NTNU

Norwegian University of
Science and Technology

Control of Six-Phase Machines

Øivind Michael Molnes Hoem

Master of Science in Energy and Environment
Submission date: June 2010
Supervisor: Tom F. Nestli, ELKRAFT
Co-supervisor: Roy Nilsen, Wärtsilä Norway

Norwegian University of Science and Technology
Department of Electric Power Engineering

Problem Description

To increase the power ratings and to reduce cost of the drive system, six-phase ma-chines are of interest to be applied in ship-propulsion. Typical maximum power rating today is 5 MW.

In a project last autumn the candidate has studied a control method for Permanent Mag-net Machines based on distributed current controllers for the two three phase groups of the six phase machine. During some transient conditions the currents are not properly controlled. In this master project the candidate should:

Investigate methods for a common control for both three phase groups; i.e. a common controller for all six phases.

Study the effect of the torque limiter chain as well as limitation in the output voltages of the inverters.

Verify the theory by help of numerical simulation in Matlab/Simulink.

Supervisor: Prof. Tom F. Nestli.
Co-supervisor: Roy Nilsen, Wärtsilä Norway

Assignment given: 19. January 2010
Supervisor: Tom F. Nestli, ELKRAFT

Preface

This master thesis was carried out at the Department of Electrical Power Engineering, Norwegian University of Science and Technology.

The time spent on this thesis has been challenging and interesting for me. Several individuals have been available to help me on my way, by producing valuable insight into the problems that I faced. I would first of all thank my supervisor Prof. 2. Tom Fagernes Nestli for his academic guidance and input. My deepest gratitude also extends to my co- supervisor Roy Nilsen whom has contributed to the process through discussions, guidance and help with constructing the modules for my simulations. A famous scientist once said that it is not difficult to see far when standing on the shoulders of giants, and this is indeed true for the help I have received in my thesis.

My fellow MSc students Martin Bråten Solhaug, Pål Kristian Vormedal and Eirik Øyslebø are also to be thanked for professional and social support throughout the past year

Øivind Michael Molnes Hoem
June, 2009
Trondheim, Norway

Abstract

The purpose of the work presented in this report was to continue the study of a six phase dual winding IPMSM with split dc-link conducted in [1]. The setup has been proposed as a means to improve the power ratings of ship-propulsion motors by increasing the number of stator windings, and thereby avoiding the problem of phase current limitations. The addition of a split dc-link gave the system increased redundancy and reliability by making the three phase inverter for each winding group capable of independently receiving power from separate sources.

The simulations performed in [1] showed unsatisfactory response in crucial fault situations that directly influence the machines reliability and redundancy. In order to improve the systems response to these faults a new control structure proposed by [2], have been constructed to replace the Double Synchronous Frame Current Control (DSFC) used in [1]. This new control structure is named Decoupled Six-Phase Current Control (DSPC) and utilizes the rotating vector space decomposition, to be introduced later, in order to successfully control both the (d,q) and (z_1,z_2) subsystem. Classical dq current controllers were used to regulate both subsystems.

The work has focused on understanding, developing and comparing the control strategy for such a machine, by theoretical modelling, analysis and analogue simulations of the machine and control structure. The new decoupled control structure will be analyzed and compared to the results of the DSFC structure. The simulations were used to verify the machines ability to perform under normal operations, as well as its response to certain fault situations. Particular effort has been made to study the transient effects of asymmetric torque limitations and dc-link undervoltage on the system.

The simulations carried out showed that the new control structures ability to respond to changes in torque reference, during normal operation, were satisfactory. The control structure was able to quickly follow the torque reference and split the load evenly on the two inverters. This was done without excitation of the (z_1,z_2) subsystem.

The simulations of the system response to asymmetric torque limitations also gave satisfactory results when including the decoupling elements for both subsystems. The direct and quadrature axis currents were rapidly regulated to their new steady state values for both inverters. This was done without considerable overshoot, and without endangering the integrity of the two inverters.

However, the system response to low dc-link voltage shows a need to implement additional control features in order to make the system successfully respond to a low dc-link voltage. This is in particular true for the step in dc-link voltage, where a large initial current peak may cause the trip of the motor drive.

It should be stressed that these are the results of analogue simulations, not including the effect of a digital control structure and the disturbance introduced by inverter switching.

Contents

List of Figures

List of Tables

Acronyms

Acronyms	*Explanation*
IPMSM	Interior Permanent Magnet Synchronous Machine
DSFC	Double Synchronous Frame Current Control
DSPC	Decoupled Six-Phase Current Control
TVSD	Traditional Vector Space Decomposition
RVSD	Rotating Vector Space Decomposition
PWM	Pulse Width Modulation
SVPWM	Space Vector Pulse Width Modulation
VCT	Vector Classification Technique

Table 1: Acronyms used in the text

List of parameters

Parameters, subscript and superscript used in the text. Lower case parameters indicate pu values. Bold specify matrixes, while underline represent vectors.

Parameter	*Explanation*
s	Parameter referred to stator
r	Parameter referred to rotating reference system
SR	Parameter referred to both stator and rotor, (vector containing several parameters referring to both stator and rotor)
z	Parameter referred to z axis
T	Transposed
*	The conjugated

Table 2: Superscript used in the text

Parameter	*Explanation*
d	Real axis of Park transform
q	Imaginary axis of Park transform
o	Zero system of Park transform
k	Order of harmonic component
s	Stator winding
r	Rotor winding
a, b, c	Phases of 3-phase system
d,q	The two axis of the (d,q) subspace
z_1,z_2	The two axis of the (z_1,z_2) subspace
0_1,0_2	The two axis of the (0_1,0_2) subspace
f	Field winding
N	Rated
n	Basis
ph	Phase
rms	Root mean square
1	Parameter related to control system 1
2	Parameter related to control system 2
σ	Leakage
dc	Direct current
ref	Reference value
max	Maximum allowed value
c	Decoupling element

Table 3: Subscript used in the text

Parameter	*Explanation*
θ_{shift}	Used to define angular difference between two basis vectors
S_k	Vector used to obtain the basis vectors used in TVSD
$S_{k,modified}$	Vector used to obtain the basis vectors used in RVSD
U	Voltage
I	Phase current
T_L	Transformation matrix introduced in [6]
R_s	Stator resistance
R_r	Rotor resistance
$L_{s\sigma}$	Stator leakage inductance, per winding
$L_{r\sigma}$	Rotor leakage inductance, per winding
L_m	Magnetizing inductance
θ_r	Rotor angular position
N	Number of turns
T_s	Sampling period
t_k	Dwell time
ψ	Flux linkage
L	Inductance
J	Moment of inertia
Ω	Angular velocity, mechanical
θ_{mech}	Angle, mechanical
p	Number of pole pairs
M_e	Electric torque
M_L	Load torque
$\mathbf{L}_g$	Position dependent leakage inductance matrix
$\mathbf{L}_{sf}$, $\mathbf{L}_{fs}$	Mutual inductance matrix between stator and field winding
$\mathbf{T}_r$	Transformation matrix
J	Matrix **J**
θ	Angle, electrical
ω	Angular velocity, electrical
P	Power
Φ	Phase angle
S	Apparent power
f	Frequency
$\mathbf{x}^r$	Inductive reactance matrix
T_m	Mechanical time constant

n	Rotational speed of the rotor
x_d	Direct axis reactance
x_q	Quadrature axis reactance
$x_{s\sigma}$	Stator leakage reactance, per winding
$x_{f\sigma}$	Field winding leakage reactance
x_{dh}	Direct axis mutual reactance
x_{qh}	Quadrature axis mutual reactance
U_{a0}, U_{b0}, U_{c0}	Inverter bridge leg voltages, with respect to the dc-link negative terminal.
u_{st}	Control voltage
α	Average time the upper bridge leg switch is on, within a switching period
ς	Voltage space vector angle
$\underline{U}_{st}$	Control voltage vector, containing control signals for all three phases
ψ_m	Rotor Magnet flux
f_s	Synchronous frequency
T	Torque
h_{oi}	Open loop transfer function
K_{pd}	Gain factor in current controller direct axis
K_{pq}	Gain factor in current controller quadrature axis
K_{pz1}	Gain factor in current controller z_1 axis
K_{pz2}	Gain factor in current controller z_2 axis
T_{id}	Time constant of the direct axis controller
T_{iq}	Time constant of the quadrature axis controller
T_{iz1}	Time constant of the z_1 axis controller
T_{iz2}	Time constant of the z_2 axis controller
T_d	Time constant direct axis
T_q	Time constant quadrature axis
T_{z1}	Time constant z_1 axis
T_{z2}	Time constant z_2 axis
T_{sum}	Sum of all small time constants
T_v	Average time delay of inverter and modulator
f_{sw}	Switching frequency [Hz]
u_{limit}	Output limit from the PI regulators.

Table 4: Parameters used in the text

1 Introduction

The aim of this thesis is to examine a six-phase machine and develop a suitable control system for the purpose of introducing it onboard offshore vessels. The propulsion systems onboard such vessels are often varying in layout and complexity depending on the application of the ship. Important concepts for most of these systems utilizing electric drives are redundancy, reliability and power ratings. Traditionally these are ensured by having several three-phase motors, connected to the onboard grid, driving one or several propellers. By utilising a six phase engine, the power rating of a motor can be greatly improved as the phase current limitations due to the converter are removed.

The motor consists of two traditional three phase windings, 30 degrees shifted and electrically isolated from each other. These winding groups are driven by two separate inverters, fed from separate dc-links. With this setup, the motor should have the capacity to utilize one set of windings even though the other has failed. However, because the two winding groups are magnetically linked, a fault concerning one winding group will affect the other. In order to take advantage of the added reliability and redundancy introduced by this setup, the control system must be robust enough to cope with faults of this nature. That is, a fault occurring in one three phase group should be controlled in such a manner that it does not cause the breakdown of the other three phase group.

In [1] a double synchronous frame current control with classical dq-current controllers was used to drive the two inverters. This is equivalent of controlling the two inverters separately without taking into consideration that they are in fact linked. Results from the simulations showed that the control system was flawed in such a way as to be inherently prone to oscillations between the two current controllers in situations regarding faults occurring in one three phase group. These oscillations had the potential of affecting the other three phase group, as it lead to increased phase currents.

In this thesis, a new control system based on the concept of a common control for both three phase groups is to be designed and evaluated. The main focus will be on the response of the given system during specific faults capable of forcing the inverters into different states. In particular this means fault capable of changing the dc-link voltage or put limitations on the amount of current each inverter is able to handle. The performance of the new system will be compared to the results of the double synchronous frame current control. This will be treated both theoretically and in simulations.

2 Background and Theory

2.1 Six-phase IPMSM layout

A six phase IPMSM (Interior Permanent Magnet Synchronous machine) consists of its rotor and its stator. The rotor is made from a permanent magnet, while the stator is constructed from six windings distributed across the 360 degree perimeter.

There are several ways in which one may distribute the six windings in the stator. In this report, one has chosen to use two identical three-phase winding sets. For each set the windings are distributed 120 degrees apart. The two sets have a displacement of 30 degrees with respect to each other. In addition the neutral points of the two three phase windings are kept electrically isolated from each other. This setup has proved to eliminate the sixth harmonic pulsating torque component [3], as well as prevent the excitation of the (0_1,0_2) subspace, see chapter 2.3.1.

A simplified scheme of the six-phase IPMSM is shown in Figure 2.1.

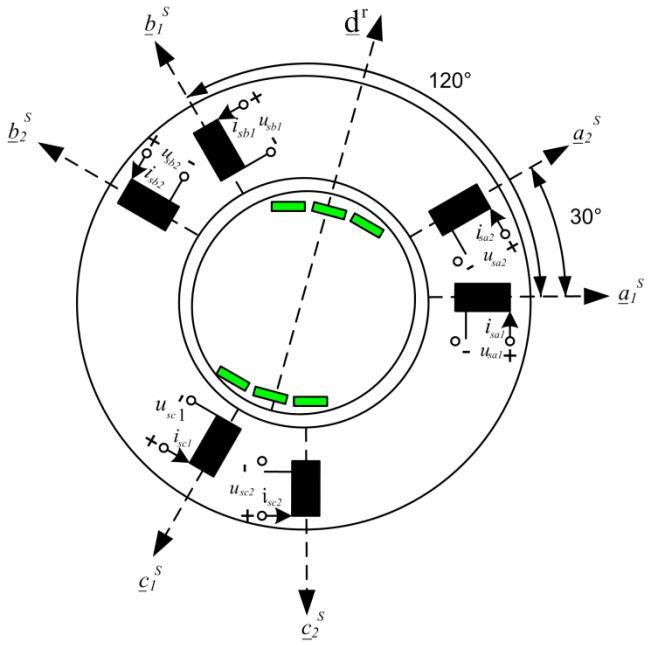

Figure 2.1: Simplified scheme of the six-phase IPMSM layout, showing rotor magnets and two three-phase groups 30° shifted [13].

2.2 Clark and Park transformation

The Clark transformation is often used to model and control a three-phase machine. It takes the three stator voltage and currents and transforms them into a spatial phasor representation. The transformation is accomplished by applying the following transformation to the voltage equations describing the physical model of the machine [4].

$$\begin{bmatrix} U_{sd}^{s} \\ U_{sq}^{s} \\ U_{0}^{s} \end{bmatrix} = \frac{1}{3} \cdot \begin{bmatrix} 2 & -1 & -1 \\ 0 & \sqrt{3} & -\sqrt{3} \\ 1 & 1 & 1 \end{bmatrix} \cdot \begin{bmatrix} U_{a} \\ U_{b} \\ U_{c} \end{bmatrix} \tag{2.1}$$

Assuming symmetrical stator windings, the sum of currents are zero. This gives, as will be shown in chapter 3.2.1, no zeros system voltage excitation. Resulting in a two dimensional control system instead of a three dimensional

By also applying the Park transformation the (d,q) system is transformed from a stationary reference frame to a synchronous rotating reference frame [5].

$$\begin{bmatrix} U_{sd}^{r} \\ U_{sq}^{r} \end{bmatrix} = \begin{bmatrix} \cos\theta & \sin\theta \\ -\sin\theta & \cos\theta \end{bmatrix} \cdot \begin{bmatrix} U_{sd}^{s} \\ U_{sq}^{s} \end{bmatrix} \tag{2.2}$$

The relations between the stationary reference frame and the rotating reference frame is illustrated in Figure 2.2.

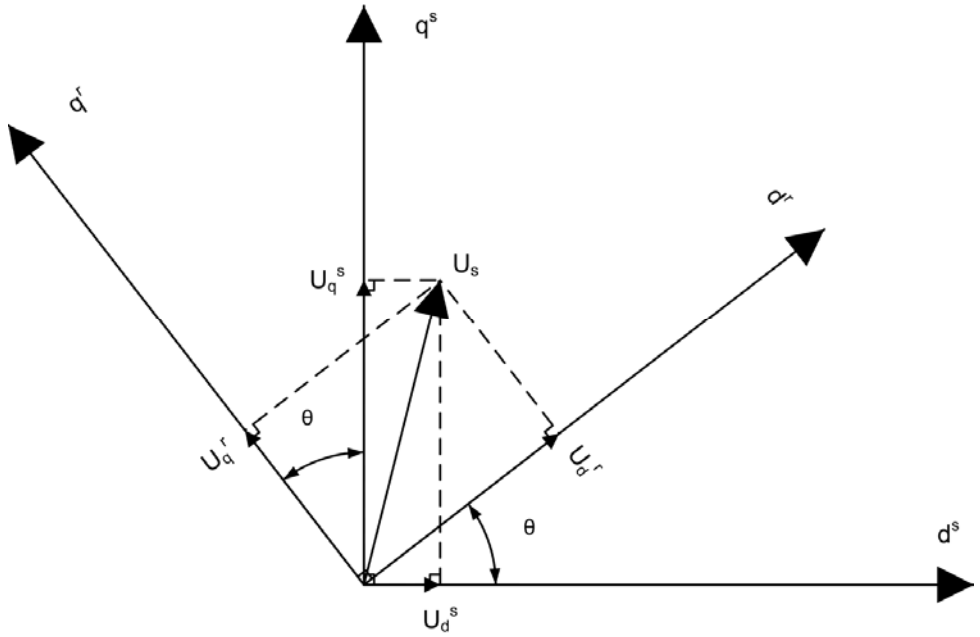

Figure 2.2: Transformation between the stationary reference frame and the rotating reference frame.

2.3 Vector Space Decomposition

The dual three-phase induction machine is a six-dimensional system since six independent currents are allowed to flow in the general case. This makes the control of the machine in the original reference frame very difficult. Geometrically, it requires the positioning of a vector on a certain surface in the six dimensional vector space, and rotating it at a desired speed.

In order to simplify the control of such a machine it would be advantageous to decompose this vector space into several orthogonal sub-systems in which one sub-system contains all the electromechanical energy conversion. This can be achieved by applying a proper transformation which maps the vectors representing the original system into a new reference frame. This is the same logic that is applied in the more familiar Clark transformation.

2.3.1 Traditional Vector Space Decomposition

In 1995 Yifan Zhao and Thomas A. Lipo introduced a powerful new method of controlling such a machine using Vector space decomposition [6]. The method is based on a vector $\underline{S_k}$ which Yifan Zhao derives in [7]. The vector is determined from the given winding distribution in fig Figure 2.1 and enables us to obtain the basis vectors for the new reference frame. This vector is given in a somewhat modified version below [8].

$$\underline{S_k}\left(\theta_k,\theta_{shift}\right)=\begin{bmatrix}\cos k(\theta_k+\theta_{shift})\\ \cos k(\theta_k+\theta_{shift}-\frac{\pi}{6})\\ \cos k(\theta_k+\theta_{shift}-\frac{4\pi}{6})\\ \cos k(\theta_k+\theta_{shift}-\frac{5\pi}{6})\\ \cos k(\theta_k+\theta_{shift}-\frac{8\pi}{6})\\ \cos k(\theta_k+\theta_{shift}-\frac{9\pi}{6})\end{bmatrix} \tag{2.3}$$

Here $k=(1,3,5)$ denotes the order of harmonics associated with the given vector and $\theta_k+\theta_{shift}$ is the angular positions in respect to the winding axis of phase one. By inserting different values of k, θ_k and θ_{shift} one can obtain the basic vectors for the new reference frame.

Two orthogonal vectors, namely d and q, can be obtained from (2.3) by mapping the first harmonic with chosen $\theta_k=0$ and $\theta_{shift}=0,\frac{\pi}{2}$.

$$\underline{\mathrm{d}} = \underline{S_1}(0,0) = \begin{bmatrix} 1 \\ \frac{\sqrt{3}}{2} \\ -\frac{1}{2} \\ -\frac{\sqrt{3}}{2} \\ -\frac{1}{2} \\ 0 \end{bmatrix} \quad \underline{q} = \underline{S_1}\left(0,\frac{\pi}{2}\right) = \begin{bmatrix} 0 \\ \frac{1}{2} \\ \frac{\sqrt{3}}{2} \\ \frac{1}{2} \\ -\frac{\sqrt{3}}{2} \\ -1 \end{bmatrix} \tag{2.4}$$

By mapping the 3 and 5 harmonic with adequate θ_k and θ_{shift} the remaining four basis vectors are obtained.

$$\underline{0_1} = \underline{S_3}(0,0) = \begin{bmatrix} 1 \\ 0 \\ 1 \\ 0 \\ 1 \\ 0 \end{bmatrix} \underline{0_2} = \underline{S_3}\left(0,\frac{\pi}{6}\right) = \begin{bmatrix} 0 \\ 1 \\ 0 \\ 1 \\ 0 \\ 1 \end{bmatrix} \quad \underline{\mathrm{Z}_1} = \underline{S_5}(0,0) = \begin{bmatrix} 1 \\ -\frac{\sqrt{3}}{2} \\ -\frac{1}{2} \\ \frac{\sqrt{3}}{2} \\ -\frac{1}{2} \\ 0 \end{bmatrix} \underline{\mathrm{Z}_2} = \underline{S_5}\left(0,\frac{\pi}{2}\right) = \begin{bmatrix} 0 \\ \frac{1}{2} \\ -\frac{\sqrt{3}}{2} \\ \frac{1}{2} \\ \frac{\sqrt{3}}{2} \\ -1 \end{bmatrix} \tag{2.5}$$

It has been shown in [7] that these vectors are orthogonal for k=1,3,5 and $0 \le (\theta_k + \theta_{shift}) \le 2\pi$. Thus the three vector spaces spanned by these basis vectors will be orthogonal to each other.

The transformation of the coordinate vectors with respect to the basis$\{\mathrm{a}_1, \mathrm{a}_2, \mathrm{b}_1, \mathrm{b}_2, \mathrm{c}_1, \mathrm{c}_2\}$ into the new reference system with basis $\{\mathrm{d}, \mathrm{q}, \mathrm{z}_1, \mathrm{z}_2, 0_1, 0_2\}$ can now be expressed as:

$$\mathbf{T}_{\mathrm{L}} = \frac{1}{3}\cdot\begin{bmatrix} 1 & \frac{\sqrt{3}}{2} & -\frac{1}{2} & -\frac{\sqrt{3}}{2} & -\frac{1}{2} & 0 \\ 0 & \frac{1}{2} & \frac{\sqrt{3}}{2} & \frac{1}{2} & -\frac{\sqrt{3}}{2} & -1 \\ 1 & -\frac{\sqrt{3}}{2} & -\frac{1}{2} & \frac{\sqrt{3}}{2} & -\frac{1}{2} & 0 \\ 0 & \frac{1}{2} & -\frac{\sqrt{3}}{2} & \frac{1}{2} & \frac{\sqrt{3}}{2} & -1 \\ 1 & 0 & 1 & 0 & 1 & 0 \\ 0 & 1 & 0 & 1 & 0 & 1 \end{bmatrix} \tag{2.6}$$

By choosing the scaling factor to $\frac{1}{3}$ rather than $\frac{1}{\sqrt{3}}$ as in [7], the length of the space vector in the two dimensional space becomes equal the peak of the phase current. Because the column vectors are mutually orthogonal, the inverse matrix T_L^{-1} exists.

Another point worth mentioning is that the voltages for the (0_1,0_2) subspace becomes zero if the stator windings have double neutral point as shown in Figure 2.3.

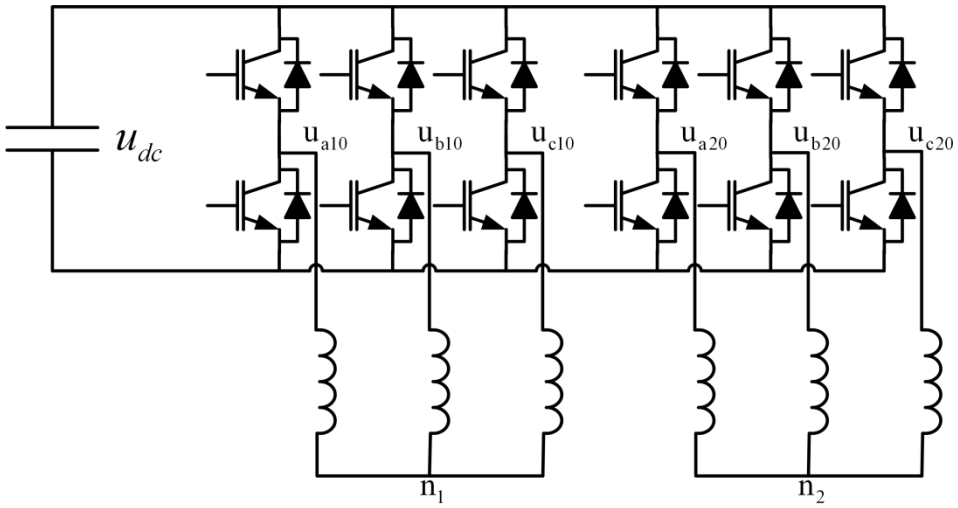

Figure 2.3: Separate neutral point for the two winding groups

This is easily verified by applying the same argument as in chapter 2.2 on both winding groups, assuming symmetrical windings in the stator. The resultant system is a four dimensional system, and the control of the dual three-phase machine is further simplified [6].

2.3.2 Rotating Vector Space Decomposition

Based on the transformation resulting from the vector space decomposition, the system can be controlled as a whole by controlling the (d,q) and (z_1,z_2) subsystem. In order to control both of these subsystems it is necessary to transform the AC quantities into DC quantities so that linear control system theory can be utilized. This will be done for the fundamental harmonic component.

In order to obtain these DC quantities, modifications were made to the original $\underline{S_k}$ vector. The modified $\underline{S_k}$ vector is given below [9].

$$S_{k,modified}\left(\theta_k,\theta_{shift}\right)=\begin{bmatrix}\cos\left(\theta_k+k(\theta_{shift})\right)\\ \cos\left(\theta_k+k(\theta_{shift}-\frac{\pi}{6})\right)\\ \cos\left(\theta_k+k(\theta_{shift}-\frac{4\pi}{6})\right)\\ \cos\left(\theta_k+k(\theta_{shift}-\frac{5\pi}{6})\right)\\ \cos\left(\theta_k+k(\theta_{shift}-\frac{8\pi}{6})\right)\\ \cos\left(\theta_k+k(\theta_{shift}-\frac{9\pi}{6})\right)\end{bmatrix} \tag{2.7}$$

In [1] it was shown that the resulting (d,q) reference vector from the traditional vector space decomposition method was rotating in the same direction and speed as the rotor, i.e. coinciding with the traditional (d,q) reference vector from the Clark transformation. The (z_1,z_2) reference vector was however found to rotate in the opposite direction of the (d,q) reference vector, with the same speed. These findings will be discussed in further detail later in the report, but the result will be utilized here to construct the new transformation matrix based on the modified $\underline{S_k}$ vector.

As stated earlier, the angular position in respect to the winding axis of phase one is given by $\theta_k + \theta_{shift}$. θ_{shift} is used to give the angular difference between the two basis vectors constituting the base for the given subsystem. This angle should be $\frac{\pi}{2}$ as the two axes should be orthogonal to each other. In the vector (2.7) this angle is multiplied by the variable k, and this needs to be taken into consideration when choosing the angle. By choosing the $\theta_k$variable for the (d,q) subsystem to be equal to the rotational speed and direction of the rotor, the basis vectors for this subsystem will follow the rotation of the (d,q) reference vector, thus giving stationary values in steady state for the first harmonic component.

The choice of harmonic components in each of the three subsystems has not been changed, thus the new basis for the (d,q) subsystem can be written as.

$$\underline{d} = \underline{S_1}(\theta,0) = \begin{bmatrix} \cos(\theta) \\ \cos(\theta-\frac{\pi}{6}) \\ \cos(\theta-\frac{2\pi}{3}) \\ \cos(\theta-\frac{5\pi}{6}) \\ \cos(\theta-\frac{4\pi}{3}) \\ \cos(\theta-\frac{3\pi}{2}) \end{bmatrix} \quad \underline{q} = \underline{S_1}\left(\theta,\frac{\pi}{2}\right) = \begin{bmatrix} -\sin(\theta) \\ -\sin(\theta-\frac{\pi}{6}) \\ -\sin(\theta-\frac{2\pi}{3}) \\ -\sin(\theta-\frac{5\pi}{6}) \\ -\sin(\theta-\frac{4\pi}{3}) \\ -\sin(\theta-\frac{3\pi}{2}) \end{bmatrix} \tag{2.8}$$

The (z_1,z_2) reference vector was found to rotate in the opposite direction of the (d,q) reference vector. By following the same logic as for the (d,q) subsystem, the θ_k variable for the (z_1,z_2) subsystem is set to $\theta_k = -\theta$. This results in the following four basis vectors.

$$\underline{0_1} = \underline{S_3}(0,0) = \begin{bmatrix} 1 \\ 0 \\ 1 \\ 0 \\ 1 \\ 0 \end{bmatrix} \underline{0_2} = \underline{S_3}\left(0,\frac{\pi}{6}\right) = \begin{bmatrix} 0 \\ 1 \\ 0 \\ 1 \\ 0 \\ 1 \end{bmatrix} \underline{Z_1} = \underline{S_5}(-\theta,0) = \begin{bmatrix} \cos\theta \\ \cos\left(\theta-\frac{7\pi}{6}\right) \\ \cos\left(\theta-\frac{2\pi}{3}\right) \\ \cos\left(\theta-\frac{11\pi}{6}\right) \\ \cos\left(\theta-\frac{4\pi}{3}\right) \\ \cos\left(\theta-\frac{\pi}{2}\right) \end{bmatrix} \underline{Z_2} = \underline{S_5}\left(-\theta,\frac{\pi}{2}\right) = \begin{bmatrix} -\sin\left(\theta-\pi\right) \\ -\sin\left(\theta-\frac{\pi}{6}\right) \\ -\sin\left(\theta-\frac{5\pi}{3}\right) \\ -\sin\left(\theta-\frac{5\pi}{6}\right) \\ -\sin\left(\theta-\frac{\pi}{3}\right) \\ -\sin\left(\theta-\frac{3\pi}{2}\right) \end{bmatrix} \tag{2.9}$$

It is vital that the properties of the original transformation, such as the basis vectors being mutually orthogonal, are kept in this new transformation. This is to ensure that the three subsystems are in fact independent of each other and that the inverse transformation exists. Although not shown in the thesis, this has been verified for the vectors given above by calculating the inner product of these vectors.

The transformation of the coordinate vectors with respect to the basis$\{a_1, a_2, b_1, b_2, c_1, c_2\}$ into the new reference system with basis $\{d, q, z_1, z_2, 0_1, 0_2\}$ can now be expressed as:

$$\mathbf{T}_{ss}^{r}=\frac{1}{3}\cdot\begin{bmatrix}\cos\theta & \cos\left(\theta-\frac{\pi}{6}\right) & \cos\left(\theta-\frac{2\pi}{3}\right) & \cos\left(\theta-\frac{5\pi}{6}\right) & \cos\left(\theta-\frac{4\pi}{3}\right) & \cos\left(\theta-\frac{3\pi}{2}\right)\\ -\sin\theta & -\sin\left(\theta-\frac{\pi}{6}\right) & -\sin\left(\theta-\frac{2\pi}{3}\right) & -\sin\left(\theta-\frac{5\pi}{6}\right) & -\sin\left(\theta-\frac{4\pi}{3}\right) & -\sin\left(\theta-\frac{3\pi}{2}\right)\\ \cos\theta & \cos\left(\theta-\frac{7\pi}{6}\right) & \cos\left(\theta-\frac{2\pi}{3}\right) & \cos\left(\theta-\frac{11\pi}{6}\right) & \cos\left(\theta-\frac{4\pi}{3}\right) & \cos\left(\theta-\frac{\pi}{2}\right)\\ -\sin\left(\theta-\pi\right) & -\sin\left(\theta-\frac{\pi}{6}\right) & -\sin\left(\theta-\frac{5\pi}{3}\right) & -\sin\left(\theta-\frac{5\pi}{6}\right) & -\sin\left(\theta-\frac{\pi}{3}\right) & -\sin\left(\theta-\frac{3\pi}{2}\right)\\ 1 & 0 & 1 & 0 & 1 & 0\\ 0 & 1 & 0 & 1 & 0 & 1\end{bmatrix} \tag{2.10}$$

For voltages this becomes.

$$\begin{bmatrix}U_{d}\\ U_{q}\\ U_{z1}\\ U_{z2}\\ U_{01}\\ U_{02}\end{bmatrix}=\mathbf{T}_{ss}^{r}\cdot\begin{bmatrix}U_{sa1}\\ U_{sa2}\\ U_{sb1}\\ U_{sb2}\\ U_{sc1}\\ U_{sc2}\end{bmatrix} \tag{2.11}$$

The inverse matrix is then given as:

$$\mathbf{T}_{ss}^{-r}=\left(\mathbf{T}_{ss}^{r}\right)^{-1}=\begin{bmatrix}\cos\theta & -\sin\theta & \cos\theta & -\sin\left(\theta-\pi\right) & 1 & 0\\ \cos\left(\theta-\frac{\pi}{6}\right) & -\sin\left(\theta-\frac{\pi}{6}\right) & \cos\left(\theta-\frac{7\pi}{6}\right) & -\sin\left(\theta-\frac{\pi}{6}\right) & 0 & 1\\ \cos\left(\theta-\frac{2\pi}{3}\right) & -\sin\left(\theta-\frac{2\pi}{3}\right) & \cos\left(\theta-\frac{2\pi}{3}\right) & -\sin\left(\theta-\frac{5\pi}{3}\right) & 1 & 0\\ \cos\left(\theta-\frac{5\pi}{6}\right) & -\sin\left(\theta-\frac{5\pi}{6}\right) & \cos\left(\theta-\frac{11\pi}{6}\right) & -\sin\left(\theta-\frac{5\pi}{6}\right) & 0 & 1\\ \cos\left(\theta-\frac{4\pi}{3}\right) & -\sin\left(\theta-\frac{4\pi}{3}\right) & \cos\left(\theta-\frac{4\pi}{3}\right) & -\sin\left(\theta-\frac{\pi}{3}\right) & 1 & 0\\ \cos\left(\theta-\frac{3\pi}{2}\right) & -\sin\left(\theta-\frac{3\pi}{2}\right) & \cos\left(\theta-\frac{\pi}{2}\right) & -\sin\left(\theta-\frac{3\pi}{2}\right) & 0 & 1\end{bmatrix} \tag{2.12}$$

2.4 Space Harmonic Components

Most industrial motors today are driven by some sort of motor drive, controlling the speed, torque and sometimes the position supplied by the motor. For ac motors this is often achieved by controlling an inverter which outputs ac voltage by using a given switching strategy. However, the use of switches to generate the set of voltages does not

give us true sinusoidal voltages. Instead the voltages can be seen to contain higher frequency components that are harmonics of the fundamental frequency.

For a six phase dual winding machine with stator windings positioned as shown in Figure 2.1 the harmonic components of the phase voltages can be written as follows.

$$\begin{aligned} a_{1,k} &= \hat{i}_{1,k} \cdot \cos\left(k \cdot (wt)\right) & a_{2,k} &= \hat{i}_{2,k} \cdot \cos\left(k \cdot (wt - 30^0)\right) \\ b_{1,k} &= \hat{i}_{1,k} \cdot \cos\left(k \cdot (wt - 120^0)\right) & b_{2,k} &= \hat{i}_{2,k} \cdot \cos\left(k \cdot (wt - 150^0)\right) \\ c_{1,k} &= \hat{i}_{1,k} \cdot \cos\left(k \cdot (wt - 240^0)\right) & c_{2,k} &= \hat{i}_{2,k} \cdot \cos\left(k \cdot (wt - 270^0)\right) \end{aligned} \quad (2.13)$$

With k stating the order of time harmonic, and being a natural number ($k = 1,2,3,4..$).

In [7] it was shown that the transformation matrix given in equation (2.6) mapped these harmonics into different subspaces depending on the frequency of the given harmonic. For instance, the k^{th} order time harmonics with $k = 12m \pm 1\ (m = 0,1,2,3,\ldots)$ were mapped into the (d,q) subspace, while the harmonics with $k = 6m \pm 1\ (m = 1,3,5,\ldots)$ and $k = 3m\ (m = 1,2,3,\ldots)$ were mapped into the (z_1,z_2) and (0_1,0_2) subspace respectively. The harmonics found to be mapped into the (d,q) subspace by [7], corresponds exactly to the space harmonics for a dual six-phase machine [10]. Therefore this subspace will produce all the rotating MMF in the machine air gap and contain the electromechanical energy conversion. This is analogous to the three phase machine, where the k^{th} order time harmonics with $k = 6m \pm 1\ (m = 0,1,2,3,\ldots)$ are mapped into the (d,q) subspace, corresponding exactly to the space harmonics for that machine. The remaining time harmonics, mapped into the (z_1,z_2) and (0_1,0_2) subspace, does not correspond with the stator space harmonic of the six-phase machine and will not contribute to the energy crossing the air gap. Because of this, the excitation of these two subsystems will lead to circulating stator current harmonics, contributing only to the total loss of the machine.

However, the analysis performed in [7] assumes that the amplitude of the bridge leg voltages from the inverters to the two three phase groups is always the same for corresponding phases. As will be shown later, this is not always the case for the setup given in this thesis. Examples of these cases could be fault situations where low dc-link voltage or current limitations affects only one of the two three-phase inverters.

It is also of interest to see, not only the harmonic components in the stationary reference frame, but the effect the rotation of the subsystems has on the harmonic components. The harmonic analysis have therefore been repeated based on the rotational transformation provided by equation (2.10) and without the assumption of equal bridge leg voltage amplitudes for corresponding phases (phase a_1 corresponding to phase a_2).

Including every harmonic component from the fundamental up to the 19 harmonic, the mapping of the harmonics into the rotating (d,q) and (z_1,z_2) subspace can be seen in Table 5 and Table 6. It is assumed that the two voltage space vector reference angles are equal as we are considering steady state operation.

k	d	q
1	$\frac{1}{2}\cdot\left(\hat{i}_{1,1}+\hat{i}_{2,1}\right)\cdot\cos\left(-\theta+\omega t\right)$	$\frac{1}{2}\cdot\left(\hat{i}_{1,1}+\hat{i}_{2,1}\right)\cdot\sin\left(-\theta+\omega t\right)$
2	$\frac{1}{2}\left(\hat{i}_{1,2}\cos\left(\theta+2\omega t\right)+\hat{i}_{2,2}\sin\left(\theta+2\omega t\right)\right)$	$\frac{1}{2}\left(-\hat{i}_{1,2}\sin\left(\theta+2\omega t\right)+\hat{i}_{2,2}\cos\left(\theta+2\omega t\right)\right)$
3	0	0
4	$\frac{1}{2}\left(\hat{i}_{1,4}\cos\left(-\theta+4\omega t\right)+\hat{i}_{2,4}\sin\left(-\theta+4\omega t\right)\right)$	$\frac{1}{2}\left(\hat{i}_{1,4}\sin\left(-\theta+4\omega t\right)-\hat{i}_{2,4}\cos\left(-\theta+4\omega t\right)\right)$
5	$\frac{1}{2}\left(\hat{i}_{1,5}-\hat{i}_{2,5}\right)\cdot\cos\left(\theta+5\omega t\right)$	$\frac{1}{2}\left(-\hat{i}_{1,5}+\hat{i}_{2,5}\right)\cdot\sin\left(\theta+5\omega t\right)$
6	0	0
7	$\frac{1}{2}\left(\hat{i}_{1,7}-\hat{i}_{2,7}\right)\cdot\cos\left(-\theta+7\omega t\right)$	$\frac{1}{2}\left(\hat{i}_{1,7}-\hat{i}_{2,7}\right)\cdot\sin\left(-\theta+7\omega t\right)$
8	$\frac{1}{2}\left(\hat{i}_{1,8}\cos\left(\theta+8\omega t\right)-\hat{i}_{2,8}\sin\left(\theta+8\omega t\right)\right)$	$\frac{1}{2}\left(-\hat{i}_{1,8}\sin\left(\theta+8\omega t\right)-\hat{i}_{2,8}\cos\left(\theta+8\omega t\right)\right)$
9	0	0
10	$\frac{1}{2}\left(\hat{i}_{1,10}\cos\left(-\theta+10\omega t\right)-\hat{i}_{2,10}\sin\left(-\theta+10\omega t\right)\right)$	$\frac{1}{2}\left(\hat{i}_{1,10}\sin\left(-\theta+10\omega t\right)+\hat{i}_{2,10}\cos\left(-\theta+10\omega t\right)\right)$
11	$\frac{1}{2}\cdot\left(\hat{i}_{1,11}+\hat{i}_{2,11}\right)\cdot\cos\left(\theta+11\omega t\right)$	$-\frac{1}{2}\cdot\left(\hat{i}_{1,11}+\hat{i}_{2,11}\right)\cdot\sin\left(\theta+11\omega t\right)$
12	0	0
13	$\frac{1}{2}\cdot\left(\hat{i}_{1,13}+\hat{i}_{2,13}\right)\cdot\cos\left(-\theta+13\omega t\right)$	$\frac{1}{2}\cdot\left(\hat{i}_{1,13}+\hat{i}_{2,13}\right)\cdot\sin\left(-\theta+13\omega t\right)$
14	$\frac{1}{2}\left(\hat{i}_{1,14}\cos\left(\theta+14\omega t\right)+\hat{i}_{2,14}\sin\left(\theta+14\omega t\right)\right)$	$\frac{1}{2}\left(-\hat{i}_{1,14}\sin\left(\theta+14\omega t\right)+\hat{i}_{2,14}\cos\left(\theta+14\omega t\right)\right)$
15	0	0
16	$\frac{1}{2}\left(\hat{i}_{1,16}\cos\left(-\theta+16\omega t\right)+\hat{i}_{2,16}\sin\left(-\theta+16\omega t\right)\right)$	$\frac{1}{2}\left(\hat{i}_{1,16}\sin\left(-\theta+16\omega t\right)-\hat{i}_{2,16}\cos\left(-\theta+16\omega t\right)\right)$
17	$\frac{1}{2}\cdot\left(\hat{i}_{1,17}-\hat{i}_{2,17}\right)\cdot\cos\left(\theta+17\omega t\right)$	$\frac{1}{2}\cdot\left(-\hat{i}_{1,17}+\hat{i}_{2,17}\right)\cdot\sin\left(\theta+17\omega t\right)$
18	0	0
19	$\frac{1}{2}\cdot\left(\hat{i}_{1,19}-\hat{i}_{2,19}\right)\cdot\cos\left(-\theta+19\omega t\right)$	$\frac{1}{2}\cdot\left(\hat{i}_{1,19}-\hat{i}_{2,19}\right)\cdot\sin\left(-\theta+19\omega t\right)$

Table 5: Harmonic components mapped into the rotating (d,q) subspace with all harmonics up to the 19th present in the stator windings.

k	z_1	z_2
1	$\frac{1}{2}\cdot\left(\hat{i}_{1,1}-\hat{i}_{2,1}\right)\cdot\cos\left(-\theta+\omega t\right)$	$\frac{1}{2}\cdot\left(-\hat{i}_{1,1}+\hat{i}_{2,1}\right)\cdot\sin\left(-\theta+\omega t\right)$
2	$\frac{1}{2}\left(\hat{i}_{1,2}\cos\left(\theta+2\omega t\right)-\hat{i}_{2,2}\sin\left(\theta+2\omega t\right)\right)$	$\frac{1}{2}\left(\hat{i}_{1,2}\sin\left(\theta+2\omega t\right)+\hat{i}_{2,2}\cos\left(\theta+2\omega t\right)\right)$
3	0	0
4	$\frac{1}{2}\left(\hat{i}_{1,4}\cos\left(-\theta+4\omega t\right)-\hat{i}_{2,4}\sin\left(-\theta+4\omega t\right)\right)$	$\frac{1}{2}\left(-\hat{i}_{1,4}\sin\left(-\theta+4\omega t\right)-\hat{i}_{2,4}\cos\left(-\theta+4\omega t\right)\right)$
5	$\frac{1}{2}\left(\hat{i}_{1,5}+\hat{i}_{2,5}\right)\cdot\cos\left(\theta+5\omega t\right)$	$\frac{1}{2}\left(\hat{i}_{1,5}+\hat{i}_{2,5}\right)\cdot\sin\left(\theta+5\omega t\right)$
6	0	0
7	$\frac{1}{2}\left(\hat{i}_{1,7}+\hat{i}_{2,7}\right)\cdot\cos\left(-\theta+7\omega t\right)$	$-\frac{1}{2}\left(\hat{i}_{1,7}+\hat{i}_{2,7}\right)\cdot\sin\left(-\theta+7\omega t\right)$
8	$\frac{1}{2}\left(\hat{i}_{1,8}\cos\left(\theta+8\omega t\right)+\hat{i}_{2,8}\sin\left(\theta+8\omega t\right)\right)$	$\frac{1}{2}\left(\hat{i}_{1,8}\sin\left(\theta+8\omega t\right)-\hat{i}_{2,8}\cos\left(\theta+8\omega t\right)\right)$
9	0	0
10	$\frac{1}{2}\left(\hat{i}_{1,10}\cos\left(-\theta+10\omega t\right)+\hat{i}_{2,10}\sin\left(-\theta+10\omega t\right)\right)$	$\frac{1}{2}\left(-\hat{i}_{1,10}\sin\left(-\theta+10\omega t\right)+\hat{i}_{2,10}\cos\left(-\theta+10\omega t\right)\right)$
11	$\frac{1}{2}\cdot\left(\hat{i}_{1,11}-\hat{i}_{2,11}\right)\cdot\cos\left(\theta+11\omega t\right)$	$\frac{1}{2}\cdot\left(\hat{i}_{1,11}-\hat{i}_{2,11}\right)\cdot\sin\left(\theta+11\omega t\right)$
12	0	0
13	$\frac{1}{2}\cdot\left(\hat{i}_{1,13}-\hat{i}_{2,13}\right)\cdot\cos\left(-\theta+13\omega t\right)$	$\frac{1}{2}\cdot\left(-\hat{i}_{1,13}+\hat{i}_{2,13}\right)\cdot\sin\left(-\theta+13\omega t\right)$
14	$\frac{1}{2}\left(\hat{i}_{1,14}\cos\left(\theta+14\omega t\right)-\hat{i}_{2,14}\sin\left(\theta+14\omega t\right)\right)$	$\frac{1}{2}\left(\hat{i}_{1,14}\sin\left(\theta+14\omega t\right)+\hat{i}_{2,14}\cos\left(\theta+14\omega t\right)\right)$
15	0	0
16	$\frac{1}{2}\left(\hat{i}_{1,16}\cos\left(-\theta+16\omega t\right)-\hat{i}_{2,16}\sin\left(-\theta+16\omega t\right)\right)$	$\frac{1}{2}\left(-\hat{i}_{1,16}\sin\left(-\theta+16\omega t\right)-\hat{i}_{2,16}\cos\left(-\theta+16\omega t\right)\right)$
17	$\frac{1}{2}\cdot\left(\hat{i}_{1,17}+\hat{i}_{2,17}\right)\cdot\cos\left(\theta+17\omega t\right)$	$\frac{1}{2}\cdot\left(\hat{i}_{1,17}+\hat{i}_{2,17}\right)\cdot\sin\left(\theta+17\omega t\right)$
18	0	0
19	$\frac{1}{2}\cdot\left(\hat{i}_{1,19}+\hat{i}_{2,19}\right)\cdot\cos\left(-\theta+19\omega t\right)$	$-\frac{1}{2}\cdot\left(\hat{i}_{1,19}+\hat{i}_{2,19}\right)\cdot\sin\left(-\theta+19\omega t\right)$

Table 6: Harmonic components mapped into the rotating (z_1,z_2) subspace with all harmonics up to the 19th present in the stator windings.

In a sinusoidal PWM, the even harmonics can be avoided by choosing to synchronise the switching frequency to be an odd integer multiple of the fundamental frequency [17]. Also for other PWM methods that are quarter wave symmetric the even harmonics will not be present in the stator. In [7] the even harmonics have been excluded from the transformation, but in Table 5 and Table 6 they have been included in order to give the full picture of the mapping of harmonics into the (d,q) and (z_1,z_2) subspace.

It can be seen from Table 5 and Table 6, that if the even harmonics exists in the stator, they will be present in the (d,q) and (z_1,z_2) subspace. The exception is the harmonics that are multiple of three, which will be mapped into the (0_1,0_2) subspace.

As seen from Table 5 and Table 6 the (d,q) and (z_1,z_2) subspace have the same properties as described in [7]. That is, if we exclude the even harmonics, disregard the rotational transformation (i.e. $\theta = 0$) and assume that the voltages from inverter one have the same amplitude as the voltages from inverter two (i.e. $\hat{i}_{1,k} = \hat{i}_{2,k}$).

If we however include the possibility of the two inverters operating at different states, the voltage amplitude of one inverter will not correspond to the amplitude of the other inverter. In this case it can be seen from Table 5 and Table 6 that the harmonic elements mapped into the (d,q) and (z_1,z_2) subspace includes the following elements $\mathrm{k} = 6\mathrm{m} \pm 1\ (\mathrm{m} = 0,1,2,3,\dots)$. For the (d,q) subsystem, this means that the harmonics that previously were mapped only into the (z_1,z_2) subspace are now included in this subsystem.

In Table 6 it can be seen that the (z_1,z_2) subspace can now be excited as a consequence of two separate incidents. One being that there exists the following stator harmonics in any of the two three phase groups: $\mathrm{k} = 3\mathrm{m} \pm 1$, where m is every natural number not a multiple of 4. The other, and far more important for the control strategy presented later, is that there exists a difference between the following corresponding harmonics from inverter one and two; $\mathrm{k} = 12\mathrm{m} \pm 1\ (\mathrm{m} = 0,1,2,3,\dots)$. This means that the excitation of the (z_1,z_2) subspace corresponding to the electromechanical energy conversion harmonics (1,11,13,23,25...) can be linked directly to the difference between the amplitude of the corresponding harmonic phase voltages for the two three phase groups. The significance of this will be more thoroughly discussed for the fundamental harmonic later in the thesis.

Including the rotational transformation (i.e. $\theta = \omega t$) the resulting harmonics mapped into the rotating (d,q) and (z_1,z_2) subspace can be seen to change their frequency. Firstly the fundamental frequency is changed into dc components for both subsystems. This is expected as the rotational transformation is designed to do precisely that. It can also be seen that for the higher harmonics, two and two harmonics are being mapped into the harmonic frequency in between them for both the (d,q) and (z_1,z_2) subspace. That is, the sum of the 5th and 7th harmonic is being mapped into the two subsystems with a frequency that corresponds to the 6th harmonic. So, for the rotating (d,q) and (z_1,z_2) subspace the following harmonics can be seen; $\mathrm{k} = 3\mathrm{m}\ (\mathrm{m} = 1,2,3,\dots)$.

For illustration purposes the harmonic components have been plotted for one axis from each subsystem, namely the direct and z_1 axis, for different scenarios. This was done by doing a Fourier analysis on a phase current containing all the harmonic frequencies. The

amplitudes of all the harmonics was set to 1, except for the case of different amplitudes where it was set to 1.5 and 0.5 respectively.

In the model presented in chapter 3.1.1 only the fundamental space harmonic is included so that only the 1st order time harmonic gives a contribution to the average torque.

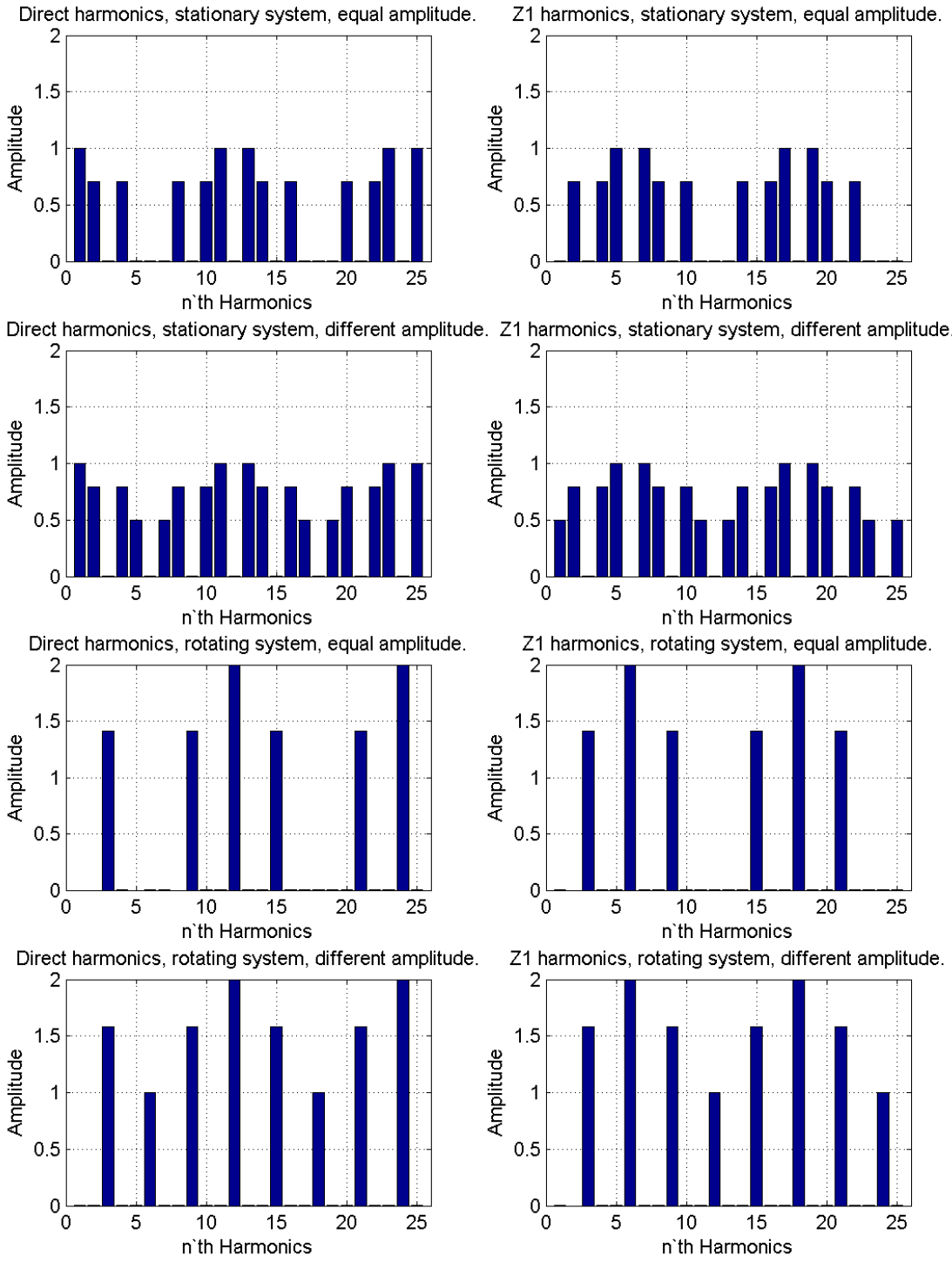

Figure 2.4: Harmonic components mapped into the (d,q) and (z_1,z_2) subspace with all harmonics up to the 25th present in the stator windings.

2.5 PWM Control Strategies

The goal of all PWM control strategies is to effectively impose the reference stator voltage generated by the control system into the (d,q) subsystem. The control strategy should also try to limit the voltage excitations in the (z_1,z_2) and $(0_1,0_2)$ subspace by keeping the average voltage vectors generated close to zero [11]. Assuming double neutral point and symmetrical windings, $(0_1,0_2)$ subspace is not excited.

To achieve these goals, a six legged two level inverter using space vector pulse width modulation (SVPWM) has 2^6=64 switching configurations. These inverter voltage vectors can be mapped in the (d,q) and (z_1,z_2) reference plane as shown in Figure 2.5

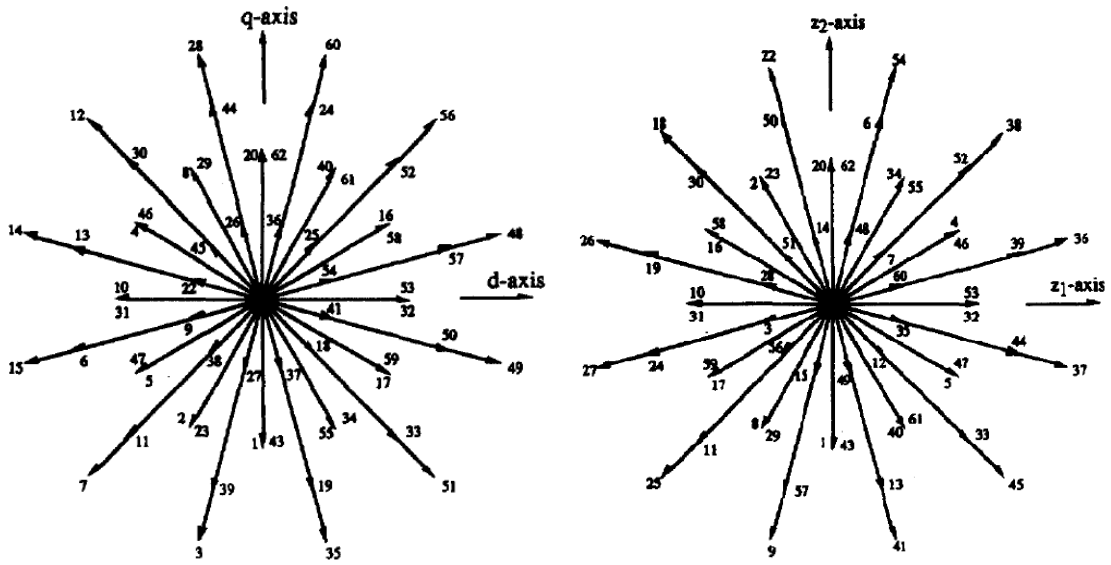

Figure 2.5: Inverter voltage vectors projected on (d,q) and (z_1,z_2) plane [6].

The numbers on each switching configuration show the switching state of the inverter as a binary number.

In order to generate the reference voltage space vector given by the control system, the (d,q) plane is divided into 12 equal size sectors. During each sampling period Ts the PWM modulator must choose a certain number of vectors (n) depending on the current sector in which the reference voltage lies. It must also allocate dwell time tk to each vector to comply with the following equation [11].

$$\sum_{k=1}^{n} t_k = T_s \tag{2.14}$$

The reference voltage space vector for the (d,q) subsystem is, according to [11], given as:

$$\begin{aligned} \sum_{k=1}^{n} u_{k,d} \cdot t_k &= u_{sd,ref} \cdot T_s & \sum_{k=1}^{n} u_{k,z_1} \cdot t_k &= 0 \\ \sum_{k=1}^{n} u_{k,q} \cdot t_k &= u_{sq,ref} \cdot T_s & \sum_{k=1}^{n} u_{k,z_2} \cdot t_k &= 0 \end{aligned} \tag{2.15}$$

2.5.1 Vector space decomposition technique

This strategy, introduced in [6], uses four vectors selected from the outermost polygon and one zero vector as shown in Figure 2.6. The chosen vectors are given from the position of the reference voltage.

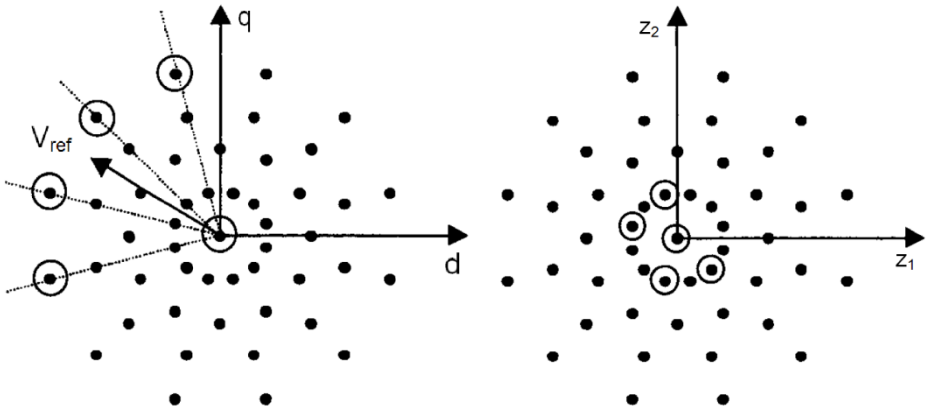

Figure 2.6: Chosen PWM vectors in the (d,q) and (z_1,z_2) plane respectively [11].

This method ensures excellent voltage output capability in the (d,q) subspace by utilizing the largest voltage vectors available in that subspace. In addition it gives ample opportunity to minimize the excitation in the (z_1,z_2) subsystem as the corresponding voltage vectors spans out to cover this system. These vectors also have the minimal amplitude which contributes to keeping the (z_1,z_2) subsystem excitation small.

2.5.2 Vector classification technique

Instead of using one six leg inverter, the authors of [12] propose to use two three legged inverters controlled by two separate modulators. This method, called the Vector classification technique (VCT), builds on the knowledge from Vector space decomposition. The exact same transformation into the (d,q) subsystem given by vector space decomposition technique, is possible to obtain by using the Clark transformation on the two separate symmetric three-phase systems. One of the transformations must then be shifted 30° in order to compensate for the spatial difference between the two three-phase groups. The two identical space vector modulators each receive a voltage reference space vector with 30° angle displacement, as pictured in Figure 2.7.

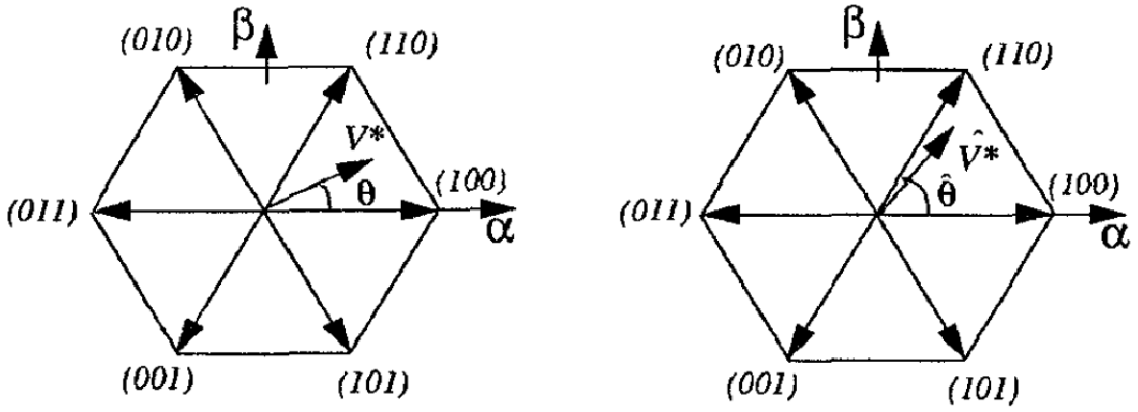

Figure 2.7: The reference voltage space vector applied to modulator 1 and 2 respectively [12].

The use of two three phase inverters introduces two sets of (d,q) systems. Using the Clark transformation described above these can be represented as:

$$\begin{bmatrix} U^s_{d1} \\ U^s_{q1} \\ U_{01} \end{bmatrix} = \frac{1}{3} \cdot \begin{bmatrix} 2 & -1 & -1 \\ 0 & \sqrt{3} & -\sqrt{3} \\ 1 & 1 & 1 \end{bmatrix} \cdot \begin{bmatrix} U_{a1} \\ U_{b1} \\ U_{c1} \end{bmatrix} \qquad \begin{bmatrix} U^s_{d2} \\ U^s_{q2} \\ U_{01} \end{bmatrix} = \frac{1}{3} \cdot \begin{bmatrix} \sqrt{3} & -\sqrt{3} & 0 \\ 1 & 1 & -2 \\ 1 & 1 & 1 \end{bmatrix} \cdot \begin{bmatrix} U_{a2} \\ U_{b2} \\ U_{c2} \end{bmatrix} \tag{2.16}$$

For the simulations presented in this report the same principle as the vector classification technique will be utilized to construct the analogue counterpart of the PWM control strategy.

2.6 Current relations

The two new (d,q) systems introduced by the vector classification technique, (d_1,q_1) and (d_2,q_2), needs to be controlled in order to successfully govern the machine. To do so, relationships between the (d,q), (z_1,z_2) subsystems from the RVSD and the (d_1,q_1), (d_2,q_2) systems from the VCT needs to be established.

Comparing the VCT transformation with the transformation of the Traditional Vector Space Decomposition technique gives the following relation for voltage, current and fluxes, exemplified with voltages:

$$\begin{bmatrix} U^s_d \\ U^s_q \end{bmatrix} = \frac{1}{2} \cdot \left\{ \begin{bmatrix} U^s_{d1} \\ U^s_{q1} \end{bmatrix} + \begin{bmatrix} U^s_{d2} \\ U^s_{q2} \end{bmatrix} \right\} \tag{2.17}$$

By applying the traditional Park transformation to the VCT transformation and comparing the results with the Rotating Vector Space Decomposition the relation given in equation (2.17) can also be found to exist in the rotating coordinate system.

$$\mathbf{T}_{ss}^{r}=\frac{1}{3}\cdot\begin{bmatrix}\cos\theta & \cos\left(\theta-\frac{\pi}{6}\right) & \cos\left(\theta-\frac{2\pi}{3}\right) & \cos\left(\theta-\frac{5\pi}{6}\right) & \cos\left(\theta-\frac{4\pi}{3}\right) & \cos\left(\theta-\frac{3\pi}{2}\right)\\ -\sin\theta & -\sin\left(\theta-\frac{\pi}{6}\right) & -\sin\left(\theta-\frac{2\pi}{3}\right) & -\sin\left(\theta-\frac{5\pi}{6}\right) & -\sin\left(\theta-\frac{4\pi}{3}\right) & -\sin\left(\theta-\frac{3\pi}{2}\right)\\ \cos\theta & \cos\left(\theta-\frac{7\pi}{6}\right) & \cos\left(\theta-\frac{2\pi}{3}\right) & \cos\left(\theta-\frac{11\pi}{6}\right) & \cos\left(\theta-\frac{4\pi}{3}\right) & \cos\left(\theta-\frac{\pi}{2}\right)\\ -\sin(\theta-\pi) & -\sin\left(\theta-\frac{\pi}{6}\right) & -\sin\left(\theta-\frac{5\pi}{3}\right) & -\sin\left(\theta-\frac{5\pi}{6}\right) & -\sin\left(\theta-\frac{\pi}{3}\right) & -\sin\left(\theta-\frac{3\pi}{2}\right)\\ 1 & 0 & 1 & 0 & 1 & 0\\ 0 & 1 & 0 & 1 & 0 & 1\end{bmatrix} \tag{2.18}$$

The remaining relations can now be derived by studying the transformation matrix given in equation (2.18). Here the 1, 3 and 5th column in row one gives us $\frac{U_{d1}^{r}}{2}$ as these are the stator related elements from winding one, see equation (2.11). The same elements are seen on the 1, 3 and 5th column in row three, allowing us to make the connection between U_{z1}^{r} and U_{d1}^{r}. By realizing that $\frac{U_{d2}^{r}}{2}$ is a result of the elements in the 2, 4 and 6th column in row one and comparing the rest of the elements in the same manner in row 1, 2, 3 and 4 the following relations can be obtained [9].

$$\begin{aligned} U_{sd}{}^{r}&=\frac{U_{d1}{}^{r}+U_{d2}{}^{r}}{2} & U_{z_1}{}^{r}&=\frac{U_{d1}{}^{r}-U_{d2}{}^{r}}{2}\\ U_{sq}{}^{r}&=\frac{U_{q1}{}^{r}+U_{q2}{}^{r}}{2} & U_{z_2}{}^{r}&=\frac{-U_{q1}{}^{r}+U_{q2}{}^{r}}{2}\end{aligned} \tag{2.19}$$

These relations can be seen to coincide with the results of the harmonic analysis performed in chapter 2.4. That is, the equations for both the (d,q) and (z_1,z_2) subsystems seen above, are the same as the governing equation for these subsystems seen in the time harmonics corresponding to the space harmonics in the machine (i.e. $k=12m\pm1\ (m=0,1,2,3,\dots)$). See Table 5 and Table 6. Equation (2.19) can therefore be said to be valid for the torque creating harmonics found in the stator. The equations can be manipulated into:

$$\begin{aligned} U_{d1}{}^{r}&=U_{sd}{}^{r}+U_{z_1}{}^{r} & U_{q1}{}^{r}&=U_{sq}{}^{r}-U_{z_2}{}^{r}\\ U_{d2}{}^{r}&=U_{sd}{}^{r}-U_{z_1}{}^{r} & U_{q2}{}^{r}&=U_{sq}{}^{r}+U_{z_2}{}^{r}\end{aligned} \tag{2.20}$$

The exact same relationship can be used to describe the corresponding currents and fluxes.

2.7 (z_1,z_2) subsystem

The Rotating Vector Space Decomposition technique leaves us with three two-dimensional subsystems instead of one six phase system. The (d,q) and (0_1,0_2) subsystem should be familiar to most readers as they are also used in the traditional control of a

three phase machine through Clark and Park transformations. The (z_1,z_2) subsystem however might not be so intuitive, and as a consequence this section will try to summarize and explain the different aspects of this system.

As mentioned in chapter 2.4 the (z_1,z_2) subsystem can in the general case contain the following stator space harmonic components $k = 3m \pm 1 (m = 0,1,2, \dots)$. These harmonics are seen by the rotating (z_1,z_2) subsystem as having the following frequencies; $k = 3m\ (m = 0,1,2 \dots)$. The harmonics can be split into two groups by differentiating on how they are formed.

The first group consists of the following stator harmonic components: $k = 3m \pm 1$, where m is every natural number not a multiple of 4. The excitation of the (z_1,z_2) subsystem by these harmonics is simply relying on the fact that they exist in the stator. Furthermore, these space harmonics does not contribute to the generated electromechanical energy conversion as they do not coincide with the time harmonics of the six-phase dual winding stator. Excitation in the (z_1,z_2) subsystem caused by these harmonics is therefore synonymous with currents circulating in the stator, creating losses and not contributing to the generated mechanical torque on the shaft. It is therefore preferable under normal conditions that this part of the (z_1,z_2) subsystem is not excited.

The second group of space harmonics contains the following components, related to the stator $k = 12m \pm 1 (m = 1,2,3, \dots)$. These harmonics will be present in the (z_1,z_2) subsystem, given that there exist a difference in amplitude between the two phase groups for that specific harmonic, see Table 6. This difference in amplitude can arise for different reasons including faults limiting the performance of one inverter, and drift resulting from controlling the two inverters separately without correcting for the deviation that might accumulate over time. Given that these harmonics are present in the (z_1,z_2) subsystem, there will be a difference in torque delivered by the two inverters as these harmonics correspond directly with the time harmonics of the six-phase dual winding stator [10]. This part of the (z_1,z_2) subsystem can in other words be used to detect and control the difference of load sharing between the two inverters. It should be pointed out that in later chapters, dealing with control theory, only the fundamental harmonic is used for this purpose.

So from a physical perspective, the excitation of the (z_1,z_2) subsystem in steady state is synonymous with the existence of harmonics with a specific frequency ($k = 3m \pm 1$, m is a natural number not multiple of 4) and/or the existence of a difference in amplitude between certain corresponding harmonics ($k = 12m \pm 1 (m = 1,2,3, \dots)$) in the two three-phase groups.

In [1],[13] the following equation was derived.

$$\underline{U_z} = \begin{bmatrix} U_{z1} \\ U_{z2} \end{bmatrix} = \frac{1}{2} \cdot \left\{ \frac{U_{dc1}}{2} \cdot u_{st1} \cdot e^{-i\zeta_1(t)} - \frac{U_{dc2}}{2} \cdot u_{st2} \cdot e^{-i\zeta_2(t)} \right\} = \frac{1}{2} \cdot \left\{ \underline{U_1}^{s*} - \underline{U_2}^{s*} \right\} \qquad (2.21)$$

It gives the relation between the excitation of the (z_1,z_2) subsystem and the dc-link voltage U_{dc}, inverter control voltages u_{st} and the voltage space vector angle ς. In short it states that a sufficiently high difference between the dc-link voltages, uncompensated by

the inverter control voltages, will lead to an excitation of the (z_1,z_2) subsystem [1]. From this equation it can also be seen that when the (z_1,z_2) subsystem is excited, it will rotate with the same speed as the voltage space vectors, but in the opposite direction. This means it will be rotating with the speed of the rotor and (d,q) subsystem, but in the opposite direction. This is shown in Figure 2.8 with $\varsigma_1 \neq \varsigma_2$ for illustration purpose.

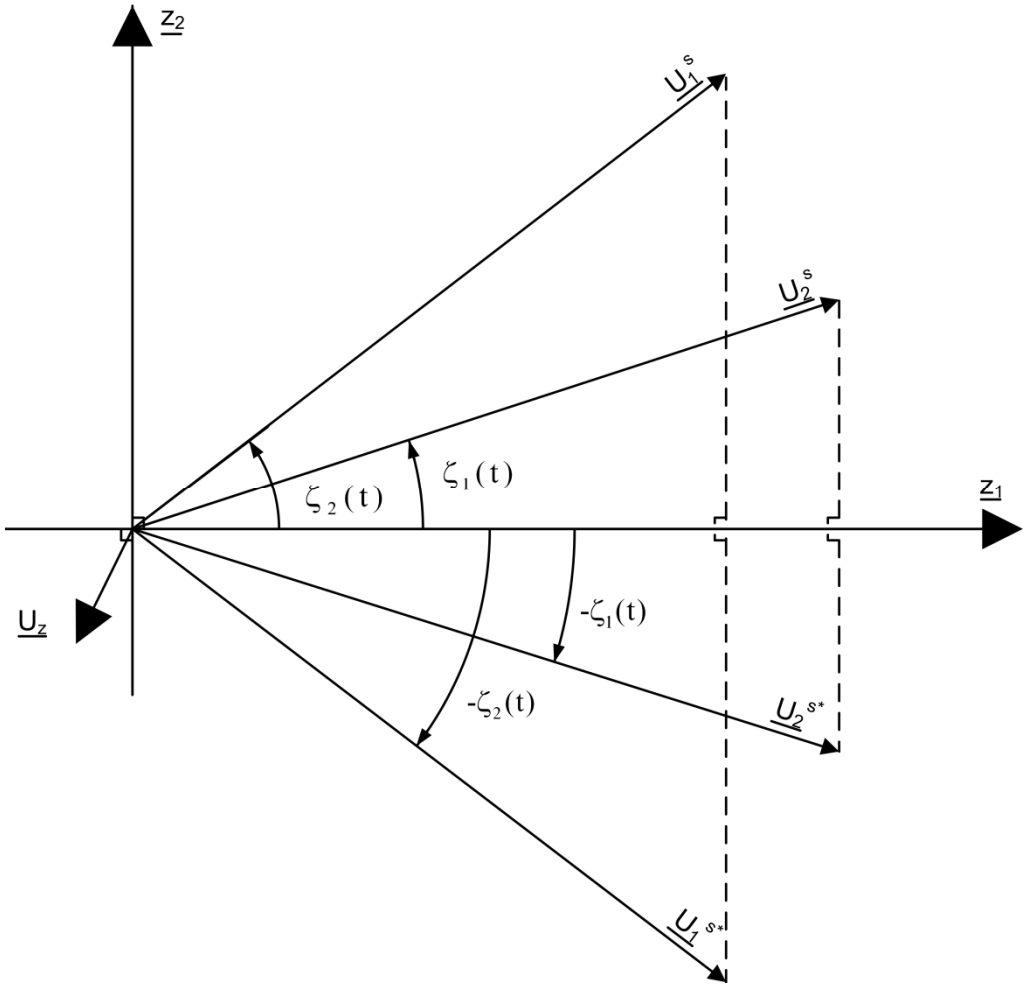

Figure 2.8: $\underline{U_z}$ with $\varsigma_1 \neq \varsigma_2$ [1]

In the previous chapter the relationship between the currents in the (z_1,z_2) subsystem and the currents governing the two inverters was found to be.

$$i_{z_1}{}^r = \frac{i_{d1}{}^r - i_{d2}{}^r}{2} \qquad i_{z_2}{}^r = \frac{-i_{q1}{}^r + i_{q2}{}^r}{2} \tag{2.22}$$

As can be seen from equation (2.22), the currents i_{z1} and i_{z2} in the (z_1,z_2) subsystem is directly related to the respective divisions of direct and quadrature axis current. That is, if part or whole of the (z_1,z_2) subsystem is excited, there will be a difference in the amount of torque or magnetizing current supplied from the inverters. This fact will be used in the control philosophy to actively control the division between the two inverters in certain fault situations.

3 Modelling

3.1 PM machine

3.1.1 Six- phase IPMSM Physical Model

The model given in this section is based on [8] with certain modifications. The model is based on the following assumptions:

- All windings give a sinusoidal distributed magnetic field around the air-gap of the machine, i.e. only the 1. harmonic component of the field is modeled. The windings are represented with concentrated coils.
- The stator windings are all equal, however, with different directions of winding axis
- Resistances and inductances are assumed to be independent of temperature and frequency
- Magnetic saturation is neglected
- Iron and eddy current losses are neglected
- Assuming symmetrical inductance matrix

In this report, only the scaled (per unit) model transformed to rotor-coordinates is presented in its whole. This derivation was also conducted in [1], and is included here because of the different basis and result.

3.1.1.1. Electromagnetic System

In a six-phase machine there are six voltage equations in the stator and one for the rotor. This can be written in matrix-form as:

$$\underline{U}^{SR} = R^{SR} \cdot \underline{I}^{SR} + \frac{d\underline{\Psi}^{SR}}{dt} \tag{3.1}$$

The flux is given as:

$$\underline{\psi}^{SR} = \mathbf{L}^{SR}(\theta) \cdot \underline{I}^{SR} \tag{3.2}$$

Where the voltage, current and flux linkage vectors as well as the resistance and inductance matrix can be found in appendix A.1.

3.1.1.2. Mechanical System

The equations for the speed and position are given as:

$$J \cdot \frac{d\Omega}{dt} = M_e - M_L \qquad \frac{d\theta_{mech}}{dt} = \Omega \qquad \theta = p \cdot \theta_{mech} \tag{3.3}$$

The torque M_e can be expressed as:

$$M_e = \frac{1}{2} \cdot \left(\underline{I}^{SR} \right)^T \cdot \frac{\partial \mathbf{L}^{SR}}{\partial \theta_{mech}} \cdot \underline{I}^{SR} = \frac{p}{2} \cdot \left(\underline{I}^{SR} \right)^T \cdot \frac{\partial \mathbf{L}^{SR}}{\partial \theta} \cdot \underline{I}^{SR} \tag{3.4}$$

3.1.2 Transformation of Physical model

3.1.2.1. Transformation Matrix

In order to simplify the model of the six-phase IPMSM, the transformation matrix from chapter 2.3.2 is utilized. This method, first introduced in [6] and later modified in [8] and in the given thesis, transforms the two three phase groups into three two dimensional orthogonal subspaces; (d,q), (z_1,z_2) and (0_1,0_2). The modifications introduced in chapter 2.3.2 allows us to make the transition from physical equations to the rotating orthogonal subspaces named (d,q) and (z_1,z_2), in one transformation. It should be noted that the (0_1,0_2) subspace is not transformed into a rotating reference frame as this subspace is proved to not be excited in the given configuration.

The rotating (d,q) subsystem in reference to the two three phase groups is shown in Figure 3.1.

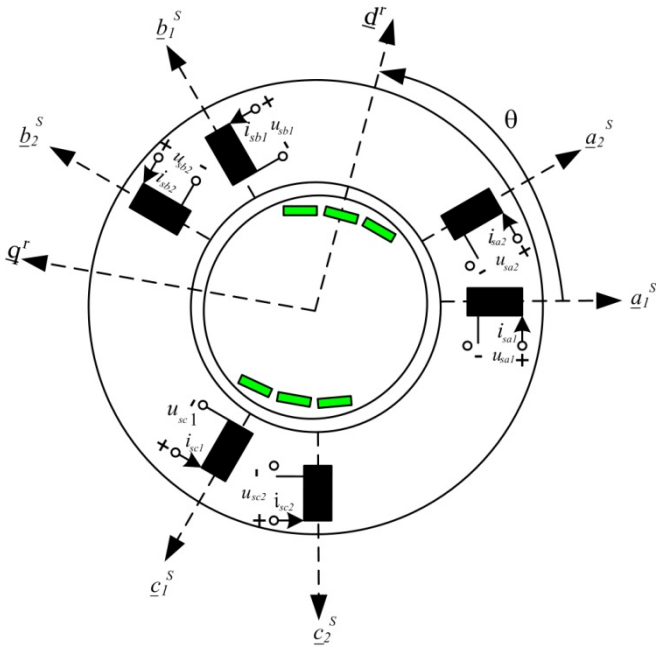

Figure 3.1: Rotating (d,q) system in relations to the physical windings in a six-phase IPMSM [13].

The transformation is achieved by applying the following relation to the IPMSM Physical Model presented above.

$$\mathbf{T}^r = \begin{bmatrix} \mathbf{T}^r_{ss} & 0 \\ 0 & \mathbf{T}^r_{rr} \end{bmatrix} \tag{3.5}$$

The $\boldsymbol{T}_{ss}{}^{r}$ component of the transformation matrix changes the reference frame of the stator related equations from stator to rotor and transforms the (d,q) and (z_1,z_2) subspace into a rotating reference frame.

$$\mathbf{T}_{ss}^{r}=\frac{1}{3}\cdot\begin{bmatrix}
\cos\theta & \cos\left(\theta-\frac{\pi}{6}\right) & \cos\left(\theta-\frac{2\pi}{3}\right) & \cos\left(\theta-\frac{5\pi}{6}\right) & \cos\left(\theta-\frac{4\pi}{3}\right) & \cos\left(\theta-\frac{3\pi}{2}\right)\\
-\sin\theta & -\sin\left(\theta-\frac{\pi}{6}\right) & -\sin\left(\theta-\frac{2\pi}{3}\right) & -\sin\left(\theta-\frac{5\pi}{6}\right) & -\sin\left(\theta-\frac{4\pi}{3}\right) & -\sin\left(\theta-\frac{3\pi}{2}\right)\\
\cos\theta & \cos\left(\theta-\frac{7\pi}{6}\right) & \cos\left(\theta-\frac{2\pi}{3}\right) & \cos\left(\theta-\frac{11\pi}{6}\right) & \cos\left(\theta-\frac{4\pi}{3}\right) & \cos\left(\theta-\frac{\pi}{2}\right)\\
-\sin(\theta-\pi) & -\sin\left(\theta-\frac{\pi}{6}\right) & -\sin\left(\theta-\frac{5\pi}{3}\right) & -\sin\left(\theta-\frac{5\pi}{6}\right) & -\sin\left(\theta-\frac{\pi}{3}\right) & -\sin\left(\theta-\frac{3\pi}{2}\right)\\
1 & 0 & 1 & 0 & 1 & 0\\
0 & 1 & 0 & 1 & 0 & 1
\end{bmatrix} \tag{3.6}$$

The $\boldsymbol{T}_{rr}{}^{r}$ component of the transformation matrix is essentially the Identity matrix since the rotor related voltage and flux equations already have the rotor as a reference frame.

$$\mathbf{T}_{rr}^{r}=1 \tag{3.7}$$

Applying the new transformation matrix:

$$\underline{U}^{r}=\mathbf{T}^{r}\cdot\underline{U}^{SR}=\mathbf{T}^{r}\cdot\mathbf{R}^{SR}\cdot\mathbf{T}^{-r}\cdot\underline{I}^{r}+\mathbf{T}^{r}\cdot\frac{d\left(\mathbf{T}^{-r}\cdot\underline{\Psi}^{r}\right)}{dt}=\mathbf{R}^{r}\cdot\underline{I}^{r}+\frac{d\underline{\Psi}^{r}}{dt}+\mathbf{T}^{r}\cdot\frac{d\mathbf{T}^{-r}}{dt}\cdot\underline{\Psi}^{r}$$

By introducing the matrix **J**, this can be written as:

$$\underline{U}^{r}=\mathbf{R}^{r}\cdot\underline{I}^{r}+\frac{d\underline{\Psi}^{r}}{dt}+\omega\cdot\mathbf{J}\cdot\underline{\Psi}^{r}\ ,\ \underline{\Psi}^{r}=\mathbf{L}^{r}\cdot\underline{I}^{r}\ ,\ \frac{d\theta}{dt}=\omega\ ,\ \mathbf{J}=\mathbf{T}^{r}\cdot\frac{d\mathbf{T}^{-r}}{d\theta} \tag{3.8}$$

The voltage, current and flux vectors, along with the resistance, inductance and **J** matrix is given in appendix A.2.

The torque can, according to [8] be expressed by help of the transformed coordinate vectors as:

$$M_e=\frac{p}{2}\cdot\left(\underline{I}^{SR}\right)^{T}\cdot\frac{\partial\mathbf{L}^{SR}}{\partial\theta}\cdot\underline{I}^{SR}=\frac{p}{2}\cdot\left(\mathbf{T}^{-r}\cdot\underline{I}^{r}\right)^{T}\cdot\frac{\partial\mathbf{L}^{SR}}{\partial\theta}\cdot\mathbf{T}^{-r}\cdot\underline{I}^{r}=\frac{p}{2}\cdot\left(\underline{I}^{r}\right)^{T}\cdot\left(\mathbf{T}^{-r}\right)^{T}\cdot\frac{\partial\mathbf{L}^{SR}}{\partial\theta}\cdot\mathbf{T}^{-r}\cdot\underline{I}^{r}$$

This can be transformed into the following equation:

$$M_e=3\cdot p\cdot\left(\underline{I}^{r}\right)^{T}\cdot\mathbf{J}\cdot\underline{\Psi}^{r}=3\cdot p\cdot\left(\Psi_d\cdot I_q-\Psi_q\cdot I_d\right) \tag{3.9}$$

3.1.2.2. Introducing the PU system

The basis for power in the AC-machine is usually the total power into the stator winding in steady state, when voltages and currents are of sinusoidal shape (or cosine). If averaging the power in each winding over one fundamental period, the power rated input power can be written as:

$$P_{sN} = 6 \cdot \frac{\hat{U}_{phN} \cdot \hat{I}_{phN}}{2} \cdot \cos\phi_N = 6 \cdot U_{phN,rms} \cdot I_{phN,rms} \cdot \cos\phi_N \tag{3.10}$$

The apparent power, which is used as basis for power in AC machines becomes:

$$S_N = 6 \cdot \frac{\hat{U}_{phN} \cdot \hat{I}_{phN}}{2} = 3 \cdot \hat{U}_{phN} \cdot \hat{I}_{phN} = 6 \cdot U_{phN,rms} \cdot I_{phN,rms} = 2 \cdot \sqrt{3} \cdot U_N \cdot I_N \tag{3.11}$$

Here U_N is the rms value of the line voltage in one of the two three-phase groups. The current is the rms-value of the current in one winding. As we understand we can have half the current rating pr. phase in a 6-phase machine compared with a 3-phase machine of same voltage and power rating.

We have 6 windings in the machine, which means that 6 basis voltages, currents and flux linkages have to be chosen when scaling the model. The rated pr. phase peak values are used as basis values in the stator windings:

$$\begin{aligned} I_{dn} &= I_{qn} = I_{z1n} = I_{z2n} = I_{01n} = I_{02n} = \hat{I}_N \\ U_{dn} &= U_{qn} = U_{z1n} = U_{z2n} = U_{01n} = U_{02n} = \hat{U}_{ph,N} \\ \Psi_{dn} &= \Psi_{qn} = \Psi_{z1n} = \Psi_{z2n} = \Psi_{01n} = \Psi_{02n} = \Psi_n = \frac{\hat{U}_{ph,N}}{\omega_n} = \frac{\hat{U}_{ph,N}}{2 \cdot \pi \cdot f_n} \end{aligned} \tag{3.12}$$

As we can see the product of the basis voltage and current in each winding becomes equal the basis for power (adding the stator windings gives 6 times):

$$U_{dn} \cdot I_{dn} = U_{qn} \cdot I_{qn} = U_{z1n} \cdot I_{z1n} = U_{z2n} \cdot I_{z2n} = U_{01n} \cdot I_{01n} = U_{02n} \cdot I_{02n} = \hat{U}_{ph,N} \cdot \hat{I}_N \tag{3.13}$$

The scaling of the power in to the stator is then given as:

$$\begin{aligned} P_s &= 3 \cdot \left(U_d \cdot I_d + U_q \cdot I_q + U_{z1} \cdot I_{z1} + U_{z2} \cdot I_{z2} + U_{01} \cdot I_{01} + U_{02} \cdot I_{02} \right) \\ S_N &= 3 \cdot \hat{U}_{phN} \cdot \hat{I}_{phN} \\ \wp_s &= \frac{P_s}{S_N} = u_d \cdot i_d + u_q \cdot i_q + u_{z1} \cdot i_{z1} + u_{z2} \cdot i_{z2} + u_{01} \cdot i_{01} + u_{02} \cdot i_{02} \end{aligned} \tag{3.14}$$

By applying this, the electromagnetic system can be written as:

$$\underline{u}^r = r^r \cdot \underline{i}^r + \frac{1}{\omega_n} \cdot \frac{d\underline{\psi}^r}{dt} + n \cdot \mathbf{J} \cdot \underline{\psi}^r \qquad \underline{\psi}^r = \mathbf{x}^r \cdot \underline{i}^r \tag{3.15}$$

Where $\mathbf{x}^r$ is given in appendix A.2.

The basis for pu-torque is:

$$M_n = \frac{S_N}{\Omega_N} = p \cdot \frac{S_N}{\omega_n} = 3 \cdot p \cdot \frac{\hat{U}_{phN} \cdot \hat{I}_{phN}}{\omega_n} = 3 \cdot p \cdot \hat{\Psi}_n \cdot \hat{I}_{phN} \tag{3.16}$$

This gives the pu torque as:

$$m_e = \frac{M_e}{M_n} = \frac{3 \cdot p \cdot \left(\Psi_d \cdot I_q - \Psi_q \cdot I_d \right)}{3 \cdot p \cdot \hat{\Psi}_n \cdot \hat{I}_{phN}} = \psi_d \cdot i_q - \psi_q \cdot i_d \tag{3.17}$$

The mechanical time constant is:

$$T_m = \frac{J \cdot \Omega_N^2}{S_N} \tag{3.18}$$

The model for the mechanical system then becomes:

$$T_m \cdot \frac{dn}{dt} = m_e - m_L \qquad \frac{d\theta}{dt} = \omega_n \cdot n \qquad \theta_{mech} = \theta / p \tag{3.19}$$

3.1.3 Transformed Six- phase IPMSM Model

When applying both the transformation matrix and the PU system the model can be written in component form. In the final model, the damper windings can be removed and the voltage equation for the field winding $L_{df} * I_f$ can then be substituted by Ψ_m. For the rest of the report the superscript ^{r} will not be used to state that a parameter is expressed using the rotating (d,q) or (z_1,z_2) subsystem. Instead it will be assumed that it is implicit.

$$\begin{aligned}
u_d &= r_s \cdot i_d + \frac{1}{\omega_n} \cdot \frac{d\psi_d}{dt} - n \cdot \psi_q & u_q &= r_s \cdot i_q + \frac{1}{\omega_n} \cdot \frac{d\psi_q}{dt} + n \cdot \psi_d \\
u_{z1} &= r_s \cdot i_{z1} + \frac{1}{\omega_n} \cdot \frac{d\psi_{z1}}{dt} + n \cdot \psi_{z2} & u_{z2} &= r_s \cdot i_{z2} + \frac{1}{\omega_n} \cdot \frac{d\psi_{z2}}{dt} - n \cdot \psi_{z1} \\
u_{01} &= r_s \cdot i_{01} + \frac{1}{\omega_n} \cdot \frac{d\psi_{01}}{dt} & u_{02} &= r_s \cdot i_{02} + \frac{1}{\omega_n} \cdot \frac{d\psi_{02}}{dt}
\end{aligned} \tag{3.20}$$

$$\begin{aligned} \psi_d &= x_d \cdot i_d + \psi_m & \psi_q &= x_q \cdot i_q \\ \psi_{z1} &= x_{s\sigma} \cdot i_{z1} & \psi_{z2} &= x_{s\sigma} \cdot i_{z2} \\ \psi_{01} &= x_{s\sigma} \cdot i_{01} & \psi_{02} &= x_{s\sigma} \cdot i_{02} \end{aligned} \tag{3.21}$$

$$x_d = x_{dh} + x_{s\sigma} \qquad x_q = x_{qh} + x_{s\sigma}$$

$$\begin{aligned} m_e &= \psi_d \cdot i_q - \psi_q \cdot i_d \\ T_m \cdot \frac{dn}{dt} &= m_e - m_L \qquad \frac{d\theta}{dt} = \omega_n \cdot n \qquad \theta_{mech} = \theta / p \end{aligned} \tag{3.22}$$

The new model with rotated (d,q) and (z_1,z_2) subspace introduces new decoupling elements in the (z_1,z_2) subspace when compared to the model in [1] where only the (d,q) subspace is rotated. The extra set of decoupling elements will be dealt with more thoroughly in the control section, see chapter 4.2.

It should be noted that the currents in the (z_1,z_2) and (0_1,0_2) subspace can become quite large if the systems are excited. This is due to the fact that they are only limited by the stator resistance and leakage reactance, as shown in equation (3.20) and (3.21).

It is important to note that in a healthy machine, with two three-phase windings electrically insulated, the sum of currents in each three-phase group is zero. This means that the zero-system can be omitted in the model, while they are not excited [13]. See chapter 2.3.1.

3.2 Inverter modell

3.2.1 Continuous model of 2-level inverter

As previously mentioned, this report will utilize two three phase inverters in order to control the six-phase machine. To accomplish this one needs a model of the three-phase inverter.

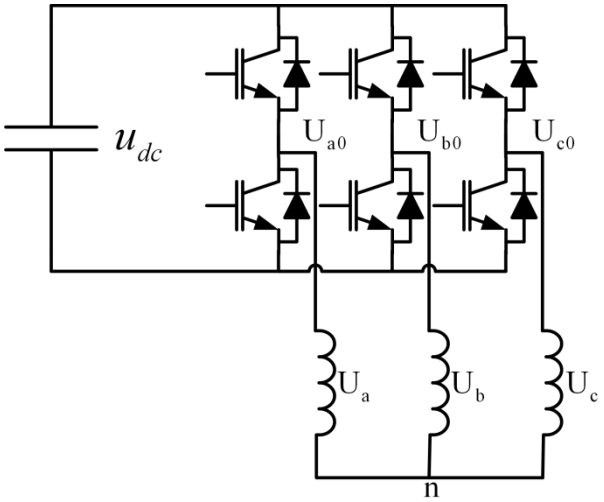

Figure 3.2: Three-phase 2-level inverter.

A three-phase inverter makes it possible to control the voltages at the bridge leg of the inverter. The implementation of this as a continuous model is described below.

The phase voltages of the motor can be expressed as:

$$\begin{aligned} U_{a0}(t) - U_{b0}(t) &= U_a(t) - U_b(t) \\ U_{b0}(t) - U_{c0}(t) &= U_b(t) - U_c(t) \\ U_{c0}(t) - U_{a0}(t) &= U_c(t) - U_a(t) \end{aligned} \tag{3.23}$$

For motors with symmetrical stator windings, i.e. equal resistance in each phase and similar windings, only 120^o displaced around the periphery of the stator, the zero system in the dq0-model becomes [13].

$$\begin{aligned} u_0(t) &= r_s \cdot i_0 + \frac{x_{s\sigma}}{\omega_n} \cdot \frac{di_0}{dt} \\ u_0(t) &= \frac{1}{3} \cdot \left(u_a(t) + u_b(t) + u_c(t)\right) \qquad i_0(t) = \frac{1}{3} \cdot \left(i_a(t) + i_b(t) + i_c(t)\right) \end{aligned} \tag{3.24}$$

Assuming that the motor has symmetrical stator windings, $u_0(t)$ will become zero. The equation (3.23) and (3.24) then gives us the following relationship between bridge leg voltages and motor phase voltages.

$$\begin{aligned} U_a(t) &= \frac{1}{3} \cdot \left(2 \cdot U_{a0}(t) - U_{b0}(t) - U_{c0}(t)\right) \\ U_b(t) &= \frac{1}{3} \cdot \left(2 \cdot U_{b0}(t) - U_{c0}(t) - U_{a0}(t)\right) \\ U_c(t) &= \frac{1}{3} \cdot \left(2 \cdot U_{c0}(t) - U_{a0}(t) - U_{b0}(t)\right) \end{aligned} \tag{3.25}$$

This result also applies to six-phase machines, provided that we have separate neutral point for the two phase windings, an assumption made in chapter 2.1. The zero system will then only influence the three-phase group it belongs to, and the zero system voltage will become zero for a symmetrical three-phase system [13].

The implementation of the PWM-modulator for the 3-phase inverters is made such that the *average* time the upper switch in a bridge leg is on (d_{au}=1) within a switching period, is given as (i.e. α_a = the average time of d_{au}=1).

$$\begin{aligned}
\bar{d}_{au} &= \alpha_a(t) = \frac{1}{2}\left(1+u_{sta}(t)\right) = \frac{1}{2}\left(1+u_{st}\cdot\cos(\zeta)\right) = \frac{1}{2}\left(1+u_{st}\cdot\cos(\omega_s t)\right)\\
\bar{d}_{bu} &= \alpha_b(t) = \frac{1}{2}\left(1+u_{stb}(t)\right) = \frac{1}{2}\left(1+u_{st}\cdot\cos(\zeta-120^0)\right) = \frac{1}{2}\left(1+u_{st}\cdot\cos(\omega_s t-120^0)\right)\\
\bar{d}_{cu} &= \alpha_c(t) = \frac{1}{2}\left(1+u_{stc}(t)\right) = \frac{1}{2}\left(1+u_{st}\cdot\cos(\zeta-240^0)\right) = \frac{1}{2}\left(1+u_{st}\cdot\cos(\omega_s t-240^0)\right)
\end{aligned} \tag{3.26}$$

$$U_{a0}(t) = U_{dc}(t)\cdot\alpha_a(t) \quad U_{b0}(t) = U_{dc}(t)\cdot\alpha_b(t) \quad U_{c0}(t) = U_{dc}(t)\cdot\alpha_c(t)$$

One then obtains.

$$\begin{aligned}
U_a(t) &= \frac{U_{dc}(t)}{2}\cdot u_{st}\cdot\cos(\zeta) \qquad U_b(t) = \frac{U_{dc}(t)}{2}\cdot u_{st}\cdot\cos(\zeta-120^0)\\
U_c(t) &= \frac{U_{dc}(t)}{2}\cdot u_{st}\cdot\cos(\zeta-240^0)
\end{aligned} \tag{3.27}$$

Where the voltage space vector reference is given as:

$$U_{ref} = u_{st}\cdot\cos(\zeta) \tag{3.28}$$

The inverter is then modelled as a vector $\underline{U_{st}}$ containing the modulated voltage space vector reference for all three phases (see equation (3.29) for signals including 3rd harmonic injection), multiplied with $\frac{U_{dc}(t)}{2}$ and including a time delay. The time delay of the inverter, due to switching, is set to be half the periodic time $T_v = \frac{1}{2*f_{sw}}$.

3.3 DC-link

In order to achieve satisfactory redundancy on the equipment, the dc-link is split in two. In this way, each of the two 3-phase inverter has its own dc supply, and can be powered from separate sources. This is shown in Figure 3.3.

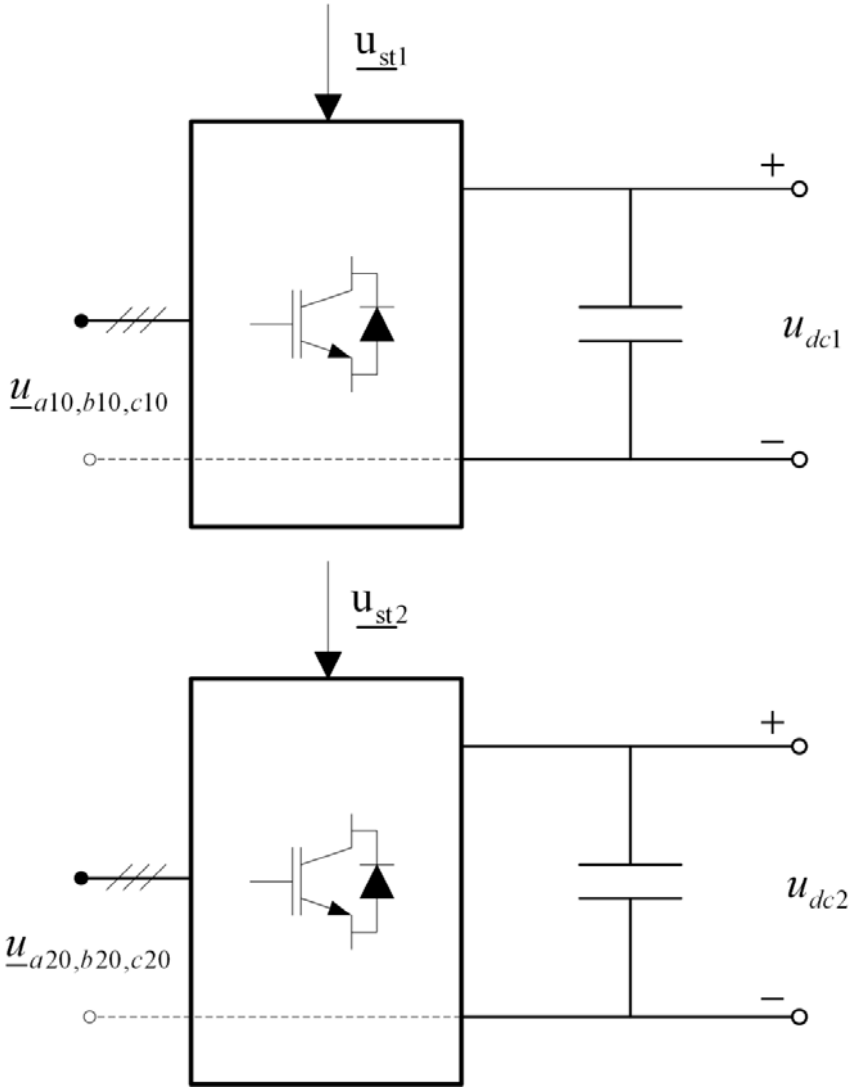

Figure 3.3: Two three-phase 2-level inverters with separate dc-links [13]

In order for the motor to fully take advantage of the split dc-link, it must be able to continue operating even after a fault causes one of the dc-link voltages to drop. To successfully test the operation of the model in a situation with low dc-link voltage, it is necessary to implement a system in which the operation of the dc-link can be simulated. In a situation with a sufficiently low dc-link voltage the control system will force the machine into generator mode for that particular three phase system. In order to take this into consideration in the analogue model, the dc-link needs to be able to receive energy from the converter and change the dc-link voltage accordingly. The system was therefore constructed as a stiff grid supplying a capacitor through a resistor. See Figure 3.4. This system will be implemented for the simulations regarding the low dc-link voltage, see chapter 5.4.

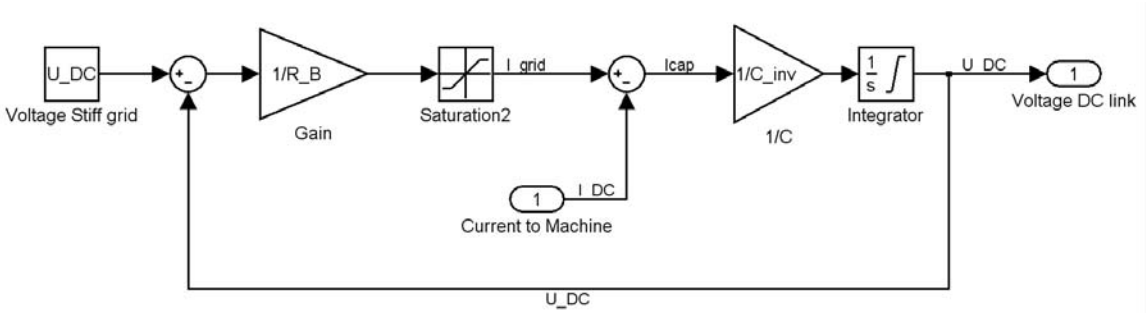

Figure 3.4: Dc-link

3.4 PWM Modulator

The control voltages u_{sta}, u_{stb} and u_{stc} for a 3-phase PWM modulator with 3rd harmonic injection are generated as follows:

$$\begin{aligned} u_{sta}(t) &= u_{st} \cdot \left[\cos(\zeta(t)) - \frac{1}{6} \cdot \cos(3 \cdot \zeta(t)) \right] \\ u_{stb}(t) &= u_{st} \cdot \left[\cos(\zeta(t) - 120^0) - \frac{1}{6} \cdot \cos(3 \cdot \zeta(t)) \right] \\ u_{stc}(t) &= u_{st} \cdot \left[\cos(\zeta(t) - 240^0) - \frac{1}{6} \cdot \cos(3 \cdot \zeta(t)) \right] \end{aligned} \tag{3.29}$$

The control signals for a six phase machine then becomes:

$$\begin{aligned} u_{sta1}(t) &= u_{st1} \cdot \left[\cos(\zeta_1(t)) - \frac{1}{6} \cdot \cos(3 \cdot \zeta_1(t)) \right] \\ u_{stb1}(t) &= u_{st1} \cdot \left[\cos(\zeta_1(t) - 120^0) - \frac{1}{6} \cdot \cos(3 \cdot \zeta_1(t)) \right] \\ u_{stc1}(t) &= u_{st1} \cdot \left[\cos(\zeta_1(t) - 240^0) - \frac{1}{6} \cdot \cos(3 \cdot \zeta_1(t)) \right] \\ u_{sta2}(t) &= u_{st2} \cdot \left[\cos(\zeta_2(t) - 30^0) - \frac{1}{6} \cdot \cos(3 \cdot (\zeta_2(t) - 30^0)) \right] \\ u_{stb2}(t) &= u_{st2} \cdot \left[\cos(\zeta_2(t) - 150^0) - \frac{1}{6} \cdot \cos(3 \cdot \zeta_2(\zeta(t) - 30^0)) \right] \\ u_{stc2}(t) &= u_{st2} \cdot \left[\cos(\zeta_2(t) - 270^0) - \frac{1}{6} \cdot \cos(3 \cdot (\zeta_2(t) - 30^0)) \right] \end{aligned} \tag{3.30}$$

This method introduces a 3rd harmonic to all phase voltages, while the line voltages remains the same, because the same 3rd harmonic is introduced in all six phases. By introducing 3rd harmonic injection, the upper limit for linear relations between u_{st} and the 1 Harmonic component of the phase voltage is increased from 1.0 pu for sinusoidal PWM to $\frac{2}{\sqrt{3}}$ pu for sinusoidal PWM with 3rd harmonic injection.

Using over-modulation it is possible to obtain higher voltages, but this causes a non-sinusoidal output and will not be considered in this report. In the simulations u_{st} will be limited to its linear range.

4 Control of six-phase IPMSM

In this chapter the control structure DSFC, presented in [1], will be explained before thoroughly going through the new control structure proposed in this report. The discussions in this chapter will be limited to the 1st harmonic component.

4.1 Double synchronous frame current control

The control philosophy cited in the following section is based on [14] and the work carried out by Roy Nilsen in [13]. For further details on this control strategy see [1].

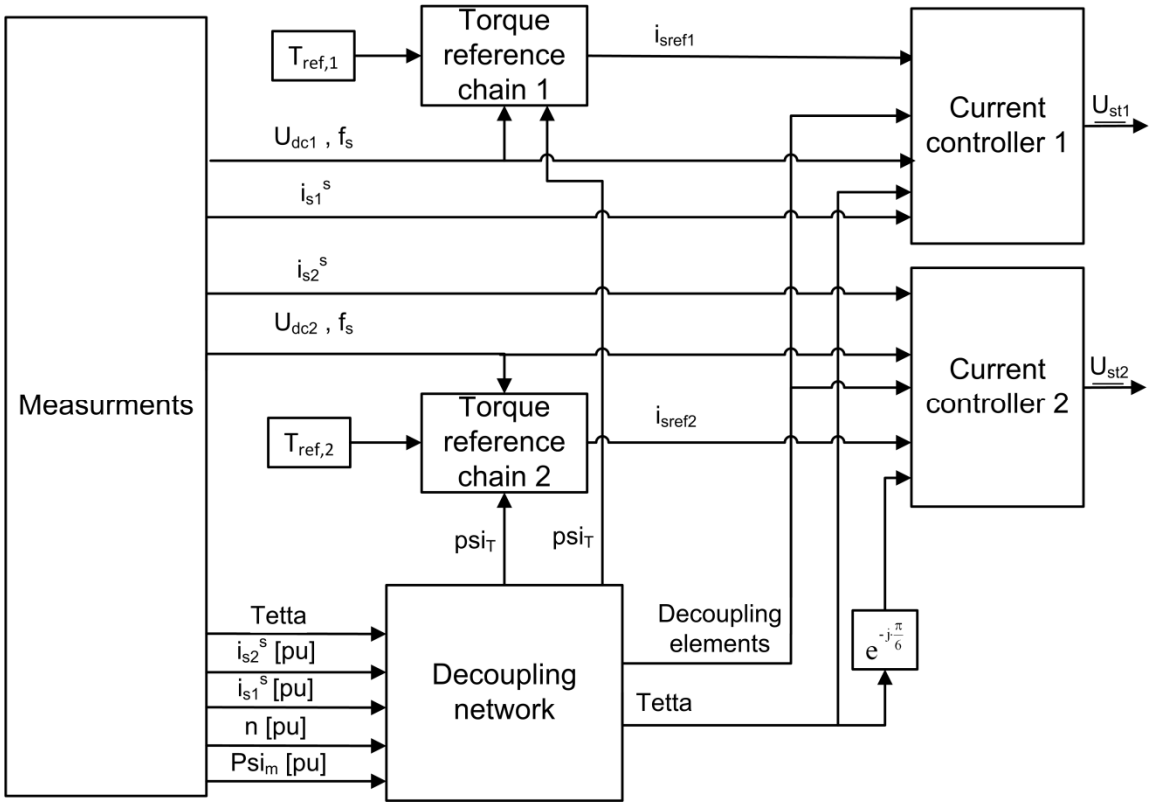

Figure 4.1: Double synchronous frame current control for six-phase dual winding machine [1].

The motor is controlled by applying two separate torque references, one for each inverter. These references pass through separate torque reference chains which is identical to the ones featured in the new control system, except for the current transformation block. There is also a decoupling network in place, responsible for providing the coupled elements in the dq subsystem, given from equation (4.1).

The control strategy utilizes two current controllers, both operating in the (d,q) subsystem and controlling one inverter each. The goal of the control philosophy is to be able to use controller 1 to control i_{d1}, i_{q1} and controller 2 to control i_{d2}, i_{q2} separately by using u_{d1}, u_{q1} and u_{d2}, u_{q2} respectively. The relation between the governing voltages and the measured currents can be seen in equation (4.1).

$$2\cdot u_d = u_{d1} + u_{d2} = r_s\cdot i_{d1} + \frac{x_d}{\omega_n}\cdot\frac{di_{d1}}{dt} - n\cdot x_q\cdot\ i_{q1} + \ r_s\cdot i_{d2} + \frac{x_d}{\omega_n}\cdot\frac{di_{d2}}{dt} - n\cdot x_q\cdot\ i_{q2}$$
$$2\cdot u_q = u_{q1} + u_{q2} = r_s\cdot i_{q1} + \frac{x_q}{\omega_n}\cdot\frac{di_{q1}}{dt} + n\cdot x_d\cdot\ i_{d1} + n\cdot\psi_m + r_s\cdot i_{q2} + \frac{x_q}{\omega_n}\cdot\frac{di_{q2}}{dt} + n\cdot x_d\cdot\ i_{d2} + n\cdot\psi_m$$

(4.1)

As can be seen from this equation the d and q axis are coupled. This is however not a significant problem, as decouple elements can be made and used in a forward connection in order to cancel out the effect of the coupled elements. The governing equation can then be written as follows.

$$\begin{aligned} 2\cdot u_d &= u_{d1} + u_{d2} = r_s\cdot i_{d1} + \frac{x_d}{\omega_n}\cdot\frac{di_{d1}}{dt} + \ r_s\cdot i_{d2} + \frac{x_d}{\omega_n}\cdot\frac{di_{d2}}{dt} \\ 2\cdot u_q &= u_{q1} + u_{q2} = r_s\cdot i_{q1} + \frac{x_q}{\omega_n}\cdot\frac{di_{q1}}{dt} + r_s\cdot i_{q2} + \frac{x_q}{\omega_n}\cdot\frac{di_{q2}}{dt} \end{aligned} \qquad (4.2)$$

However, there exists a more severe problem with this control structure. By studying equation (4.2) it can be seen that an attempt to control i_{q1} with u_{q1} inevitably will affect i_{q2} as well. This in turn invokes the controller responsible for regulating i_{q2} which will counter the effect of the first controller, thus leading to dangerous oscillations in the system. These oscillations could contain high frequency components as the derivatives of the currents are included, with $\frac{x_d}{\omega_n} \ll r_s$. These oscillations where observed in [1] and is given in Figure 4.2.

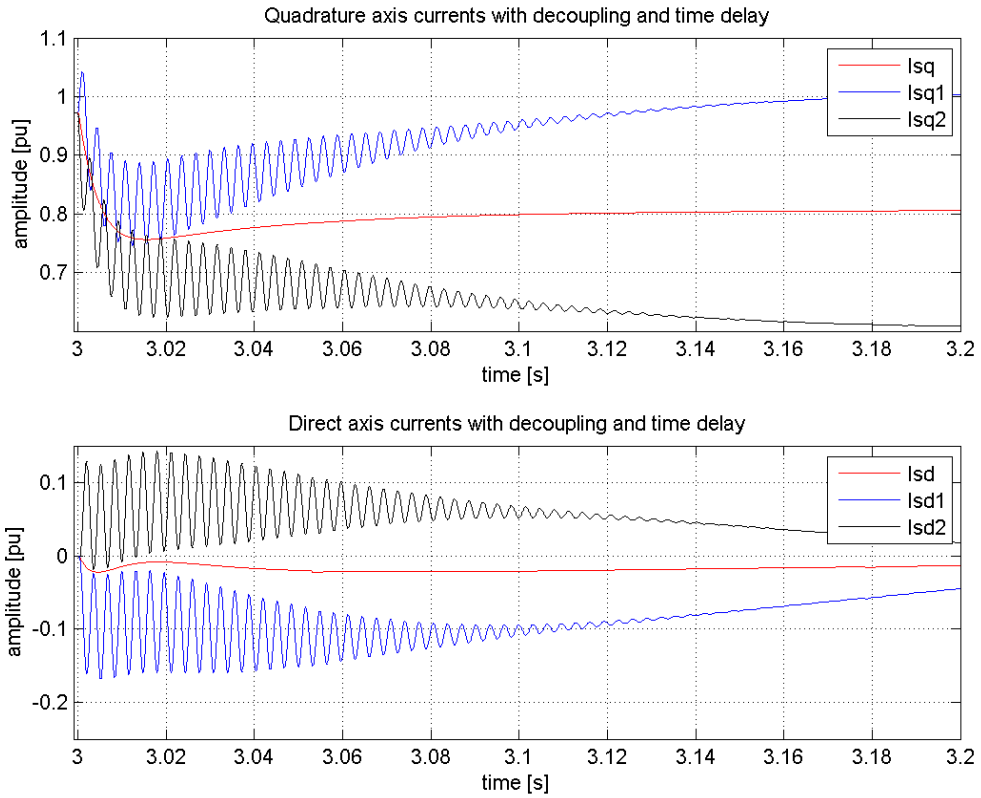

Figure 4.2: Close up of transient direct and quadrature axis current response to negative step in torque reference 2, using DSFC, with decoupling and time delay enabled [1].

The reason for these oscillations could be explained by taking into account the fact that in this control structure two regulators are trying to control one half each of the total (d,q) subsystem. Considering the Transformed Six- phase IPMSM Model given in equation (3.20), it is evident that only the whole voltages u_d and u_q from the total (d,q) system is controlling the motor. By splitting the control of this system into four voltages u_{d1}, u_{d2}, u_{q1}, u_{q2} and using two regulators, both in the (d,q) subsystem, to control one half each of the direct and quadrature axis currents, you create a potential for oscillations between the two regulators.

It must be stressed that these oscillations may only occur in situations requiring that the two inverters operate at different states, such as certain fault situations where their current reference or dc-link voltage differs.

4.2 New control structure

The control philosophy cited in the following section is made based on the idea of Roy Nilsen [2].

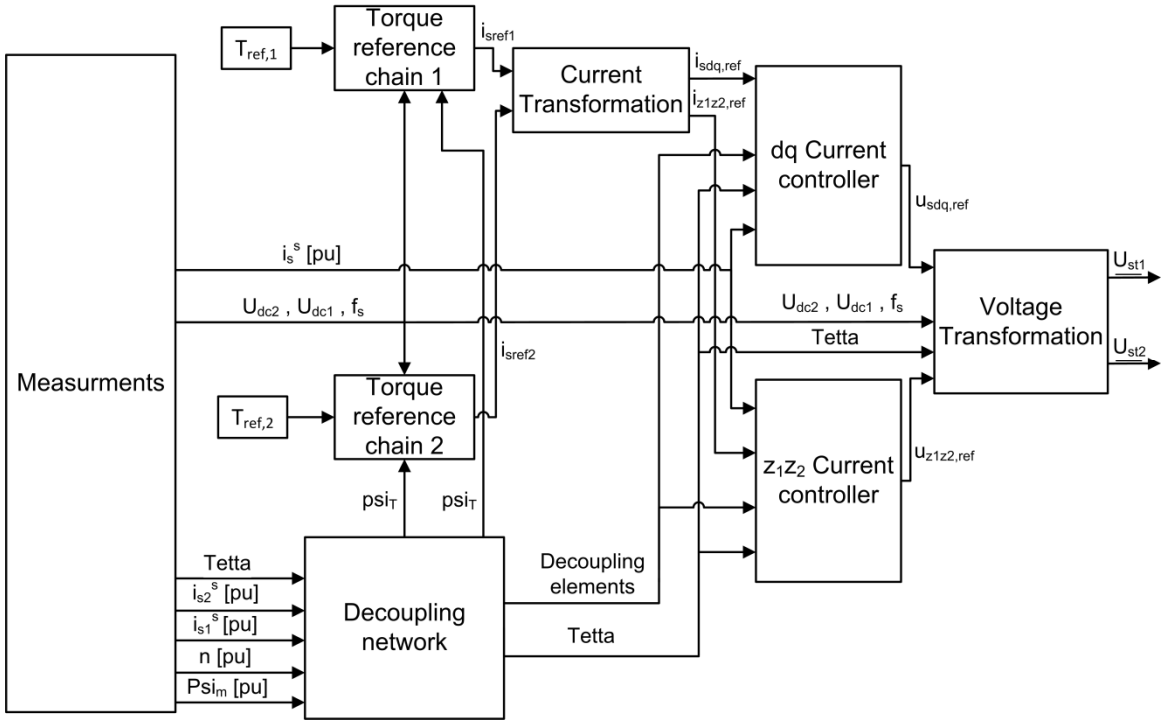

Figure 4.3: New control structure for six-phase dual winding machine.

4.2.1 Torque reference chain

The control of the six-phase IPMSM is carried out utilizing two analogue current controllers, each controlled by separate current reference signals. These signals are given through two separate torque reference chains consisting of a current calculator, a torque limiter and a current transformation block. The function of these components will be discussed in the following.

4.2.1.1. Torque limiter

The torque limiter gives torque reference limits to the current calculator in the event of over- and undervoltage on the dc-link, and in the case of overspeed in the rotor. If one of the dc-links drops below a certain threshold, the torque limiter will change the quadrature axis current of the corresponding three phase system into a negative value. This will force the three phase system into generator mode in order to pump up the dc-link voltage. It is important that the undervoltage regulators threshold voltage is not set to high, as this might affect the normal operations of the motor drive. However, if it is set to low, it will allow for a too low dc-link voltage without changing the reference value. In the simulations performed in chapter 5 the threshold limit is set to 650 V. The torque limiter is implemented in order to secure safe operating conditions for the system as a whole.

4.2.1.2. Current calculator

In order to obtain the correct stator current references, for the current transformation block, two current calculators were applied. The current calculators applied in this control scheme employ the torque reference signal from the torque limiter and the torque creating flux from the decoupling element, see chapter 4.2.4. By dividing the torque reference with the given flux you obtain the reference signal for i_{sq}. The reference signal for i_{sd} is naturally zero since this is a permanent magnet motor and we disregard situations requiring field weakening.

When supplying the control currents reference signal, it is important that this reference does not make the inverters supply a current that is beyond the safe operating conditions of the system. For this purpose limitations are added to the reference signal. These limitations come from the torque limiter or from an internal process in the current calculator, depending on who has the strictest limitations. This last method is based on the assumption that we know the maximum stator current allowed in the motor. It is then possible to use the following relation to find the maximum allowable q-axis current

$$i_{sq,ref,max} = \sqrt{\left(i_{s,max}\right)^2 - \left(i_{sd,ref}\right)^2} \tag{4.3}$$

4.2.1.3. Current transformation

The Current transformation block is used to transform the reference signal from the Current calculators into reference signals for the dq and z_1z_2 current controllers. This is achieved by using the relation between i_{q1}, i_{d1}, i_{q2}, i_{d2} and i_q, i_d, i_{z1}, i_{z2} given by equation (4.4)

$$\begin{aligned} i_{d,ref} &= \frac{i_{d1,ref} + i_{d2,ref}}{2} & \qquad i_{z_1,ref} &= \frac{i_{d1,ref} - i_{d2,ref}}{2} \\ i_{q,ref} &= \frac{i_{q1,ref} + i_{q2,ref}}{2} & \qquad i_{z_2,ref} &= \frac{-i_{q1,ref} + i_{q2,ref}}{2} \end{aligned} \tag{4.4}$$

4.2.2 Current controllers

In order to control the two three-phase inverters, two current controllers are used. These will be used to control the (d,q) and (z_1,z_2) subsystems and will be referred to as dq controller and z_1z_2 controller. The current controllers consist of two disconnected PI-regulators operated in parallel, each controlling one of the axes of the given subsystem. This is shown for the z_1z_2 controller in Figure 4.4 .

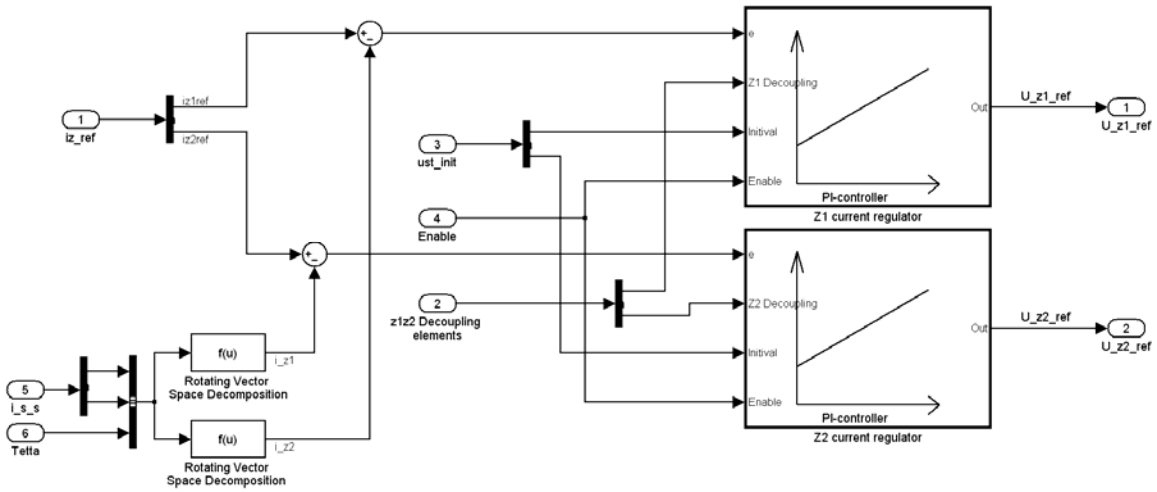

Figure 4.4: z_1z_2 Current controller layout

4.2.2.1. Control strategy

The goal of the new control philosophy is to control i_{d1}, i_{q1}, i_{d2} and i_{q2} by using the voltages u_d, u_q, u_{z1} and u_{z2}. This is obtained through letting the dq current controller control i_d, i_q and the z_1z_2 current controller control i_{z1}, i_{z2}. The currents are controlled by using u_d, u_q and u_{z1}, u_{z2} respectively. The relation between the governing voltages and the corresponding currents can be seen in equation (4.5).

$$\begin{aligned} u_d &= r_s \cdot i_d + \frac{x_d}{\omega_n} \cdot \frac{di_d}{dt} - n \cdot x_q \cdot i_q & u_{z_1} &= r_s \cdot i_{z_1} + \frac{x_{s\sigma}}{\omega_n} \cdot \frac{di_{z_1}}{dt} + n \cdot x_{s\sigma} \cdot i_{z_2} \\ u_q &= r_s \cdot i_q + \frac{x_q}{\omega_n} \cdot \frac{di_q}{dt} + n \cdot x_d \cdot i_d + n \cdot \psi_m & u_{z_2} &= r_s \cdot i_{z_2} + \frac{x_{s\sigma}}{\omega_n} \cdot \frac{di_{z_2}}{dt} - n \cdot x_{s\sigma} \cdot i_{z_1} \end{aligned} \tag{4.5}$$

As can be seen from equation (4.5), the two subsystems both have internal coupled equations. In order to control each axis of the two subsystems separately it is necessary to remove this disturbance. A forward connection from the decoupling network is therefore utilized, cancelling out the effect of the decoupling elements. The correlation between the controlling voltages and the given currents then become.

$$\begin{aligned} u_d &= r_s \cdot i_d + \frac{x_d}{\omega_n} \cdot \frac{di_d}{dt} & u_{z_1} &= r_s \cdot i_{z_1} + \frac{x_{s\sigma}}{\omega_n} \cdot \frac{di_{z_1}}{dt} \\ u_q &= r_s \cdot i_q + \frac{x_q}{\omega_n} \cdot \frac{di_q}{dt} & u_{z_2} &= r_s \cdot i_{z_2} + \frac{x_{s\sigma}}{\omega_n} \cdot \frac{di_{z_2}}{dt} \end{aligned} \tag{4.6}$$

Where the decoupling elements are given as:

$$\begin{aligned} u_{d,c} &= -n \cdot x_q \cdot i_q & u_{z_1,c} &= n \cdot x_{s\sigma} \cdot i_{z_2} \\ u_{q,c} &= n \cdot x_d \cdot i_d + n \cdot \psi_m & u_{z_2,c} &= -n \cdot x_{s\sigma} \cdot i_{z_1} \end{aligned} \tag{4.7}$$

Considering equation(4.6), it is clear that a properly tuned PI regulator should have no problem controlling any of the four currents by means of the four available voltages.

The correlation between the controlled currents i_d, i_q, i_{z1}, i_{z2} and the four currents controlling the two converters are given by the following equation.

$$\begin{aligned} i_d &= \frac{i_{d1} + i_{d2}}{2} & i_{z_1} &= \frac{i_{d1} - i_{d2}}{2} \\ i_q &= \frac{i_{q1} + i_{q2}}{2} & i_{z_2} &= \frac{-i_{q1} + i_{q2}}{2} \end{aligned} \tag{4.8}$$

These equations can be manipulated into:

$$\begin{aligned} i_{d1} &= i_d + i_{z_1} & i_{q1} &= i_q - i_{z_2} \\ i_{d2} &= i_d - i_{z_1} & i_{q2} &= i_q + i_{z_2} \end{aligned} \tag{4.9}$$

By combining equation (4.6) and (4.8) the governing equations can then be written as.

$$\begin{aligned} 2 \cdot u_d &= r_s \cdot i_{d1} + \frac{x_d}{\omega_n} \cdot \frac{di_{d1}}{dt} + r_s \cdot i_{d2} + \frac{x_d}{\omega_n} \cdot \frac{di_{d2}}{dt} & 2 \cdot u_{z_1} &= r_s \cdot i_{d1} + \frac{x_{s\sigma}}{\omega_n} \cdot \frac{di_{d1}}{dt} - r_s \cdot i_{d2} - \frac{x_{s\sigma}}{\omega_n} \cdot \frac{di_{d2}}{dt} \\ 2 \cdot u_q &= r_s \cdot i_{q1} + \frac{x_q}{\omega_n} \cdot \frac{di_{q1}}{dt} + r_s \cdot i_{q2} + \frac{x_q}{\omega_n} \cdot \frac{di_{q2}}{dt} & 2 \cdot u_{z_2} &= -r_s \cdot i_{q1} - \frac{x_{s\sigma}}{\omega_n} \cdot \frac{di_{q1}}{dt} + r_s \cdot i_{q2} + \frac{x_{s\sigma}}{\omega_n} \cdot \frac{di_{q2}}{dt} \end{aligned} \tag{4.10}$$

By examining equation (4.10) it is evident that the dq controller controls the sum of both controllers with respect to the direct and quadrature axis current. In other words, it is controlling the total amount of torque delivered to the machine, as well as the amount of magnetizing current.

The z_1z_2 controller on the other hand is controlling the balance of the direct and quadrature axis current from the two inverters. Thereby it is controlling the load sharing between the two inverters both in respect to torque and magnetizing current. In normal operation the z_1z_2 controller will make sure the inverters are equally loaded by regulating the excitation of the (z_1,z_2) subsystem to zero. In certain fault situations, requiring that the two inverters be run at different states, the z_1z_2 controller will make sure that the correct amount of excitation is applied to the (z_1,z_2) subsystem so that the two inverters can quickly reach and operate in their new respective state.

In the DSFC control structure, the two controllers both tried to control one half each of the total direct and quadrature current by dividing the controlling voltages and currents into two parts that where controlled directly. This philosophy had an inherent problem with direct and quadrature current oscillations, as trying to control one part of the quadrature current will inevitably affect the other part of the quadrature current. By instead using one controller to control the total amount of direct and quadrature current while the other controller regulates the allocation of these currents between the two inverters, the cur-

rents are completely controlled without the same risk of oscillations between the two controllers.

4.2.2.2. Dimensioning the PI regulators

The correlation between the controlling voltages and the corresponding currents are given by the following equation.

$$\begin{aligned} u_d &= r_s \cdot i_d + \frac{x_d}{\omega_n} \cdot \frac{di_d}{dt} \qquad & u_{z_1} &= r_s \cdot i_{z_1} + \frac{x_{s\sigma}}{\omega_n} \cdot \frac{di_{z_1}}{dt} \\ u_q &= r_s \cdot i_q + \frac{x_q}{\omega_n} \cdot \frac{di_q}{dt} \qquad & u_{z2} &= r_s \cdot i_{z_2} + \frac{x_{s\sigma}}{\omega_n} \cdot \frac{d\psi_{z_2}}{dt} \end{aligned} \tag{4.11}$$

By introducing PI-regulators, inverter models, serial gain inverse of the dc-link voltage and ignoring the time delay of the inverter, the open loop transfer functions for the dq and z_1z_2 current controller can be written as:

$$\begin{aligned} h_{oid} &= \frac{i_d}{i_{d1ref}} = K_{pd} \frac{1+T_{id} \cdot s}{T_{id} \cdot s} \cdot \frac{\omega_n \cdot T_d}{x_d \cdot (1+T_d \cdot s) \cdot (1+T_{sum} \cdot s)} \\ h_{oiq} &= \frac{i_q}{i_{q1ref}} = K_{pq} \frac{1+T_{iq} \cdot s}{T_{iq} \cdot s} \cdot \frac{\omega_n \cdot T_q}{x_q \cdot (1+T_q \cdot s) \cdot (1+T_{sum} \cdot s)} \end{aligned} \tag{4.12}$$

$$\begin{aligned} h_{oiz_1} &= \frac{i_{z_1}}{i_{z_1ref}} = K_{pz_1} \frac{1+T_{iz_1} \cdot s}{T_{iz_1} \cdot s} \cdot \frac{\omega_n \cdot T_{z_1}}{x_{s\sigma} \cdot (1+T_{z_1} \cdot s) \cdot (1+T_{sum} \cdot s)} \\ h_{oiz_2} &= \frac{i_{z_2}}{i_{z_2ref}} = K_{pz_2} \frac{1+T_{iz_2} \cdot s}{T_{iz_2} \cdot s} \cdot \frac{\omega_n \cdot T_{z_2}}{x_{s\sigma} \cdot (1+T_{z_2} \cdot s) \cdot (1+T_{sum} \cdot s)} \end{aligned} \tag{4.13}$$

In the implementation, the serial gain inverse of the dc-link voltage is added after the transformation back into u_{d1}, u_{q1}, u_{d2} and u_{q2} is accomplished.

The regulator parameters K_{pd}, K_{pq}, T_{id}, T_{iq} for the dq controller and K_{pz1}, K_{pz2}, T_{iz1}, T_{iz2} for the z_1z_2 controller are chosen as follows, based on the modulus optimum criterion.

$$\begin{aligned} K_{pd} &= \frac{x_d}{2 \cdot \omega_n \cdot T_{sum}} = \frac{x_d}{2 \cdot \omega_n \cdot (T_v)} = 0.6795 & K_{pz_1} &= \frac{x_{s\sigma}}{2 \cdot \omega_n \cdot T_{sum}} = \frac{x_{s\sigma}}{2 \cdot \omega_n \cdot (T_v)} = 0.1910 \\ K_{pd} &= \frac{x_q}{2 \cdot \omega_n \cdot T_{sum}} = \frac{x_q}{2 \cdot \omega_n \cdot (T_v)} = 0.6795 & K_{pz_2} &= \frac{x_{s\sigma}}{2 \cdot \omega_n \cdot T_{sum}} = \frac{x_{s\sigma}}{2 \cdot \omega_n \cdot (T_v)} = 0.1910 \\ T_{id} &= T_d = \frac{x_d}{\omega_n \cdot r_s} = 0.050 & T_{iz_1} &= T_{z_1} = \frac{x_{s\sigma}}{\omega_n \cdot r_s} = 0.014 \\ T_{iq} &= T_q = \frac{x_q}{\omega_n \cdot r_s} = 0.050 & T_{iz_2} &= T_{z_2} = \frac{x_{s\sigma}}{\omega_n \cdot r_s} = 0.014 \end{aligned} \tag{4.14}$$

In order to make the comparison with the simulation performed in [1] the regulator parameters used in the simulations are chosen to give corresponding values.

$$K_{pd} = \frac{x_d}{9 \cdot \omega_n \cdot T_{sum}} = \frac{x_d}{9 \cdot \omega_n \cdot (T_v)} = 0.1510 \qquad K_{pz_1} = \frac{x_{s\sigma}}{9 \cdot \omega_n \cdot T_{sum}} = \frac{x_{s\sigma}}{9 \cdot \omega_n \cdot (T_v)} = 0.0424$$

$$K_{pd} = \frac{x_q}{9 \cdot \omega_n \cdot T_{sum}} = \frac{x_q}{9 \cdot \omega_n \cdot (T_v)} = 0.1510 \qquad K_{pz_2} = \frac{x_{s\sigma}}{9 \cdot \omega_n \cdot T_{sum}} = \frac{x_{s\sigma}}{9 \cdot \omega_n \cdot (T_v)} = 0.0424$$

$$T_{id} = T_d = \frac{x_d}{\omega_n \cdot r_s} = 0.050 \qquad T_{iz_1} = T_{z_1} = \frac{x_{s\sigma}}{\omega_n \cdot r_s} = 0.014$$

$$T_{iq} = T_q = \frac{x_q}{\omega_n \cdot r_s} = 0.050 \qquad T_{iz_2} = T_{z_2} = \frac{x_{s\sigma}}{\omega_n \cdot r_s} = 0.014$$

(4.15)

From the regulator parameters it is clear that the z_1z_2 controller needs to be at least three times faster than the dq controller. This imposes new demands on the realization of such a system as a fast regulator demands a high switching frequency. In some applications, such as medium voltage components, this switching frequency might be hard to obtain due to high switching losses.

The reason why the z_1z_2 controller needs to be so much faster than the dq controller is due to the different reactance in the two subsystems. While the (d,q) system reactance consists of the leakage and the mutual reactance, the reactance in the (z_1,z_2) system only consists of the leakage reactance. Since the mutual reactance is considerably larger than the leakage reactance, the total reactance of the (d,q) subsystem is much larger than the total reactance of the (z_1,z_2) subsystem.

The coil pitch should be considered as a method for increasing the leakage reactance and thereby reduce the speed in which the z_1z_2 controller needs to operate. In [15] the effect the coil pitch has on the leakage reactance has been studied. Here it was concluded that full pitch is required in order to maximize the leakage reactance. In traditional three-phase machines the coil pitch is commonly designed to be 5/6 to minimize the 5^{th} and 7^{th} time and space harmonics, and thereby the influence they have on the torque ripple. A six-phase machine does not have the same restrictions on the coil pitch as it has no space harmonic below the 11^{th} harmonic, and therefore the lower order circulating stator time harmonics does not contribute to the generated torque ripple. This leads us to the conclusion that full pitch should be chosen in order to increase the leakage reactance and thereby decrease the necessary switching frequency. An increased leakage reactance also reduces the amount of current in the (z_1,z_2) subspace, thereby reducing losses resulting from the excitation of the (z_1,z_2) subsystem. See equation (3.20).

Another solution could be to place external inductances in series with the motor in order to increase the leakage reactance. This method is however not preferable as it also increases the stator reactance.

The control scheme for one of the PI-regulators is represented in Figure 4.5.

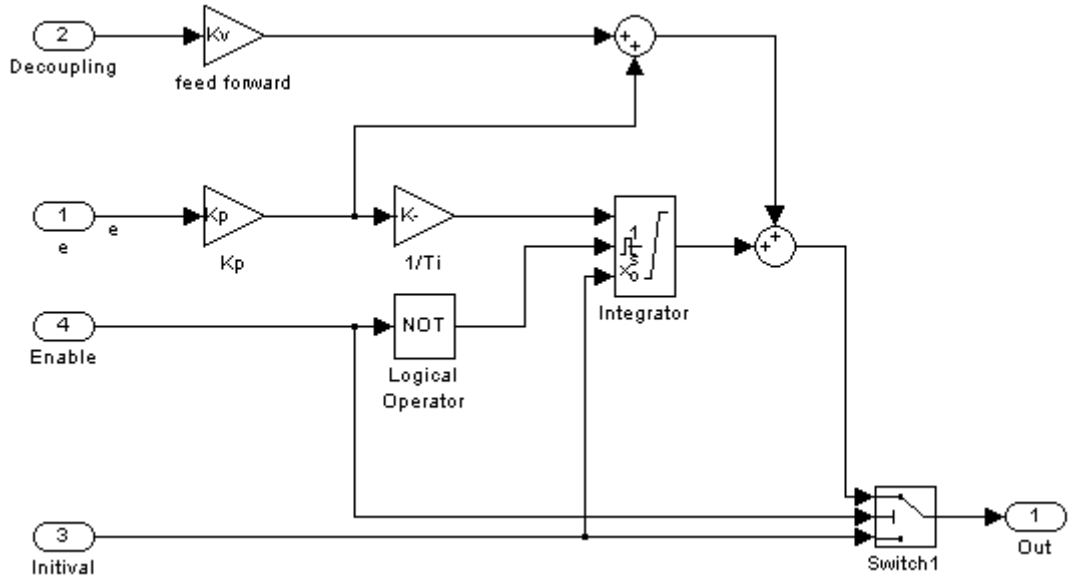

Figure 4.5: PI-regulator layout

4.2.3 Voltage transformation

The voltage transformation block is used to convert the voltages from the dq and z_1z_2 controller into the voltages u_{d1}, u_{d2}, u_{q1} and u_{q2}. This is accomplished by using the equations found in chapter 2.6. These voltages can then be used to find the control voltages u_{st1} and u_{st2} used by the PWM modulator to create the control signals for the inverter. It should be mentioned that the serial gain inverse of the dc-link voltage introduced in chapter 4.2.2.2 is implemented as a part of the voltage transformation block.

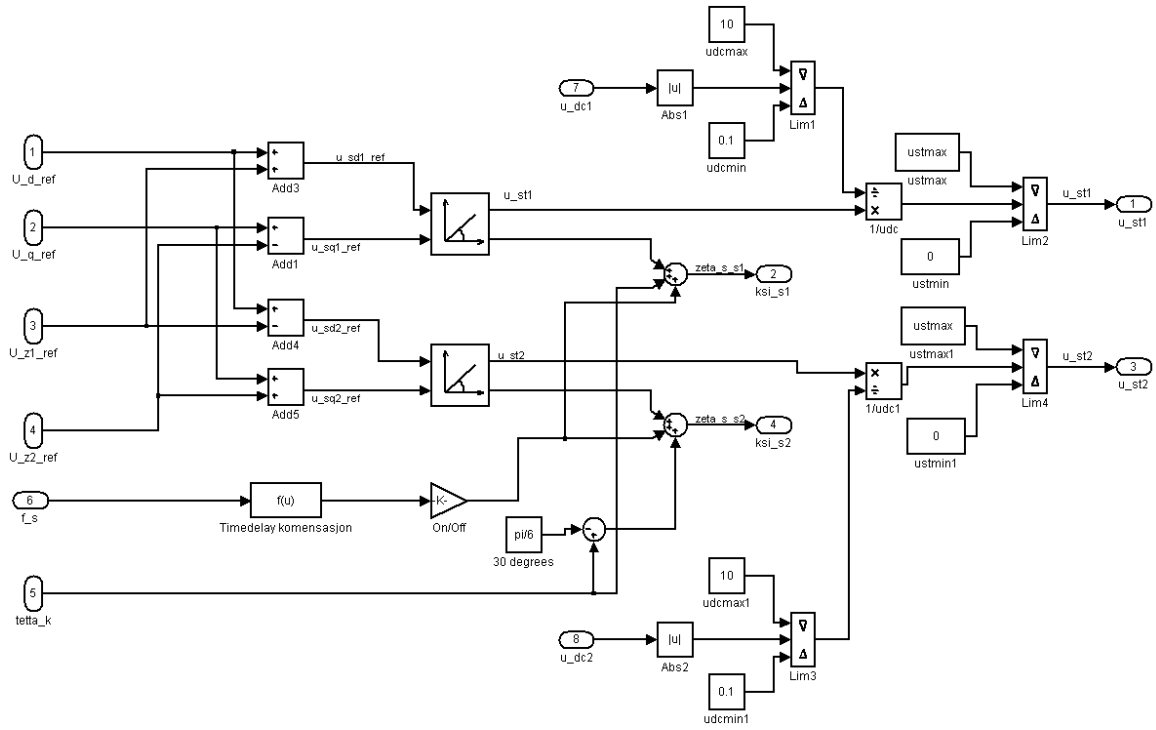

Figure 4.6: Voltage transformation block

As seen in Figure 4.6 the voltage transformation block also includes a time delay compensation unit. This method for vector control systems is used to compensate for voltage and current distortions resulting from a time delay in the overall system. The compensation is made possible by adding an angle $\Delta\zeta$ to $\zeta_1(t)$ in order to compensate for the angle travelled by the rotor and reference vector during the delay of the system [9]. If set correctly, this is an effective way of dealing with time delay induced distortions.

In these simulations the only time delay in the system comes from the introduced time delay in the inverters. The time delay compensation unit is therefore set to match this, unless otherwise specified. It should however be noted that it is difficult to make a perfect match between the compensating time delay and the actual time delay of the physical system. Simulations will therefore include situations where the time delay compensator is disabled, in order to investigate how the system responds to time delay.

4.2.4 Decoupling network

The decoupling network calculates the value of the decoupling elements, for both current controllers, as well as the torque flux used by the current calculator. It is vital that the decoupling elements are calculated correctly since the assumption of decoupling the axis in each subsystem depends on the accuracy in which the decoupling network is able to compensate the cross-coupled terms given in equation (4.5). An overview of the decoupling network can be found in appendix C.

As can be seen from equation (4.7), the decoupling elements in the (d,q) system contains the unregulated elements of the quadrature and direct axis currents. Any high frequency disturbance or oscillations in these currents will directly influence the reference voltage and may cause undesired effects or even instability. An option to be considered in the simulations is therefore to remove the current dependent part of the dq decoupling, thus making a modified decoupling consisting of merely induced voltage compensation. This approach will not decouple the direct and quadrature axis current, and the response of the (d,q) system will therefore be governed by equation (4.5), without the induced voltage elements. This configuration will become more relevant when including the effect of harmonics due to inverter switching.

4.3 Fault conditions

In order to take advantage of the increased reliability offered by the split dc-link, it is essential that the motor is able to continue operation after the occurrence of a fault related to one of the two inverters. The theoretical response of the control system to such faults will be discussed in the following.

4.3.1 Faults leading to different torque reference

Under normal conditions the currents i_{d1}, i_{q1}, i_{d2} and i_{q2} would be controlled by applying the same step in both torque references. This results in changing both $i_{q1,ref}$ and $i_{q2,ref}$ at the same time. According to equation (4.4) this does not change the reference value of the (z_1,z_2) subsystem currents. It does however change the reference value of the total quadrature axis current, making the corresponding PI regulator increase both i_{q1} and i_{q2} simultaneously by controlling the total quadrature axis voltage u_q, see equation (4.10). From this equation it is also possible to conclude that since both components of the total

quadrature current are changed simultaneously this will not affect the actual currents in the (z_1,z_2) subsystem.

However, for certain transient fault conditions the reference value of one current controller may change without the same change occurring in the other. This may be because of limitations added to the torque reference of one controller in order to protect the corresponding inverter of overload. With these limitations added, the quadrature reference current corresponding to that inverter, for example i_{q2}, will be lowered to meet the new requirements. In this situation the reference value of i_{z2} will change from zero to its new value, corresponding to the given difference in the two quadrature axis reference currents. See equation (4.4). The PI regulator responsible for the control of the z_2 axis current will change the voltage u_{z2} so that i_{z2} becomes equal to its new reference value. By doing so it also forces the two quadrature axis currents into obtaining the correct values for uneven load sharing between the two inverters. While the z_2 regulator changes the difference between the two quadrature currents, the quadrature axis regulator will make sure that the new reference value for the total quadrature current is kept. Considering equation (4.9) it is clear that as long as the dq controller and z_1z_2 controller are tuned to give the same response for their currents, the two quadrature axis currents can be controlled separately. The same can be shown for the direct axis currents. This theory will be tested in the analogue simulations in chapter 5.3.

4.3.2 Faults leading to drop in dc-link voltage

With the introduction of a split dc-link, certain faults such as trip of the circuit breaker at the grid side of one dc-link would give different voltage levels on the two dc-links. Because the dc-link voltage directly influences the inverters ability to output the desired phase voltages, it can also have a devastating effect on the current controller's ability to regulate the currents to their designated values. This connection is shown for one inverter in equation (3.27). Assuming the motor is operating below its rated capacity, this drop in dc-link voltage will be compensated for by the current controller's increase of the control voltage u_{st}. As long as the control voltage is in the linear region ($u_{st} \leq \frac{2}{\sqrt{3}}$) this will hold.

The problem arise the moment u_{st} reaches saturation. In this situation the controllers can no longer hold the corresponding currents to their reference values. This will happen for a given threshold voltage, depending on how much the motor is loaded, i.e. the initial value of u_{st} at the time the fault occurs. Given that u_{st2} reach saturation the output of inverter two will begin to drop as the dc-link voltage drops below the threshold voltage, see equation (3.27). This will cause both the direct and quadrature currents of inverter two to decline. If this drop occurs as a step in the dc-link voltage it will not only affect the currents of inverter two, but also cause the direct and quadrature currents of inverter one to respond. This can be seen in equation (4.10), where a negative step in i_{d2} and i_{q2} will cause i_{d1} and i_{q1} to increase, given that the regulators do not respond fast enough.

If the reference value $i_{q2,ref}$ is not changed, i.e. the torque limiter is disabled or tuned for a lower dc-link voltage, there will exist a permanent difference between the reference value and actual value of i_{q2}. This difference will cause the quadrature and z_2 axis PI regulators to increase their output voltage as this also gives a difference in i_q and i_{z2}. This can be seen in equation (4.16), repeated here for clarity.

$$\begin{aligned} i_d &= \frac{i_{d1} + i_{d2}}{2} & i_{z_1} &= \frac{i_{d1} - i_{d2}}{2} \\ i_q &= \frac{i_{q1} + i_{q2}}{2} & i_{z_2} &= \frac{-i_{q1} + i_{q2}}{2} \end{aligned} \tag{4.16}$$

The quadrature axis PI regulator will try to increase both i_{q1} and i_{q2} in order to bridge the gap between the reference value and real value of i_q. However, the z_2 axis PI regulator will also try to reach its reference value by increasing i_{q2} and decreasing i_{q1}. Since i_{q2} is limited because of the low dc-link voltage, the two regulators will counteract each other's influence on i_{q1}. This will last until one regulators integrator reaches saturation or until the dc-link voltage drops low enough to invoke the undervoltage regulator.

When the dc-link voltage is lowered beyond a certain threshold voltage, the Torque limiters undervoltage regulator will lower the quadrature axis current reference value corresponding to the faulty dc-link. With this change in reference value there will again be correspondence between the available output of the inverters and the output demanded by the reference values. This will eventually lead to u_{st2} going out of saturation, giving control of inverter two back to the current controllers. If necessary, the undervoltage regulator changes the quadrature axis current into a negative value, forcing the given three phase group into generator mode. This is done in order to pump up the dc-link voltage.

In order to improve the transient response of the control structure, new output limits have been introduced on each PI regulator so that they do not exceed the available output limits of the inverters [16]. The modified output boundaries coincide with the available output limits from the inverters and are given in the following equation.

$$u_{limit} = u_{st,max} \cdot \left(\frac{u_{dc1} + u_{dc2}}{2} \right) \tag{4.17}$$

Using the limit from equation (4.17), rather than simply $u_{st,max}$, ensures that each regulator do not demand a higher output from the inverters than what is available, even in situations with low dc-link voltage. In addition an anti windup scheme was connected to the new output limits to stop the integrator from winding up when the output is limited. See Figure D.1 in appendix D for the new PI regulator structure.

5 Matlab-Simulink simulations

5.1 Introduction

The simulations described in this section were carried out in order to test the transient performance of the new control structure during fault conditions. This performance will be compared with the performance of the DSFC [1]. Of particular interest is the effect of split dc-link during transient fault situations, the transient control of the the (z_1,z_2) subsystem, and the transient response of the phase currents.

Several simulations will be conducted, with focus on faults that will cause the inverters to supply different outputs. This includes simulations of faults leading to different torque reference to the current controllers and faults leading to drop in the dc-link voltage. The faults will be tested with different attributes of the control system enabled in order to analyze the effect of certain parts of the motor control. Particular attention will be given to the effect of decoupling and the effect of time delay in the control circuit. There will also be a control simulation corresponding to normal operation of the six-phase motor.

The continuous model allows for the study of the effect of faults in transient states without the harmonic disturbance from the inverter switches. All the simulations were tested with a step from steady state, except from the ones conducted in chapter 5.4 where both a start-up and a step from steady state were performed. The machine is loaded with a centrifugal load, modeled as the square of the angular velocity.

Simulations were run in continuous mode. Unless otherwise specified the dc-link voltage, supplying the inverters are set to a constant value of 1 kV. The outputs of the current controllers were limited to $\underline{u_{st}}$ linear range. In all figures, the corresponding reference signals are given in dashed lines.

The parameters used are given in appendix B, and are identical for the two control configurations, namely the DSFC and the DSPC introduced in this thesis.

The results of the simulations are presented in the following subsections.

5.2 Normal operation

In the following a negative step torque of 0.3 pu was applied to both inverters, starting from a torque reference of 0.9 pu. The simulation is what would be considered normal operation for a six-phase motor. It has been conducted in order to clarify the significance of certain control elements and for use as a reference in the following fault simulations. Corresponding simulations have been conducted with the DSFC structure in [1].

5.2.1 Perfect time delay compensation

The following simulations were conducted with the time delay compensator matching exactly the time delay introduced in the control structure. This idealized case is presented in order to show the control structures inherent response.

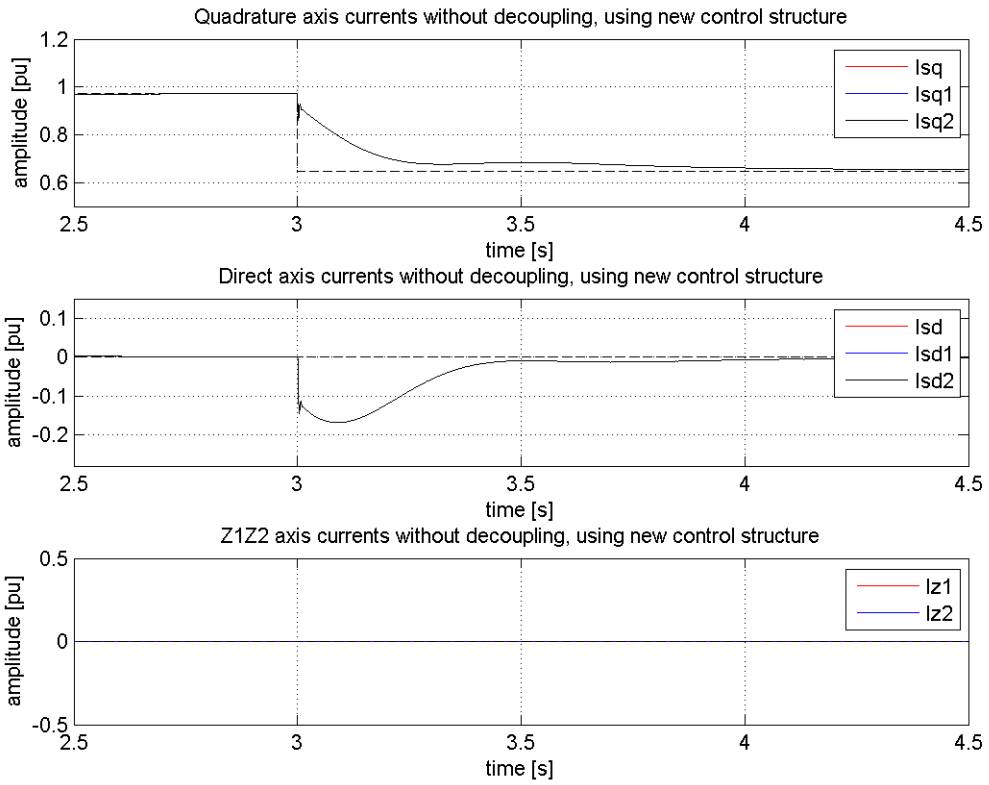

Figure 5.1: Transient current response to negative step in torque reference 1 and 2 with perfect time delay compensation, no decoupling, using new control structure.

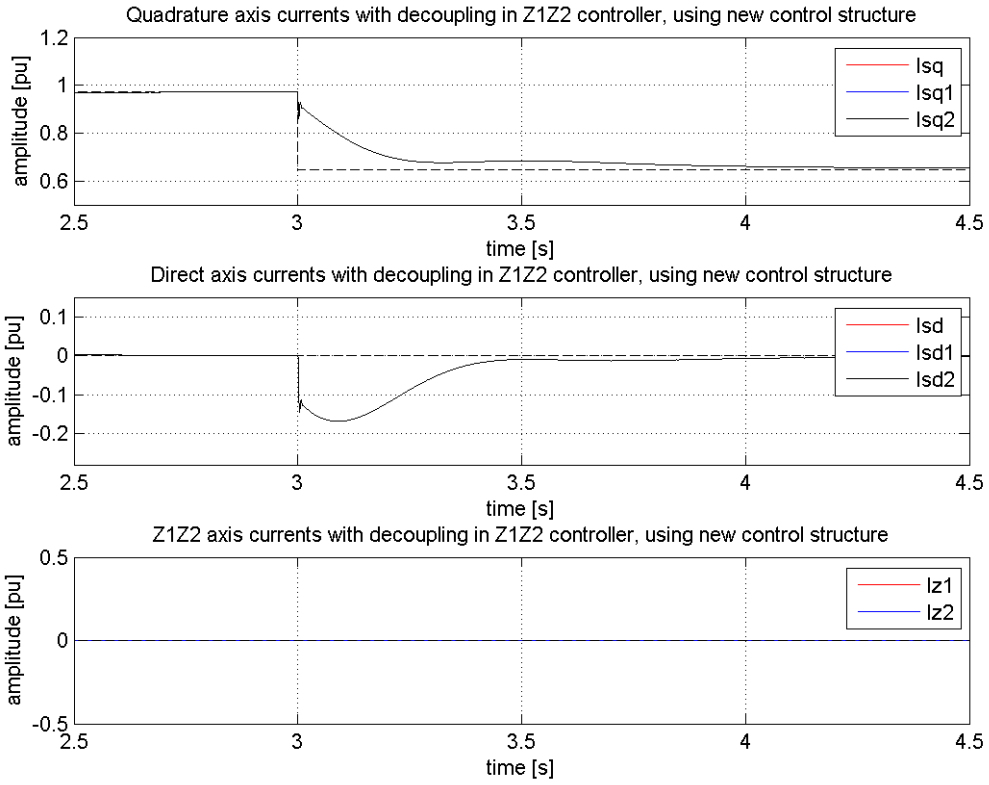

Figure 5.2: Transient current response to negative step in torque reference 1 and 2 with perfect time delay compensation, z_1z_2 decoupling, using new control structure.

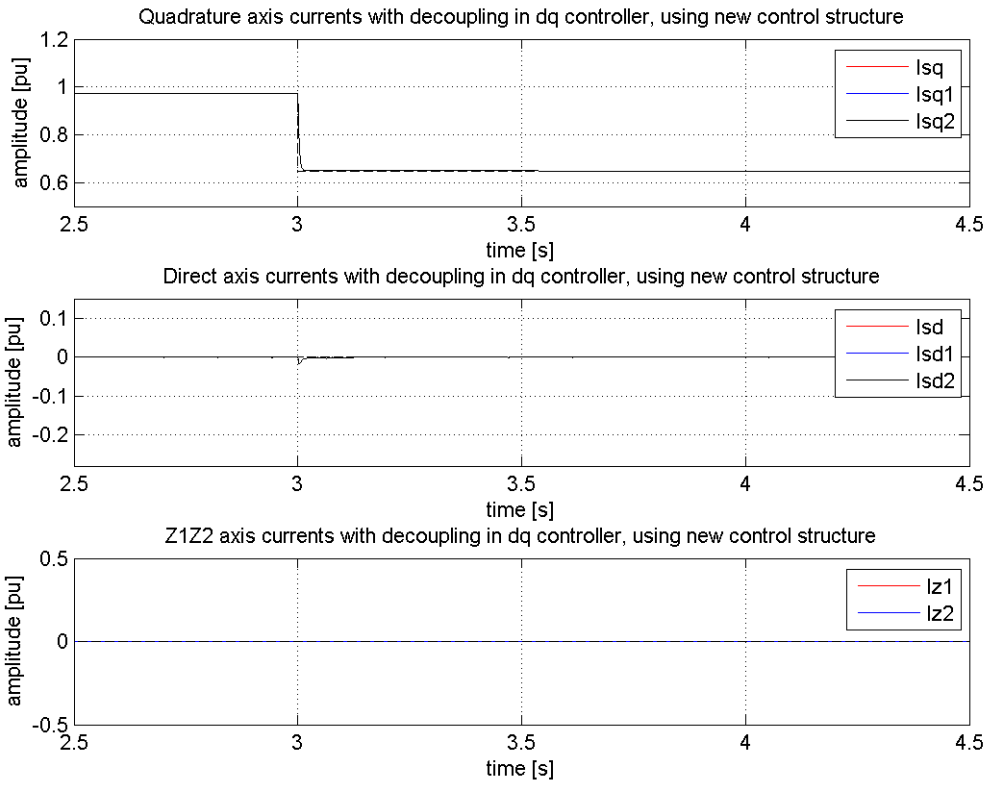

Figure 5.3: Transient current response to negative step in torque reference 1 and 2 with perfect time delay compensation, dq decoupling, using new control structure.

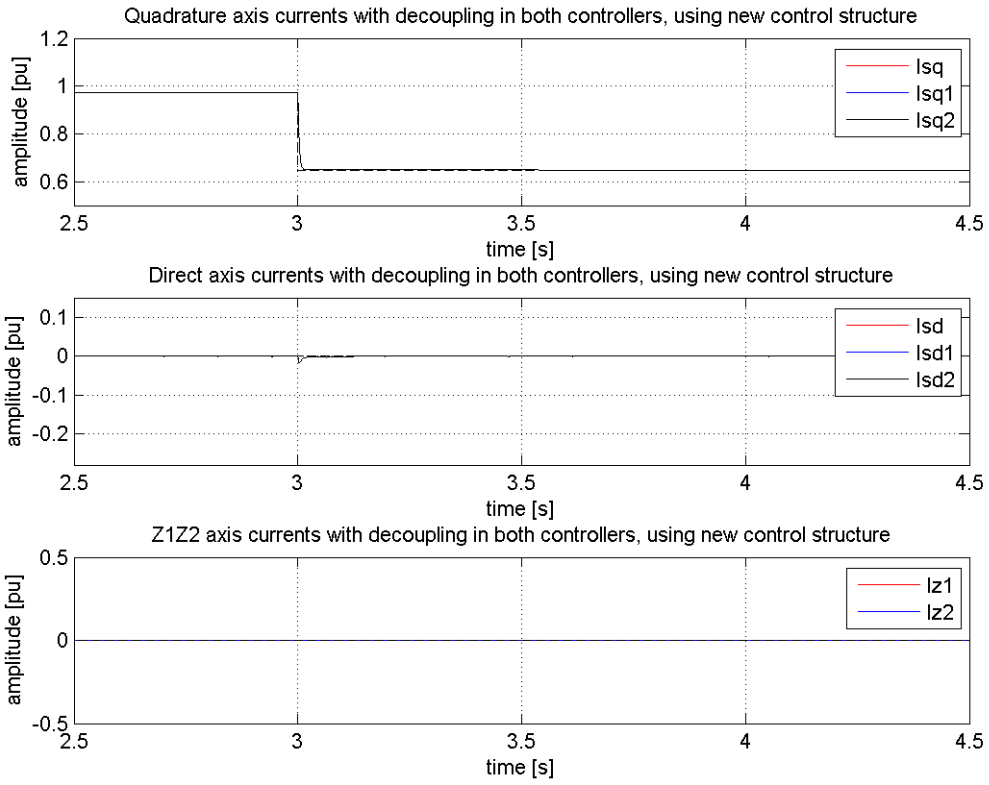

Figure 5.4: Transient current response to negative step in torque reference 1 and 2 with perfect time delay compensation, decoupling in both controllers, using new control structure.

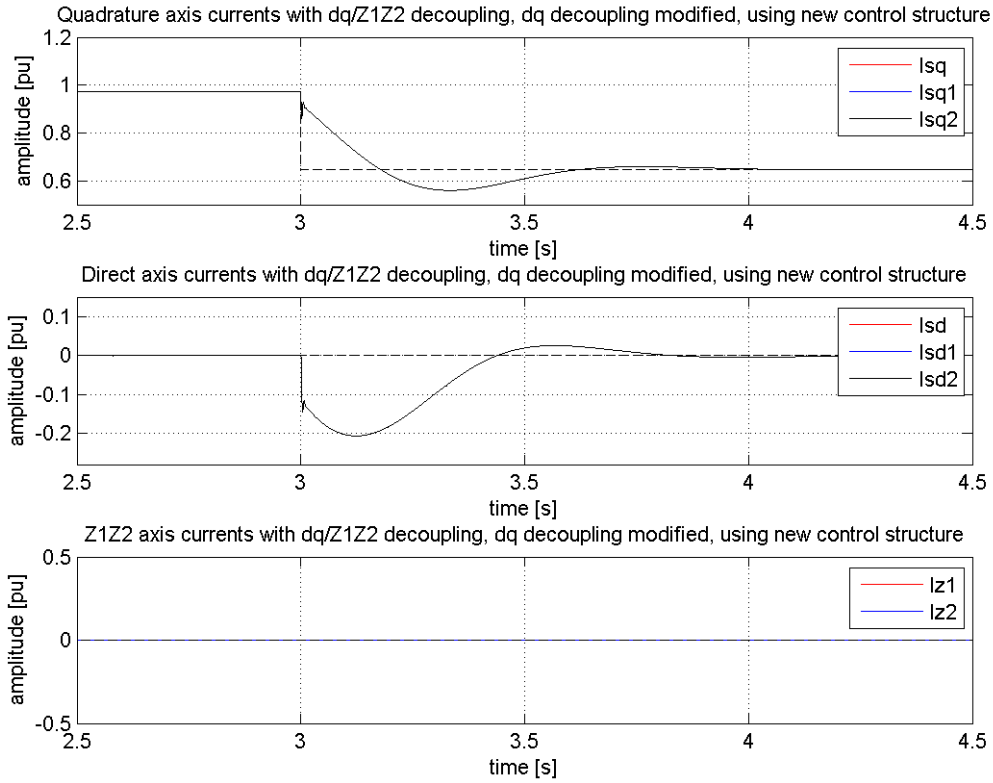

Figure 5.5: Transient current response to negative step in torque reference 1 and 2 with perfect time delay compensation, z_1z_2 decoupling and modified dq decoupling, using new control structure.

The quadrature and direct axis response, given in the figures above, show that the controller is able to reach its new steady state value after a given time. This is independent of the chosen decoupling scheme. The load is split evenly on the two inverters, even in transient state. This is confirmed by the fact that the current component from each converter follows the total current for both direct and quadrature axis.

The effect of the various decoupling elements can also be observed quite clearly. Including the z_1z_2 decoupling elements have no influence on the observed results. This is expected as the two inverters are given the same reference values and will behave identically in an analogue model. The z_1z_2 controller, and indeed the excitation of the entire (z_1,z_2) subsystem, is dependent on their being a difference in the two inverters direct and quadrature axis currents. This could also be seen in that the (z_1,z_2) subsystem is not excited.

Without the dq decoupling elements, the direct and quadrature axis have a distinct coupling that results in oscillations and contributes to the time it takes the controller to reach steady state, see equation (4.5). The modified decoupling element given in Figure 5.5 is, as expected, unable to remove this disturbance as it does not eliminate the current related coupling, see equation (4.7). In fact it increases the oscillations. The response of the current components of the quadrature and direct axis is considerably faster with the decoupling network enabled. The coupling between the quadrature axis and the direct axis have been close to eliminated, as the direct axis current is no longer significantly affected by the step in quadrature current, see Figure 5.3 and equation (4.6). By introducing this decoupling to the dq regulator it is able to control the two axes separately,

and efficiently regulate the total direct and quadrature currents to their new reference values. When the common dq decoupling elements is included the response is satisfactory.

For comparison, a plot of the results from the DSFC control structure with decoupling enabled in both controllers is given below [1]. This simulation is conducted with exactly the same premises as the simulations shown in Figure 5.1 to Figure 5.5. In order to compare the two structures, the (z_1,z_2) subsystem have been mapped using the Rotating Vector Space Decomposition so that the currents are represented as dc quantities.

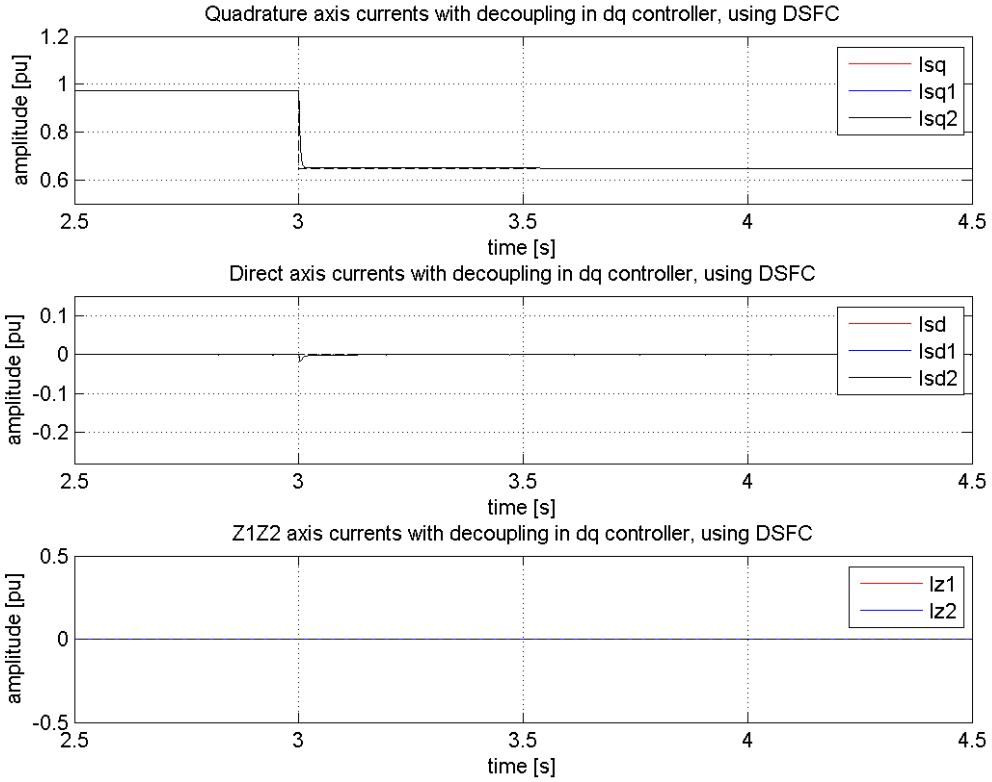

Figure 5.6: Transient current response to negative step in torque reference 1 and 2 with perfect time delay compensation, decoupling in both controllers, using DSFC [1].

Comparing Figure 5.4 with Figure 5.6 it is clear that the results are identical.

Although not presented in this report, all the corresponding results from the DSFC are identical to the results for normal operation from the new control structure. That is, the two control systems behave in a similar manner when there is no need for an excitation of the (z_1z_2) subsystem (i.e. the controlling currents for the two inverters are equal).

5.2.2 Excluding time delay compensation

The simulations performed in section 5.2.1 were repeated without perfect time delay compensation. This introduces a disturbance to the system that the control system

needs to cope with. The results given in this section are chosen because they represent the most important configurations and because they illustrate the effect of unsuccessful time delay compensation.

Although not included in this section, the results of the simulations with the DSFC control structure were exactly the same as the results from the new control structure presented below. This could be explained in the same manner as in the previous chapter, and the arguments will not be repeated here.

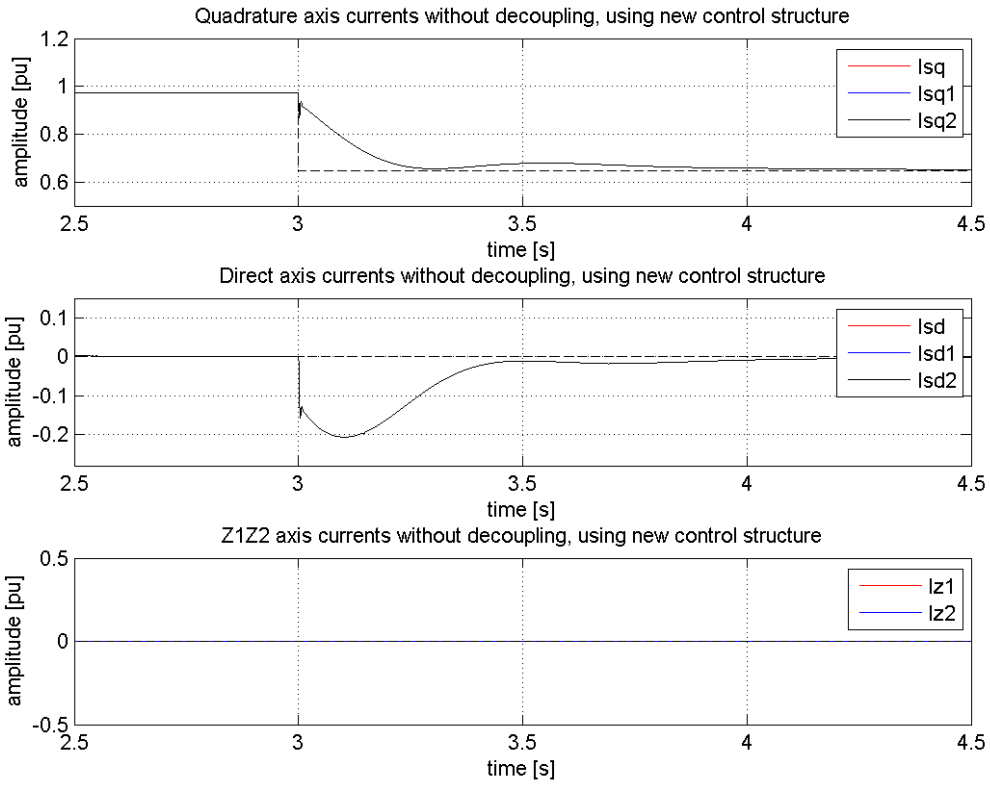

Figure 5.7: Transient current response to negative step in torque reference 1 and 2 without time delay compensation, no decoupling, using new control structure.

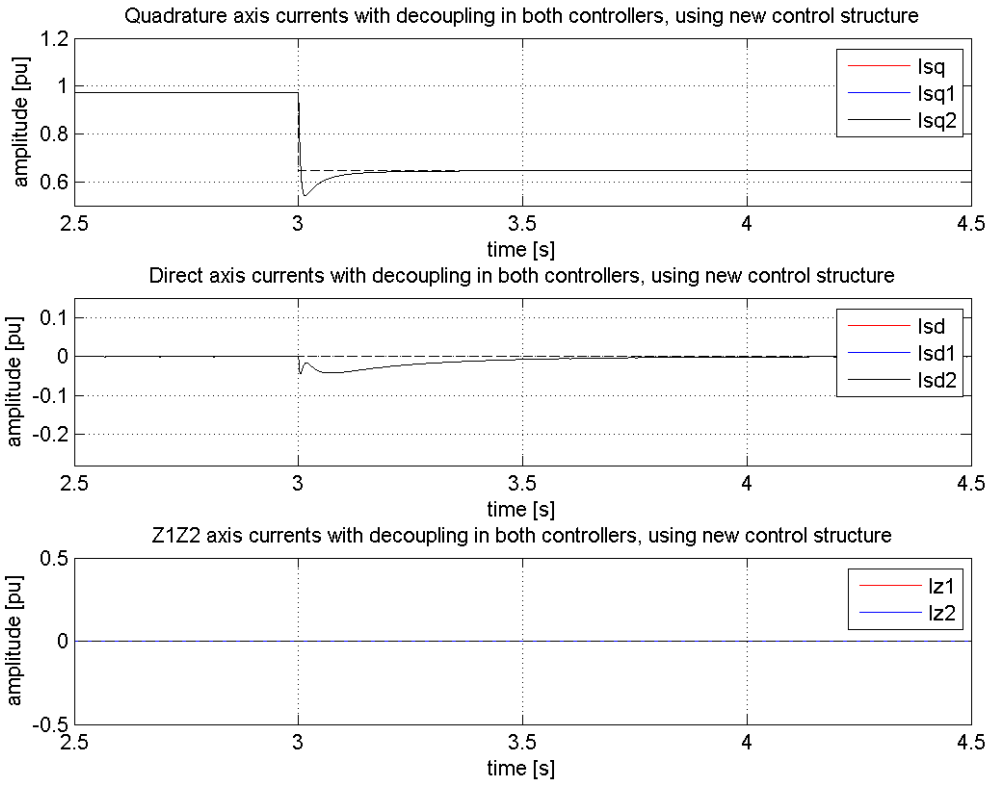

Figure 5.8: Transient current response to negative step in torque reference 1 and 2 without time delay compensation, including decoupling in both controllers, using new control structure.

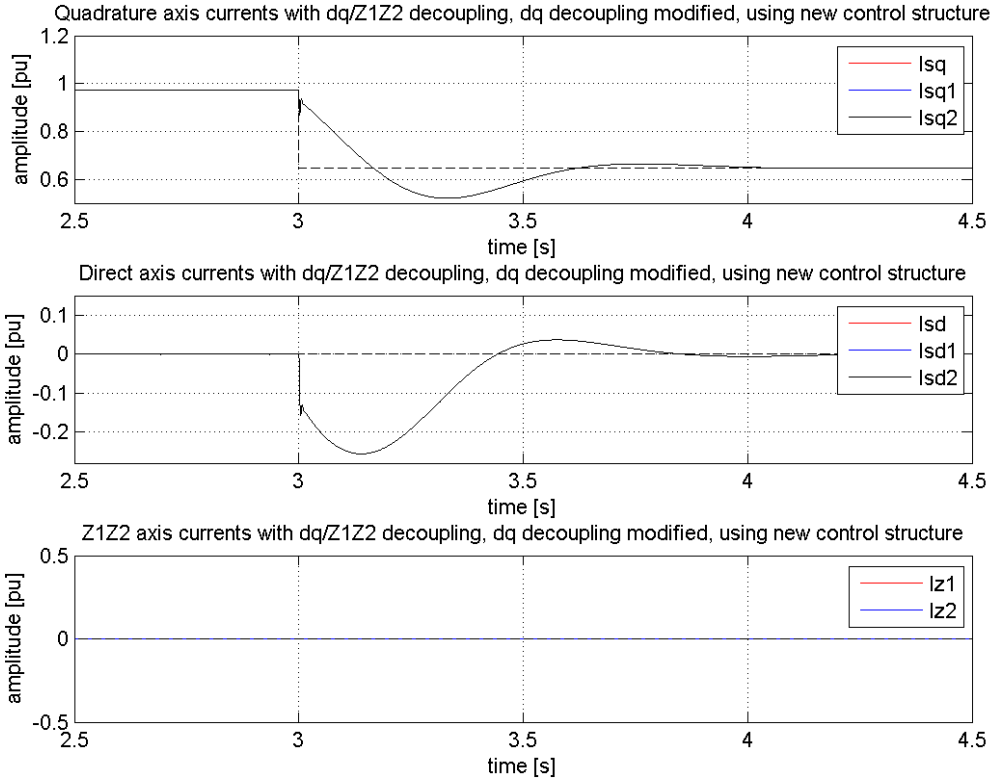

Figure 5.9: Transient current response to negative step in torque reference 1 and 2 without time delay compensation, including z_1z_2 decoupling and modified dq decoupling, using new control structure.

Comparing the results given in the above figures with the results from section 5.2.1, it is clear that the exclusion of the time delay compensation leads to increased direct and quadrature transient oscillations in all configurations. However, the control system is still capable of reaching its new steady state. In the case where both dq and z_1z_2 decoupling is enabled it gives a small deviation from the reference value, where previously the regulator managed to follow the reference with great precision. The flawed time delay compensator can be seen to have no effect on the division of power between the two inverters and consequently the excitation of the (z_1z_2) subsystem remains zero.

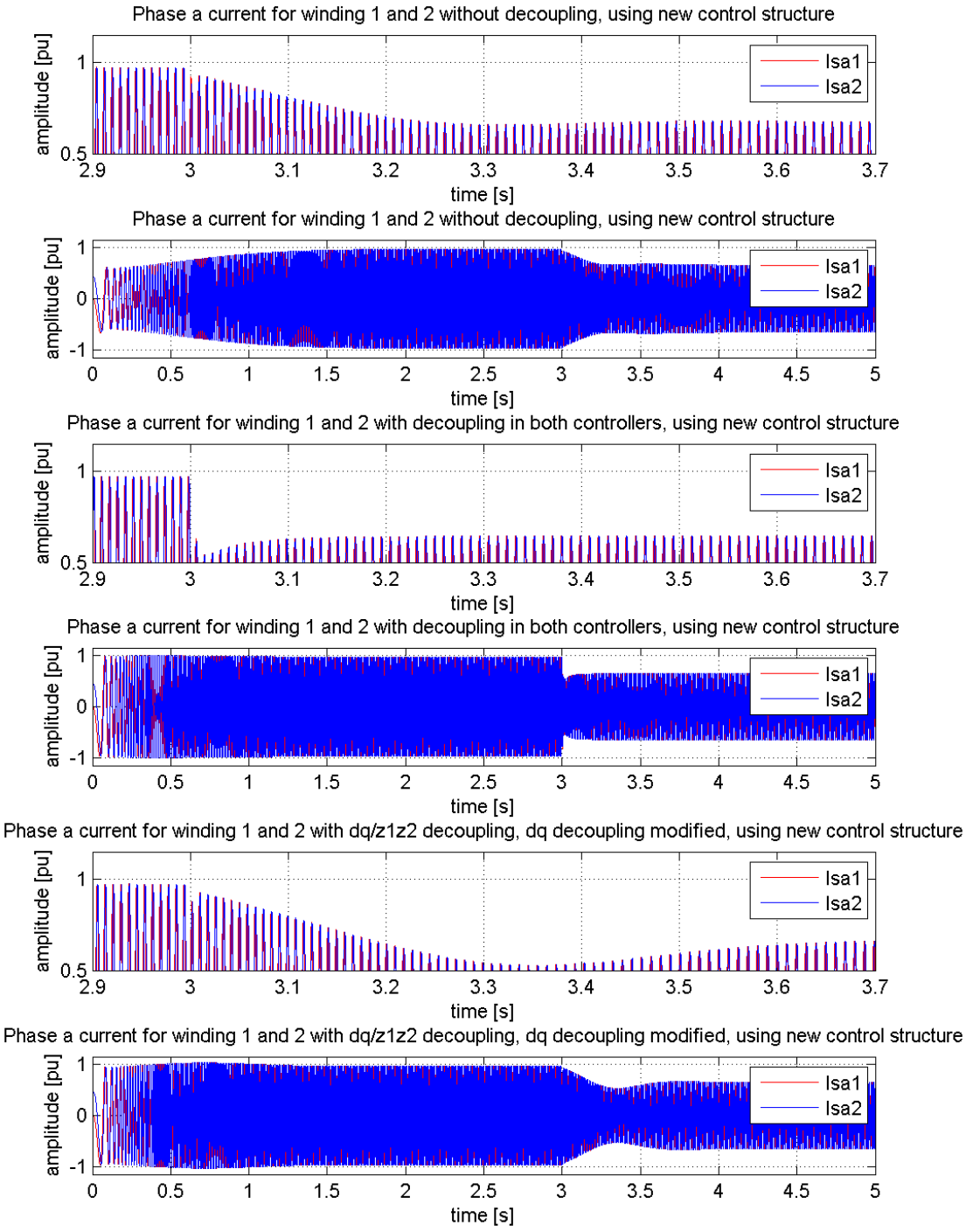

Figure 5.10: Transient phase a current response to negative step in torque reference 1 and 2, without time delay compensation, using new control structure.

From Figure 5.10 one can see the transient response of the phase currents to a negative step in both torque references. The oscillations seen in the (d,q) subspace can clearly be seen to influence the phase currents. The relation between the (d,q) subsystem, the (z_1,z_2) subsystem and the phase currents is given from the transformation matrix in equation (2.10). With both the subsystems decoupling elements enabled the phase currents can be seen to respond satisfactory, with only a slight overshoot.

Summarizing results of the normal operation

In the previous sections the function of the motor in regular operating conditions are documented. The new current control scheme is found to work satisfactorily under these conditions.

The effect of the dq decoupling has been found to drastically increase the performance of the control system during normal operation. The z_1z_2 controller seems to have no effect on the simulation results. This can be explained by considering the fact that we are dealing with analogue simulations, and that the two inverter systems are identical and receives the same reference values. The dq controller was therefore able to divide the load equally on the two inverters without invoking the z_1z_2 controller.

It has also been demonstrated that the new control system behaves identical to the DSFC system during normal operation.

Although it has not been documented in this report, the result of the six-phase machine running in normal mode is similar to that of a normal three-phase machine. With the dq current controller controlling the (d,q) system and no excitation of the (z_1,z_2) subsystem.

5.3 Different torque reference operation

In the following, a step torque of 0.3 pu was applied to inverter two, giving the two inverters a different torque reference value. This decrease in torque reference in one of the inverters can be caused by a number of faults including; failure to supply power to dc-link resulting in the over- and under voltage regulator limiting the torque reference, and because of limitations added to the torque reference of one controller in order to protect the corresponding inverter of overload.

5.3.1 Perfect time delay compensation

The following simulations were conducted with the time delay compensator matching exactly the time delay introduced in the control structure. This idealized case is presented in order to show the control structures inherent response. This gave the following results.

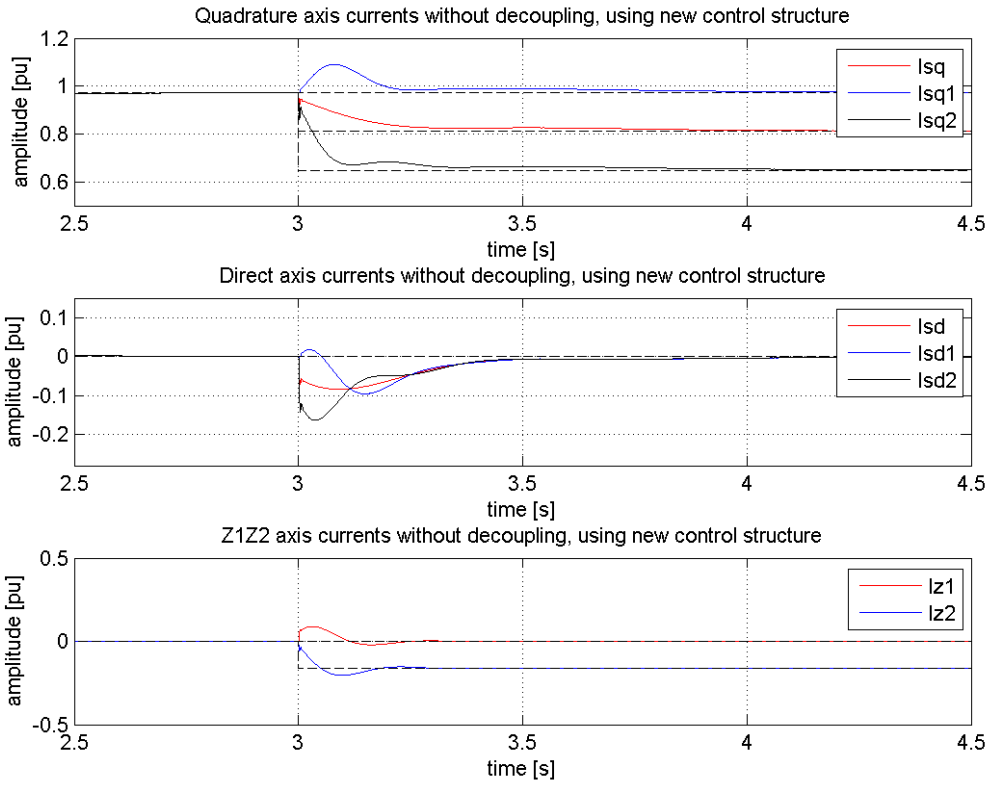

Figure 5.11: Transient current response to negative step in torque reference 2 with perfect time delay compensation, no decoupling, using new control structure.

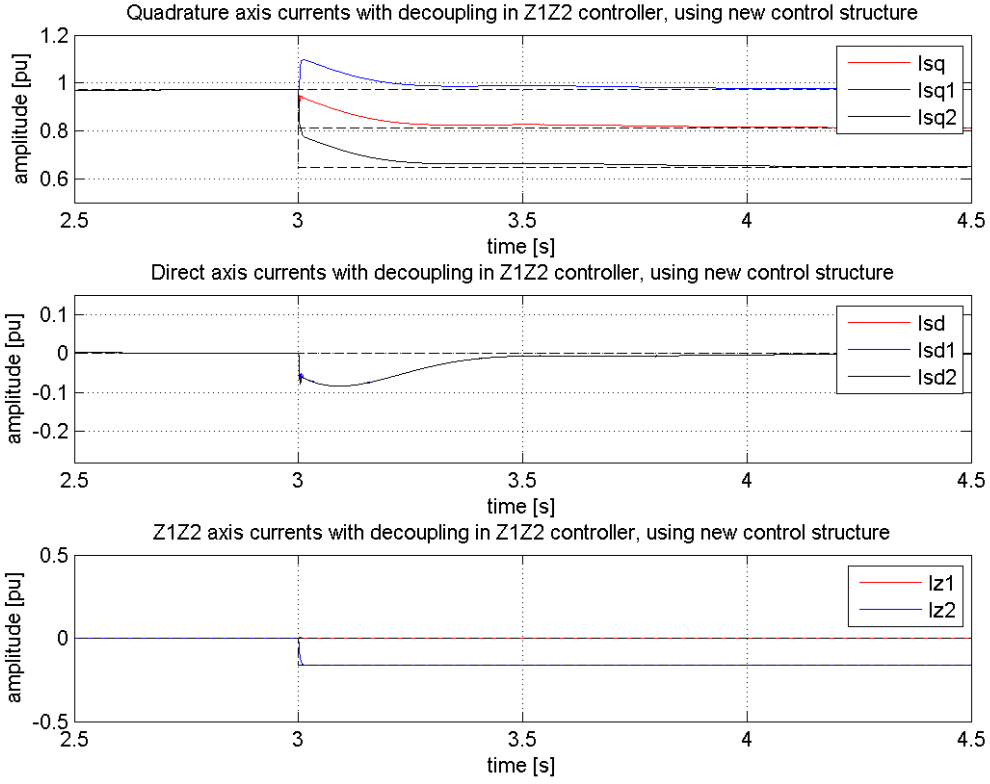

Figure 5.12: Transient current response to negative step in torque reference 2 with perfect time delay compensation, z_1z_2 decoupling, using new control structure.

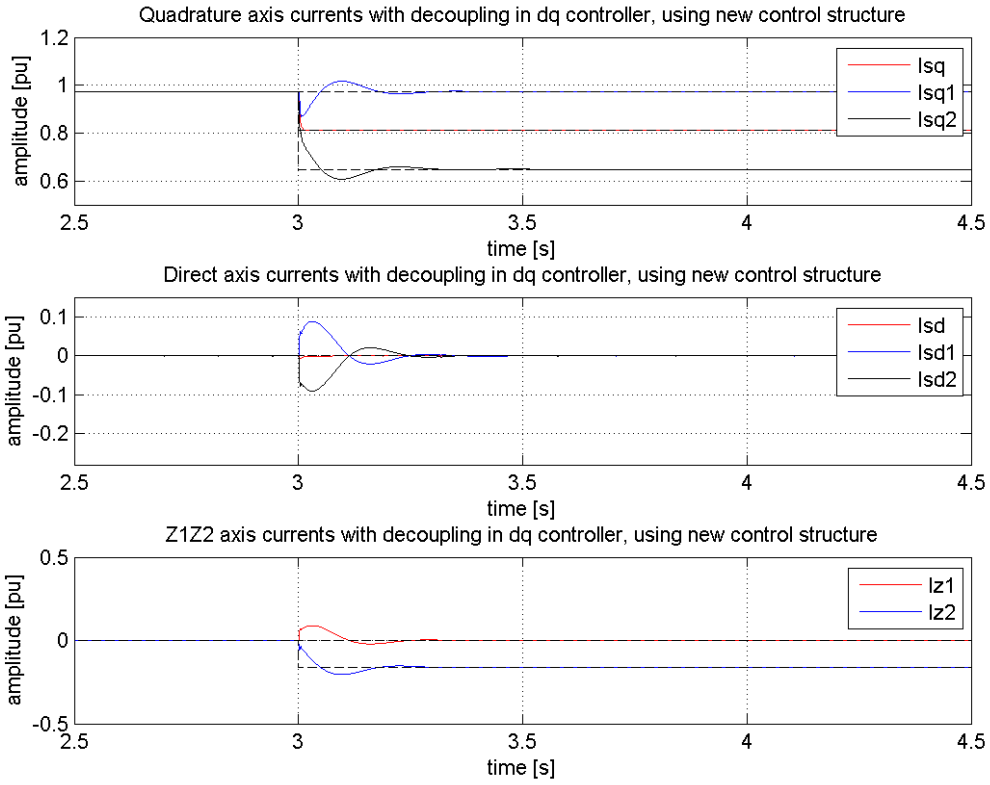

Figure 5.13: Transient current response to negative step in torque reference 2 with perfect time delay compensation, dq decoupling, using new control structure.

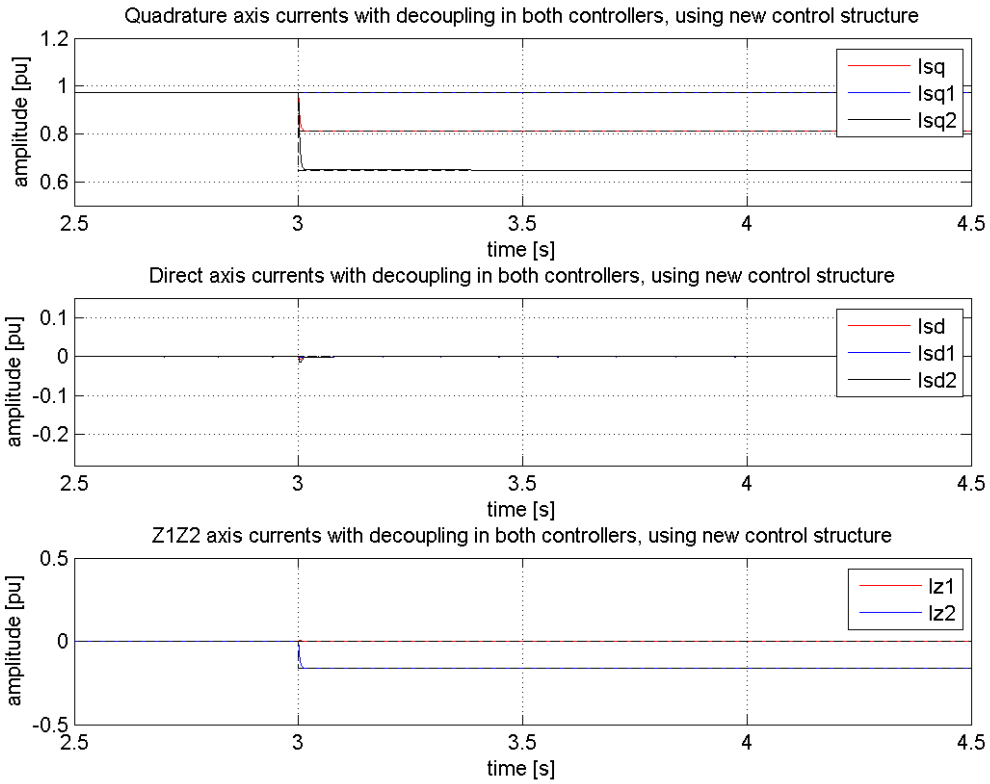

Figure 5.14: Transient current response to negative step in torque reference 2 with perfect time delay compensation, decoupling in both controllers, using new control structure.

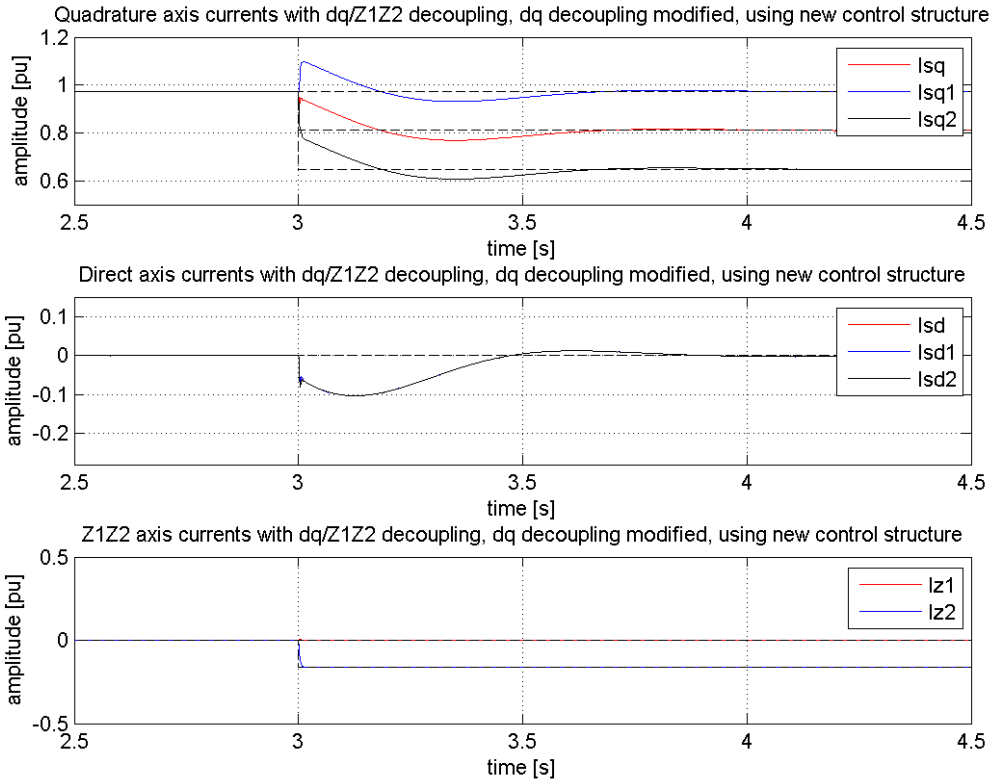

Figure 5.15: Transient current response to negative step in torque reference 2 with perfect time delay compensation, z_1z_2 decoupling and modified dq decoupling, using new control structure.

The results show that the new control structure is able to direct the two inverters to their new steady state reference frames. That is, both the i_{q1}, i_{q2} and the i_{d1}, i_{d2} reach their designated reference values after some time. This is accomplished for all the chosen decoupling schemes. It is also worth mentioning that all the simulations show excitation of the (z_1,z_2) subsystem, something that corresponds to the theory given from equation (4.8). This system is now represented as dc quantities because of the new transformation matrix presented in chapter 2.3.2.

From Figure 5.11 it can be seen that lack of decoupling in both the dq and z_1z_2 controller leads to oscillations in the (d,q) and (z_1,z_2) subsystem. This corresponds to the theory given by equation (4.5) and (4.8). The results also show that the total direct and quadrature current has a slow response to the change in reference value.

As seen in Figure 5.12 the introduction of the z_1z_2 decoupling element removes the oscillations in the (z_1,z_2) subsystem. The (z_1,z_2) subsystem is now governed by equation (4.6) , making it possible for the PI regulators to effectively control each axis to its designated value. By controlling the excitation of the (z_1,z_2) subsystem the z_1z_2 controller is able to remove the oscillations between the direct and quadrature currents belonging to inverter one and two. The difference between the quadrature currents i_{q1} and i_{q2} is now locked to twice the value of $|i_{z2}|$, while the difference between the direct currents is zero as $|i_{z1}| = 0$. This follows from equation (4.10).

When only the dq decoupling is included, as seen in Figure 5.13, the oscillation between the two inverters persists. This is due to the oscillations between i_{z1} and i_{z2} governed by equation (4.5). As mentioned in the previous paragraph, the (z_1,z_2) subsystem controls the differences between the quadrature and direct axis components from inverter one and two. The oscillating i_{z1} and i_{z2} will therefore induce oscillations in these axes. The effect of the dq decoupling element can be seen in that the total quadrature axis current follows the new reference value swiftly without affecting the total direct axis current. See equation (4.11).

In Figure 5.14 the results of including both the dq and z_1z_2 decoupling can be seen. The response to the changing torque reference in inverter two is very good. The two decoupling elements are accomplishing their tasks of decoupling their respective subsystem without interfering with each other. The new control structures ability to avoid oscillations in these kinds of situations is vital to the machines capability to continue operations. This is because large oscillations in the direct and quadrature axis will directly influence the phase currents and may lead to trip of the motor drive.

Simulations with the modified dq decoupling element are included in Figure 5.15. The response of the system is similar to that of Figure 5.12 where merely the z_1z_2 decoupling is included. The response in Figure 5.15 is however seen to be slightly more oscillatory.

In order to compare the given results of the new control structure with the results of the DSFC structure given in [1], some of the DSFC results are repeated in the following figures. For comparison, the (z_1,z_2) subsystem have been mapped using the Rotating Vector Space Decomposition so that the currents are represented as dc quantities.

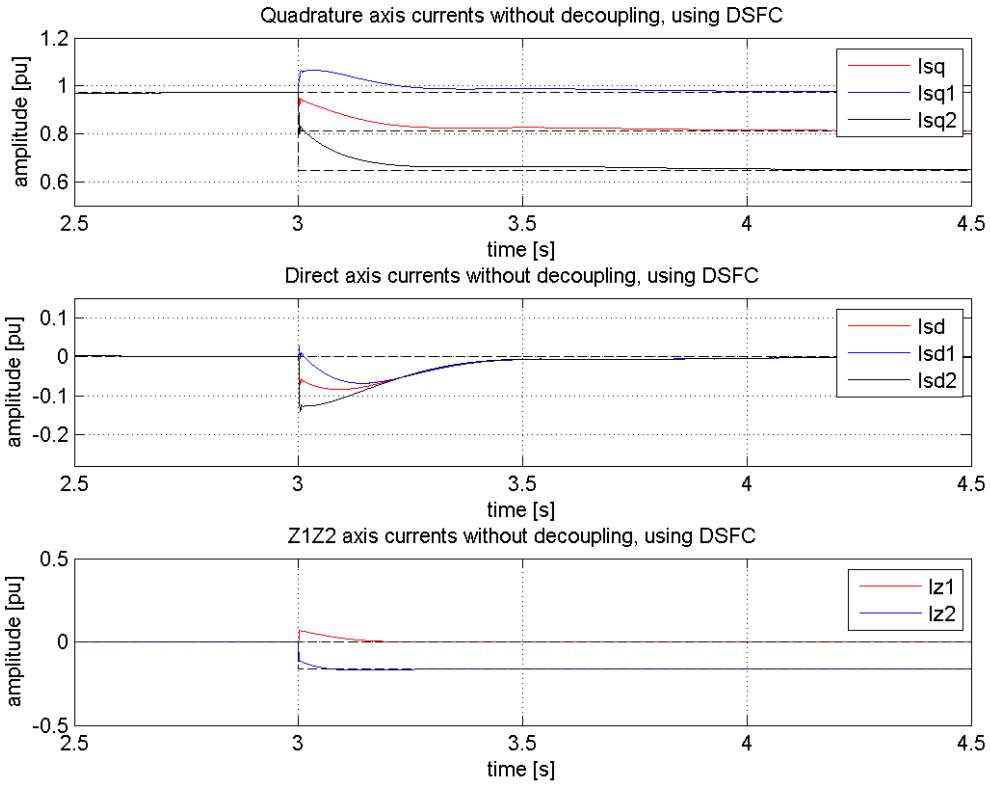

Figure 5.16: Transient current response to negative step in torque reference 2 with perfect time delay compensation, no decoupling, using DSFC [1].

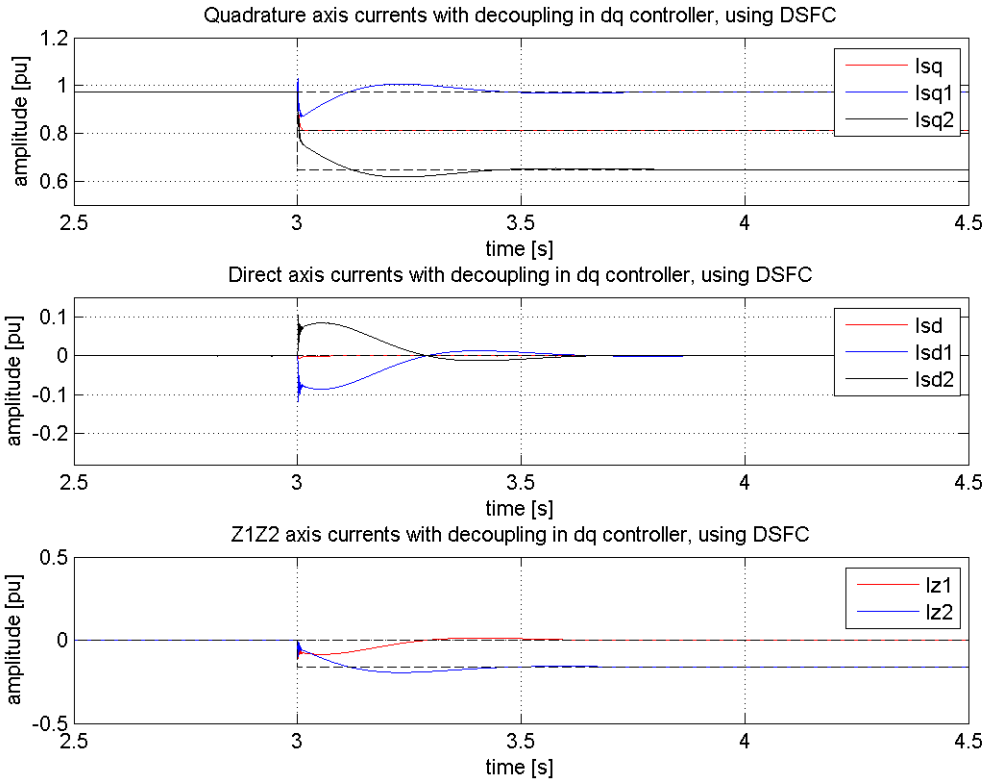

Figure 5.17: Transient current response to negative step in torque reference 2 with perfect time delay compensation, decoupling in both controllers, using DSFC [1].

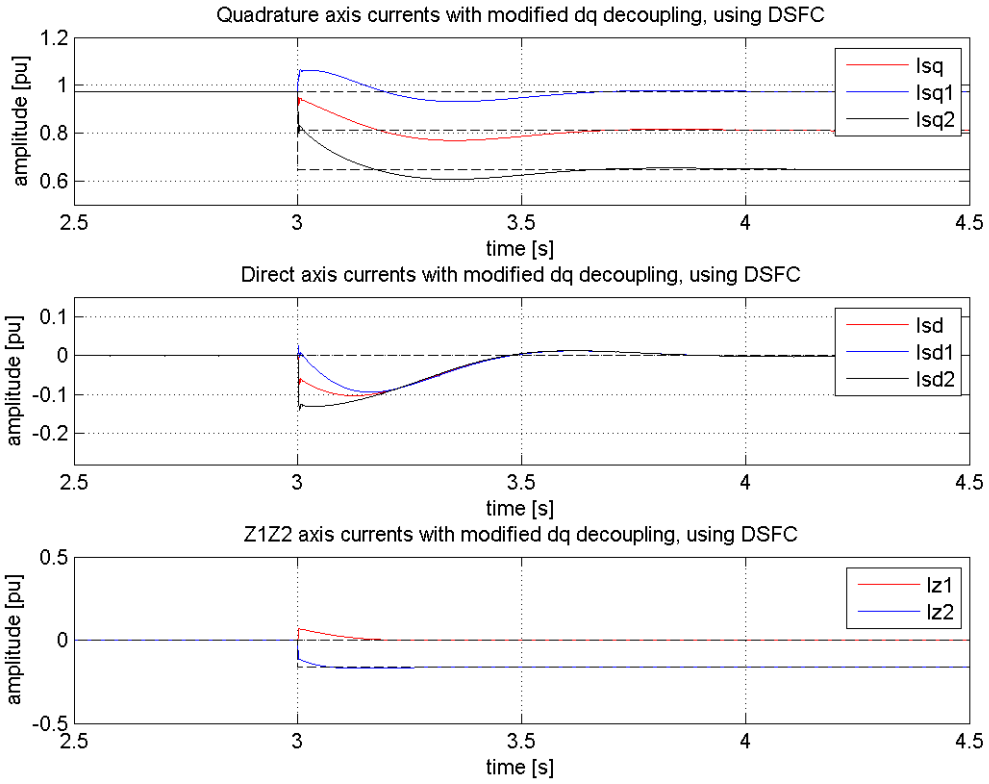

Figure 5.18: Transient current response to negative step in torque reference 2 with perfect time delay compensation, modified dq decoupling in both controllers, using DSFC [1].

Comparing the response of the new control structure with the response from the DSFC, some interesting points can be made. With both controllers operating with no decoupling, as seen in Figure 5.11 and Figure 5.16, the new control structure can be seen to oscillate more than the DSFC structure. This can be explained by realizing that the results seen are in fact the same, only with the added oscillations in the (z_1,z_2) subsystem caused by the coupling elements in the z_1z_2 controller.

It is worth mentioning that the control of the (z_1,z_2) system has no effect on the resulting steady state excitation of that system. The control is only there to give a faster response of the system. In other words, the additional losses induced by exciting the (z_1,z_2) subsystem are the same whether the system is controlled or not.

Including all the decoupling elements in both control structures shows the advantage of the new control structure versus the DSFC, see Figure 5.14 and Figure 5.17. Whereas the currents in the new control structure follows their reference values, the currents of the DSFC structure tend to oscillate against each other. That is, even though the decoupling elements are enabled, the design of the control strategy is flawed in such a way as to be inherently prone to oscillations between the two current controllers, see equation (4.2). This is explained in more detail in chapter 4.1. These low frequency oscillations are mirrored in the phase currents, and have the potential to trip the motor drive when these types of fault occur.

5.3.2 Excluding time delay compensation

The simulations performed in section 5.3.1 were repeated without perfect time delay compensation. This introduces a disturbance to the system that the control system needs to cope with. All the simulated configurations from chapter 5.3.1 are included, as the combination of excluding time delay compensation and including decoupling elements was shown to be a crucial case in the analysis of the DSFC structure [1].

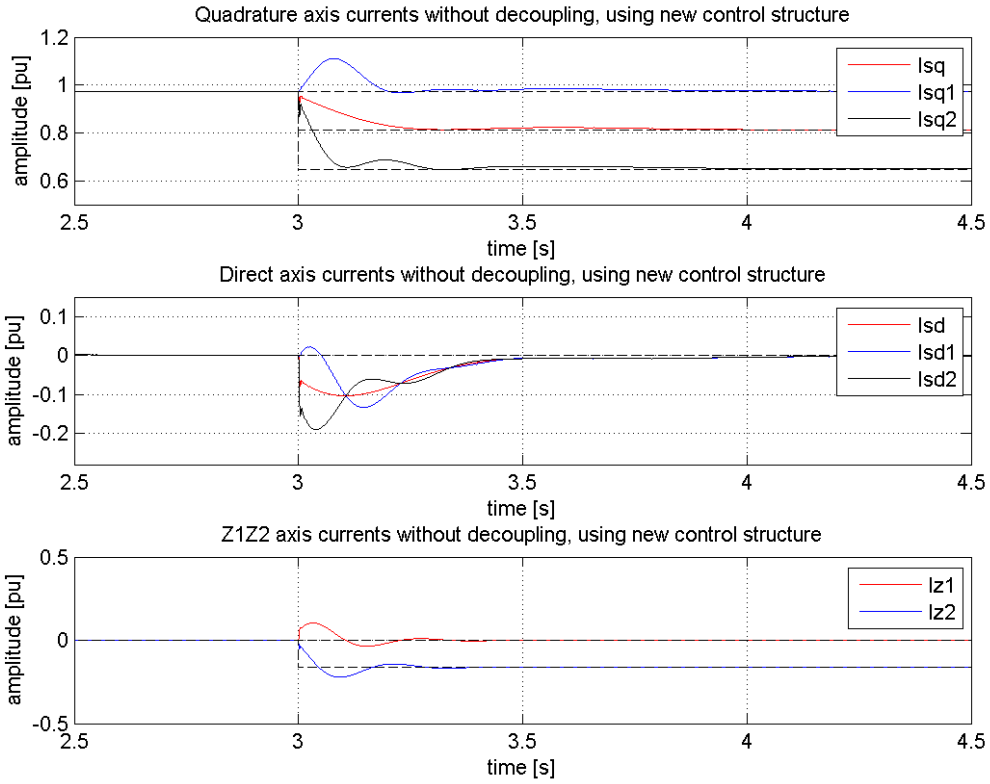

Figure 5.19: Transient current response to negative step in torque reference 2 without time delay compensation, no decoupling, using new control structure.

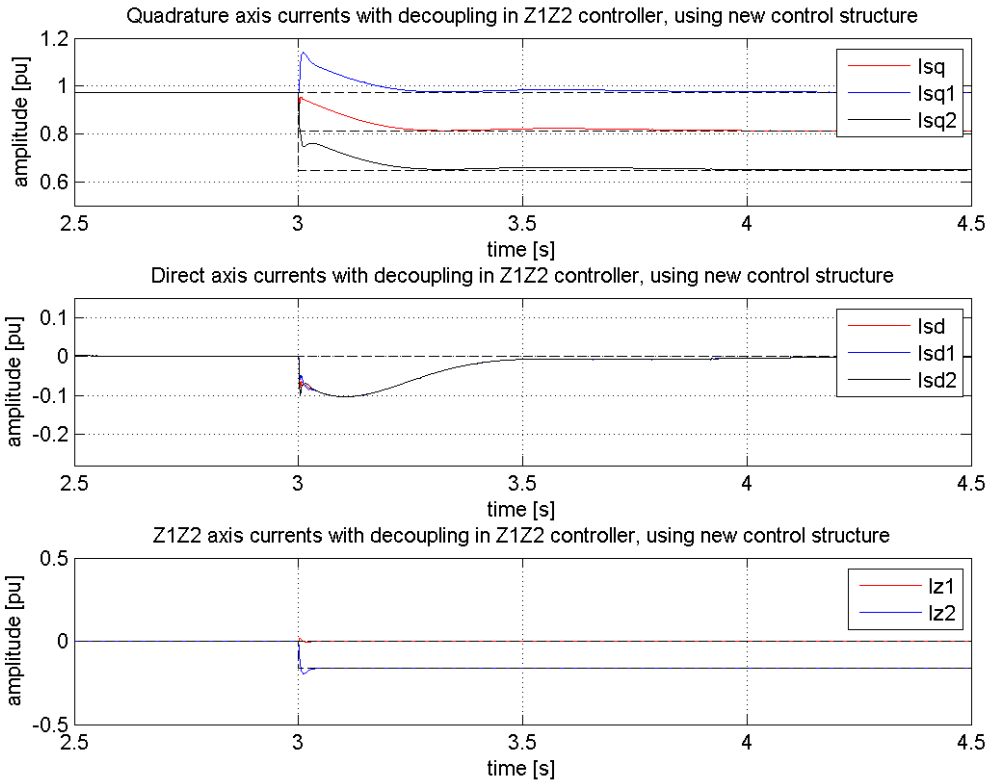

Figure 5.20: Transient current response to negative step in torque reference 2 without time delay compensation, including z_1z_2 decoupling, using new control structure.

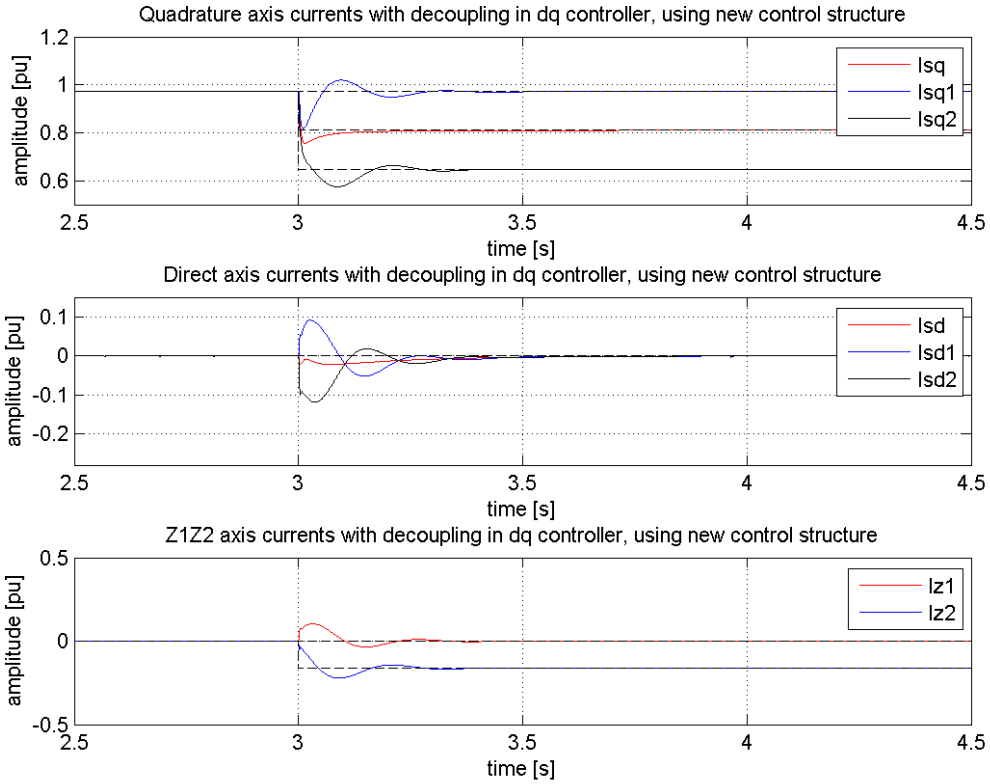

Figure 5.21: Transient current response to negative step in torque reference 2 without time delay compensation, including dq decoupling, using new control structure.

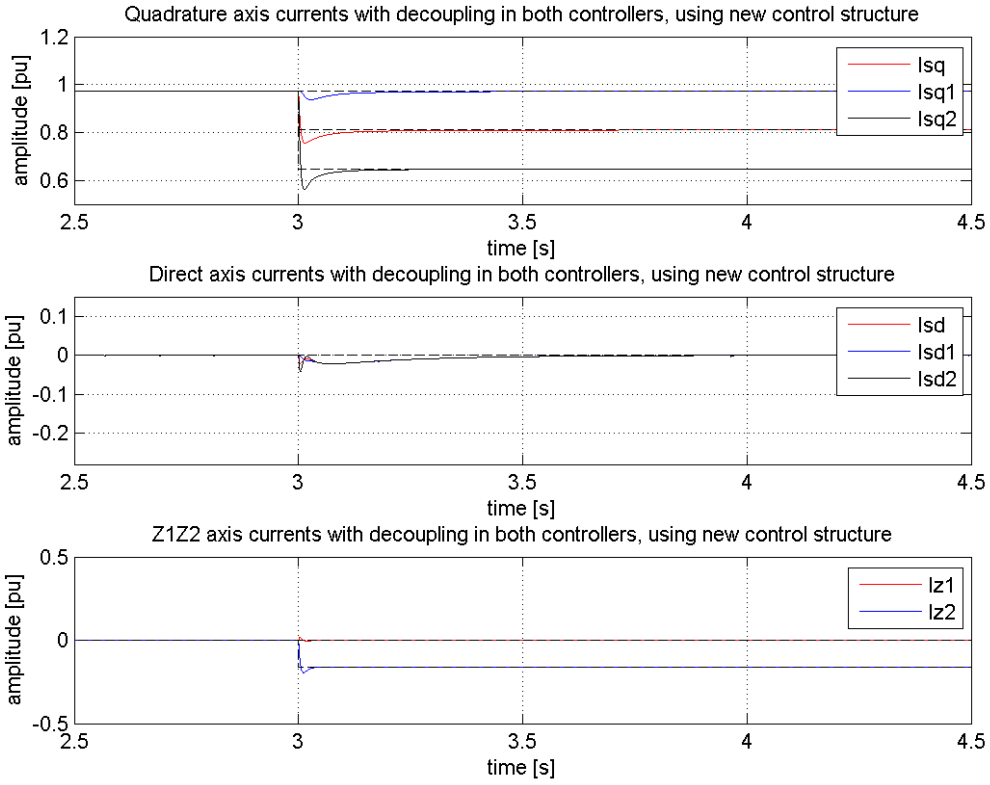

Figure 5.22: Transient current response to negative step in torque reference 2 without time delay compensation, including decoupling in both controllers, using new control structure.

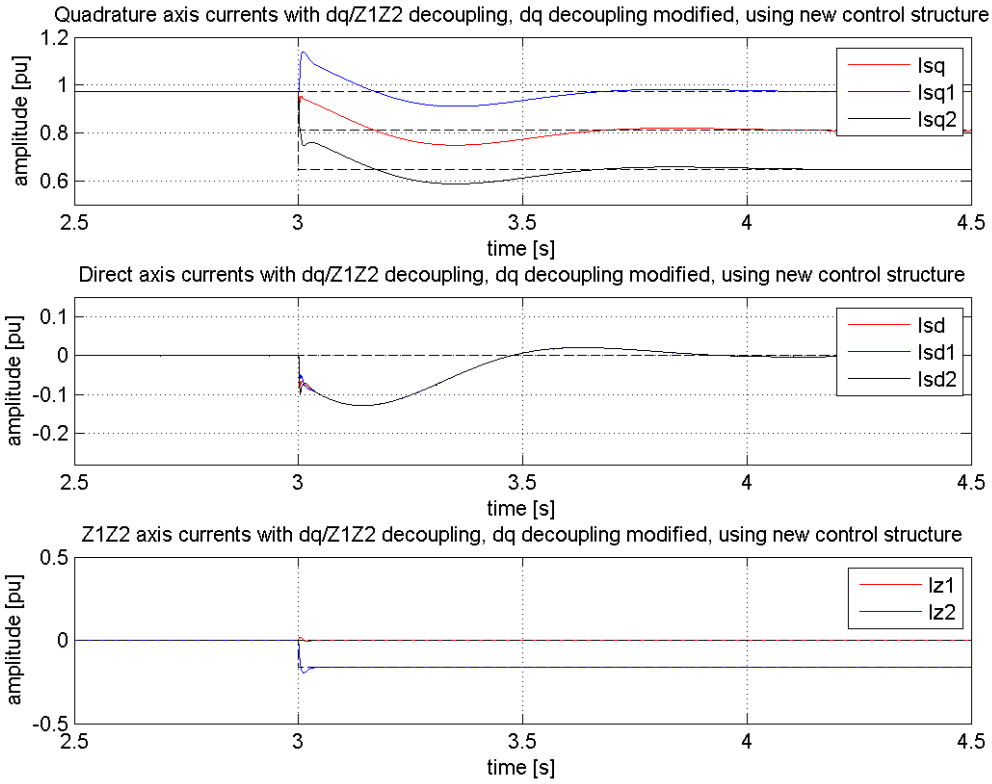

Figure 5.23: Transient current response to negative step in torque reference 2 without time delay compensation, including z_1z_2 decoupling and modified dq decoupling, using new control structure.

Comparing the results given in the above figures with the results from section 5.2.1, it is clear that the exclusion of the time delay compensation unit leads to increased direct and quadrature axis oscillations in all configurations. However, that is the only effect it can be seen to have, and the effect is not drastic in the sense that the oscillations are only slightly increased and the control system is still capable of reaching its new steady state.

The effects of the various decoupling elements can still be seen in that the z_1z_2 controller is still regulating the difference between the controlling currents for inverter one and two, and the dq controller is still controlling the sum of these currents. This coincides with the results found in chapter 4.2.2.

In the case where both dq and z_1z_2 decoupling is enabled it gives a small deviation from the reference value, where previously the regulator managed to follow the reference with great precision. None the less, the results look very promising as no oscillations of any significance could be seen to influence the controlling currents i_{d1}, i_{q1}, i_{d2} and i_{q2}.

In order to compare the given results of the new control structure with the results of the DSFC structure given in [1], some of the DSFC results are repeated in the following figures. For comparison, the (z_1,z_2) subsystem have been mapped using the Rotating Vector Space Decomposition so that the currents are represented as dc quantities.

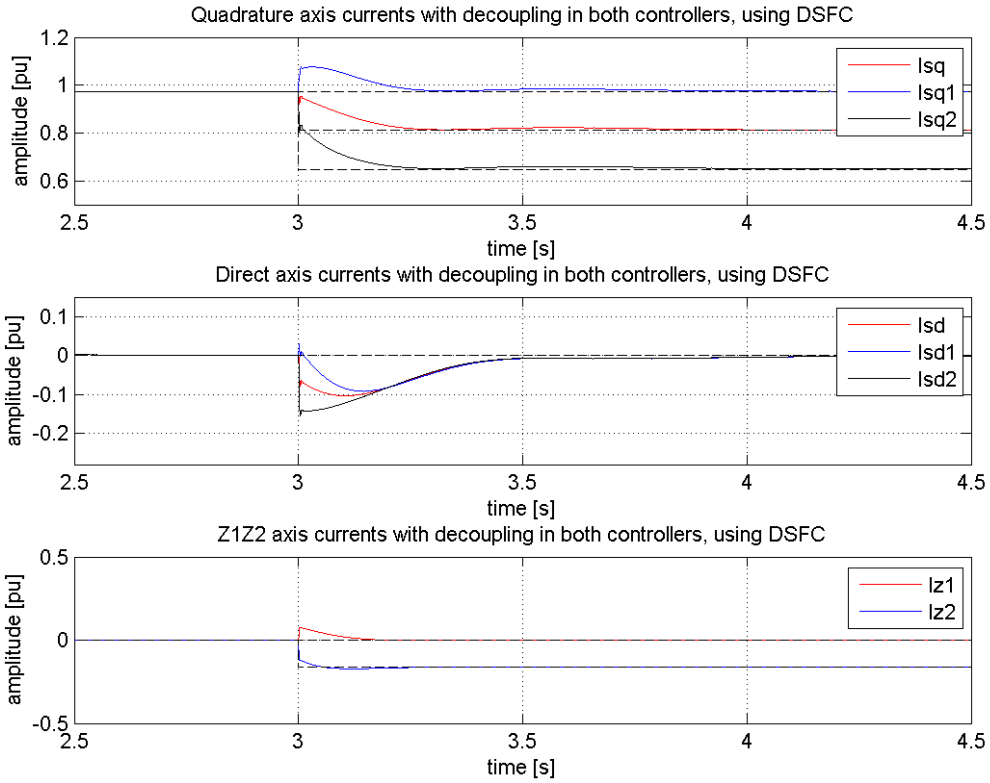

Figure 5.24: Transient current response to negative step in torque reference 2 without time delay compensation, no decoupling, using DSFC [1].

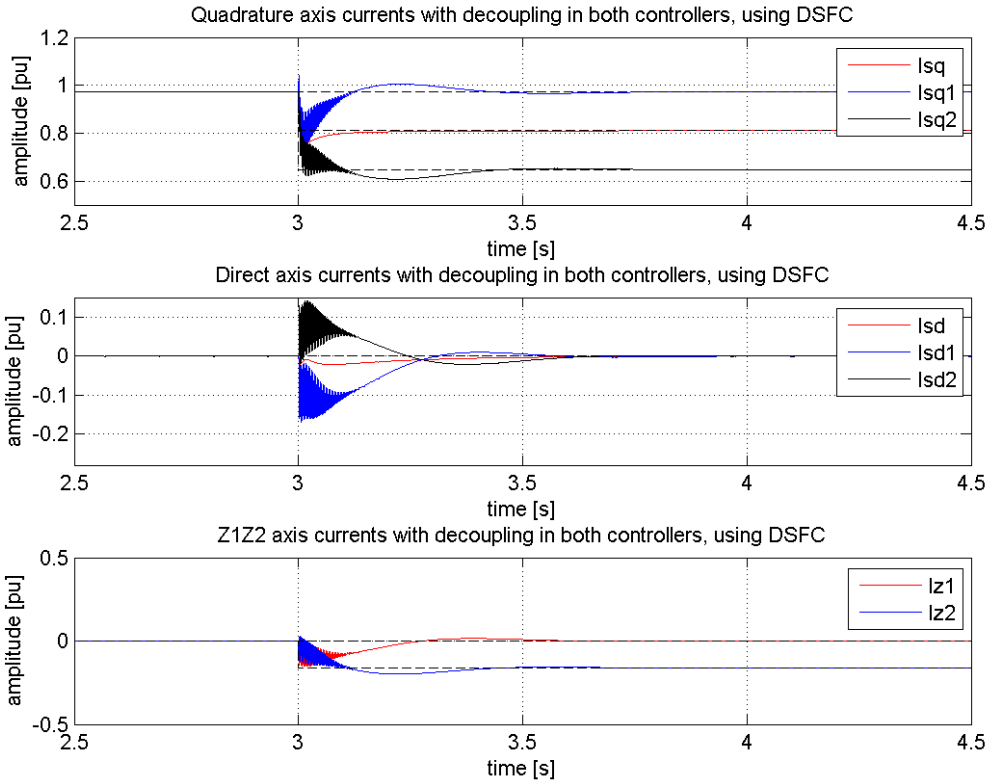

Figure 5.25: Transient current response to negative step in torque reference 2 without time delay compensation, decoupling in both controllers, using DSFC [1].

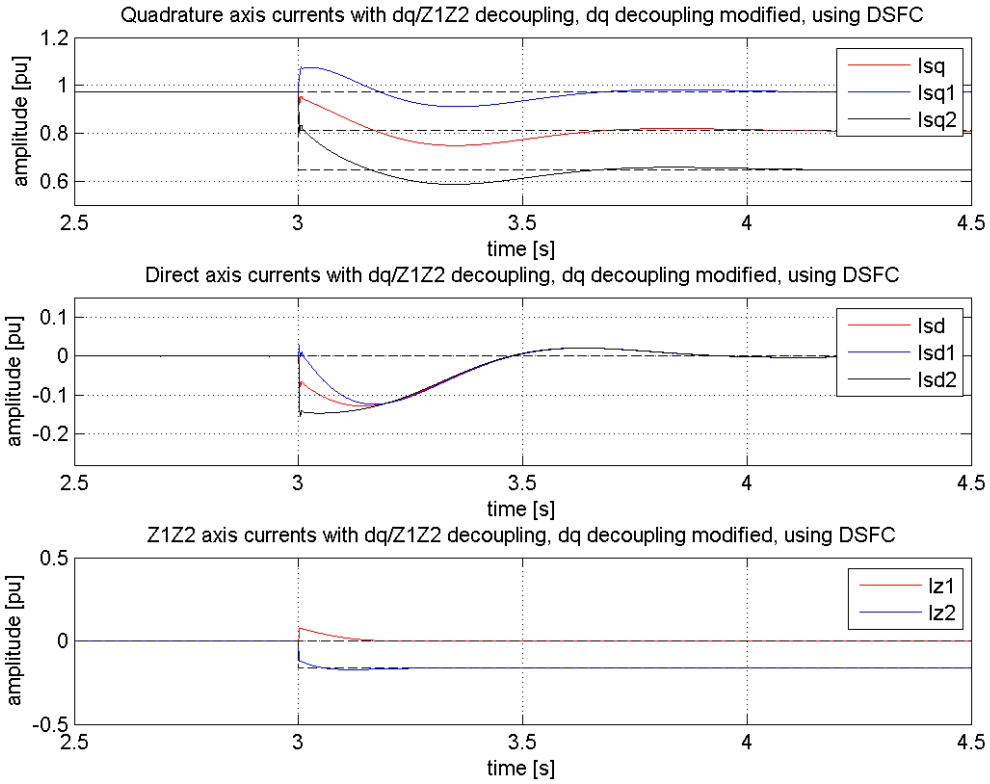

Figure 5.26: Transient current response to negative step in torque reference 2 without time delay compensation, modified dq decoupling in both controllers, using DSFC [1].

The results of the simulations with the DSFC structure show similar behavior to that of the new control structure in that the only effect of excluding the time delay compensation is slightly increased oscillations. The exception is the simulations including the decoupling elements in the current controllers. Including the decoupling elements in the new control system successfully decouples the direct and quadrature axis as well as the z_1 and z_2 axis, as shown in Figure 5.22 and equation (4.6). In the DSFC structure however, the inclusion of the decoupling elements leads to additional high frequency oscillations on top of the oscillations already present. The decoupling elements are not able to decouple the direct and quadrature axis, and instead introduce high frequency oscillations between the two controllers. As can be seen from Figure 5.25 the high frequency oscillations affecting i_{d1}, i_{q1}, i_{d2} and i_{22} do not affect the total direct and quadrature currents. These oscillations can therefore be seen to be directly dependent on the two controllers, and a consequence of choosing to control each part of the total direct and quadrature current directly with two controllers.

In order to see the effect these results have on the phase currents, they have been plotted for both control structures in Figure 5.27 and Figure 5.28.

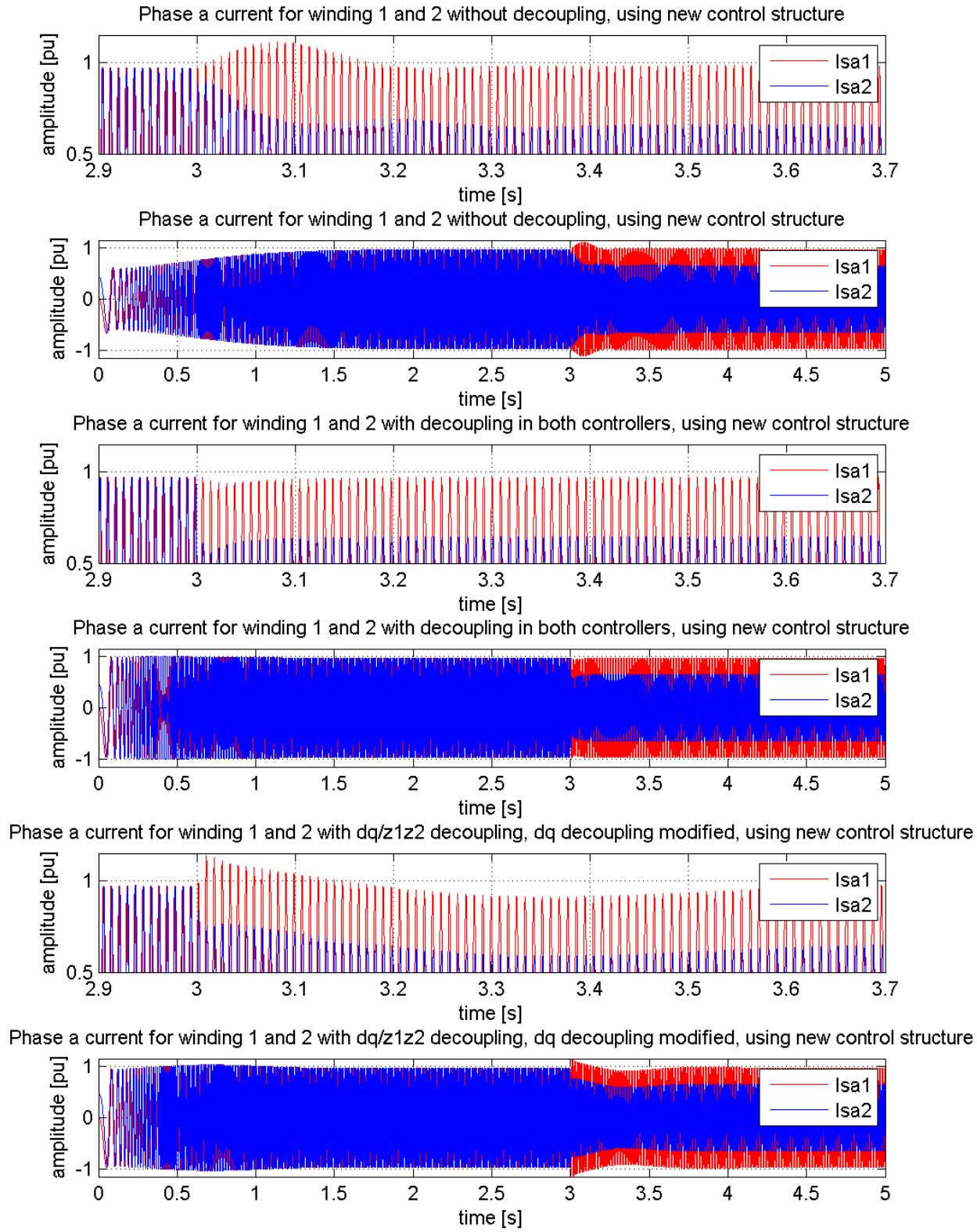

Figure 5.27: Transient phase a current response to negative step in torque reference 2, without time delay compensation, using new control structure.

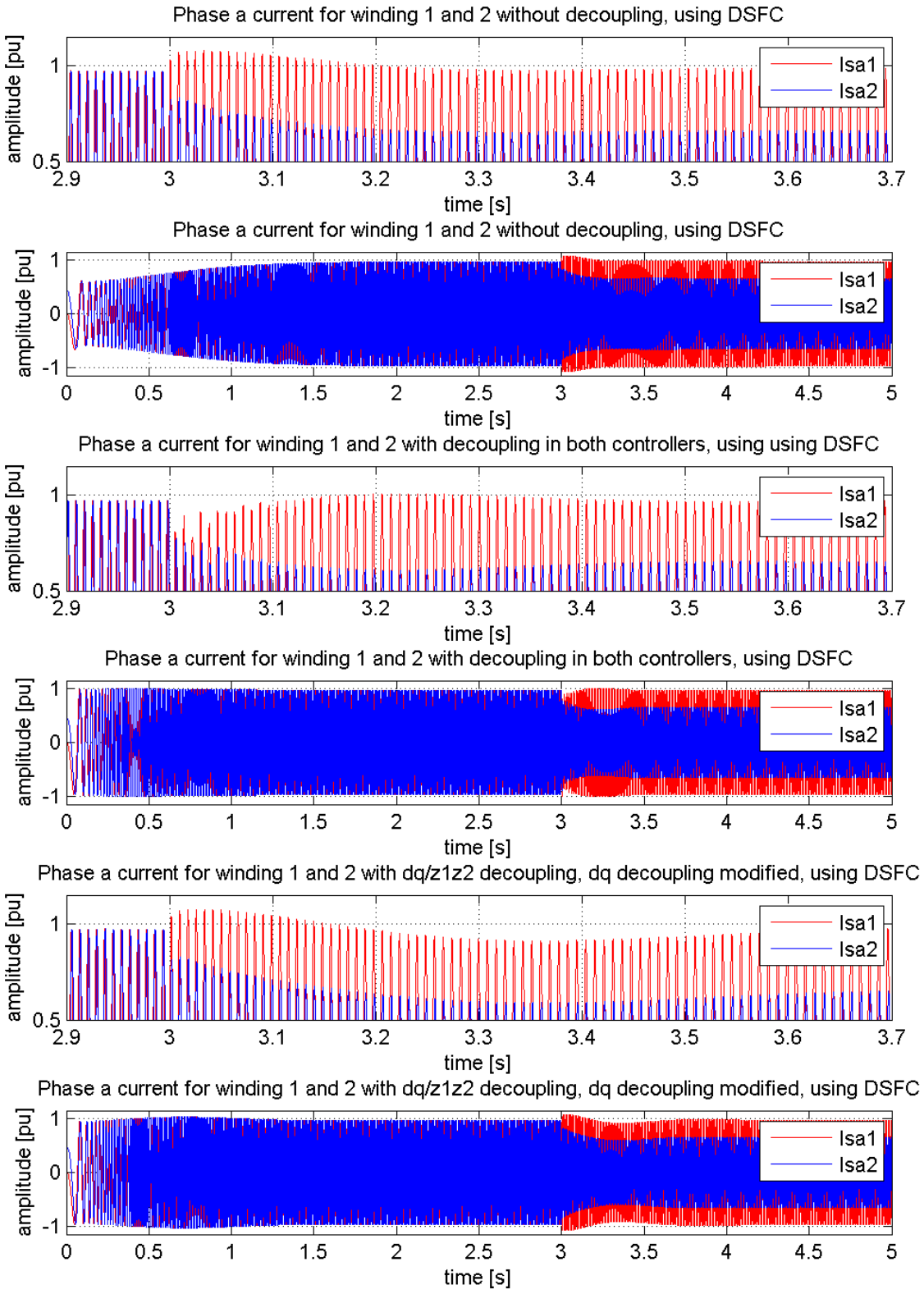

Figure 5.28: Transient phase a current response to negative step in torque reference 2, without time delay compensation, using DSFC [1].

As seen in Figure 5.27 and Figure 5.28 the oscillations first seen in the direct and quadrature axis is being mirrored in the phase currents. Using the DSFC structure, the low

frequency oscillations is seen to raise the phase current of inverter one in all simulations. This raising of the phase currents represents a threat to the inverters ability to continue operation after these types of faults. This is because of the possibility that the increased current might cause the trip of the motor drive if $i_{sa} > i_{trip}$ [1]. In the new control structure, this oscillation of the phase current is no longer seen when the decoupling elements are enabled. This means that this kind of fault can occur in one of the inverters, without it affecting the operations of the second inverter, thus increasing the reliability of the machine.

5.3.3 Summarizing results of the different torque operation

By introducing different torque reference values to the two current controllers, the two controllers stop operating in unison and the load is no longer shared equally between the two. As verified by simulations and theory this causes the excitation of the (z_1,z_2) subsystem which increases the stator loss. However, the controlling currents for the two inverters manage to reach their designated steady state reference values.

The two current controllers of the new control structure have been found to govern different aspects of the control entity. The dq current controller has been shown to control both the sum of the direct currents and the sum of the quadrature currents. Including the dq decoupling elements, this feature of the control system was effectively regulated during transient states. By also controlling the (z_1,z_2) subsystem, the oscillations between the governing currents for inverter one and two could be effectively controlled. This is particularly evident when considering the effect of including the z_1z_2 decoupling elements, see Figure 5.19 and Figure 5.20. Because the two controllers are no longer trying to control different parts of the same elements directly, i.e. parts of i_d and i_q, the introduction of decoupling elements does not lead to unwanted oscillations as they did in the DSFC structure. Instead, the introduction of the decoupling elements eliminates the low frequency oscillations due to coupling of the axes within a subsystem, see equation(4.5).

Because of these features, the transient response of the direct and quadrature currents for inverter one and two are now satisfactory when dealing with these particular faults. The introduction of time delay to the new control structure introduces a slight increase in the oscillations. The performance of the system is never the less satisfactory when including the decoupling elements for both subsystems. This is reflected in the transient response of the phase currents without time delay compensation, seen in Figure 5.27.

5.4 Low dc-link voltage operation

In this section, the dc-link system described in chapter 3.3 will be implemented in order to simulate the response of the system during undervoltage operation. The system will be tested with voltage drops of 200 V and 600 V in the dc-link connected to inverter number two. The voltage drop of 200 V is done in order to test the system response to a voltage drop that does not invoke the undervoltage regulator. The step in 600 V is performed in order to see the behavior of the system when the undervoltage regulator threshold voltage is exceeded. Both the voltage drops are chosen to give saturation in the control voltage of inverter two, u_{st2}.

Based on the simulations performed in the previous sections, the simulations in this chapter have been limited to include simulations with time delay compensation and both the dq and z_1z_2 decoupling enabled. This is the setup that is the most the most promising

when studying the results presented in chapter 5.2 and 5.3, and will give an indication on how well the control strategy copes with a drop in dc-link voltage.

In order to show the problems related to low dc-link voltage for the controllers, simulations of both a low voltage start-up and a step in voltage from steady state will be conducted.

5.4.1 Voltage drop from steady state

The voltage drop was conducted with a stiff grid voltage at 1 kV and the torque reference at 0.9 pu. The drop in dc-link voltage two was conducted from steady state after 2 seconds.

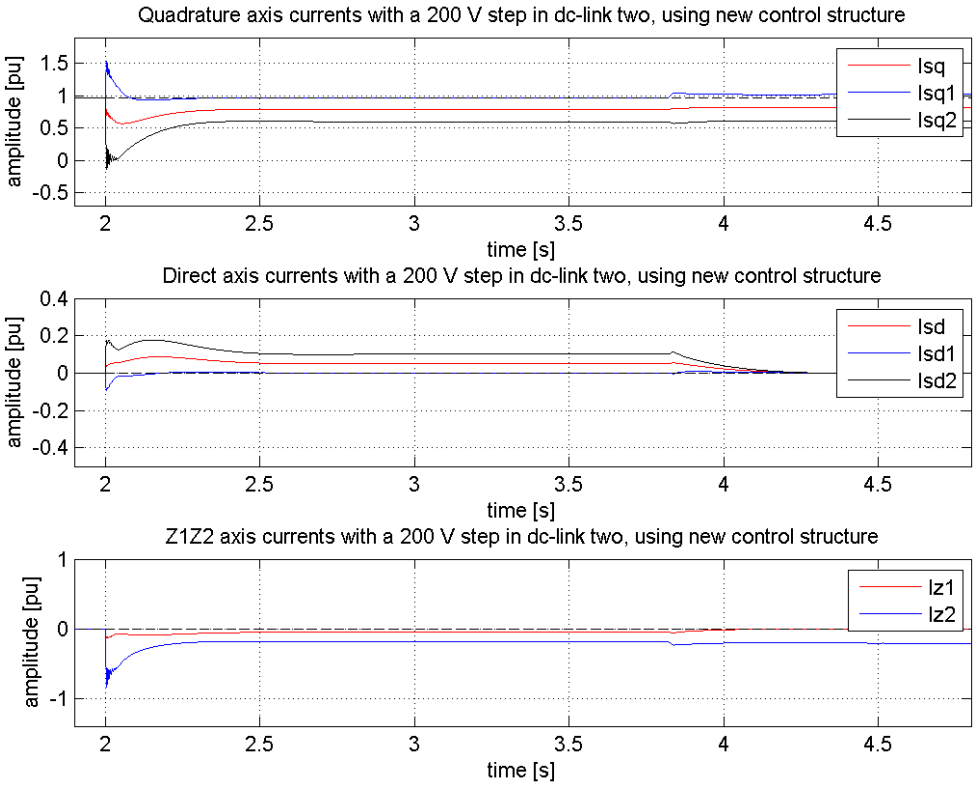

Figure 5.29: Transient current responses to a negative 200 V step in dc-link voltage 2 with no output limitations to the regulators, using new control structure.

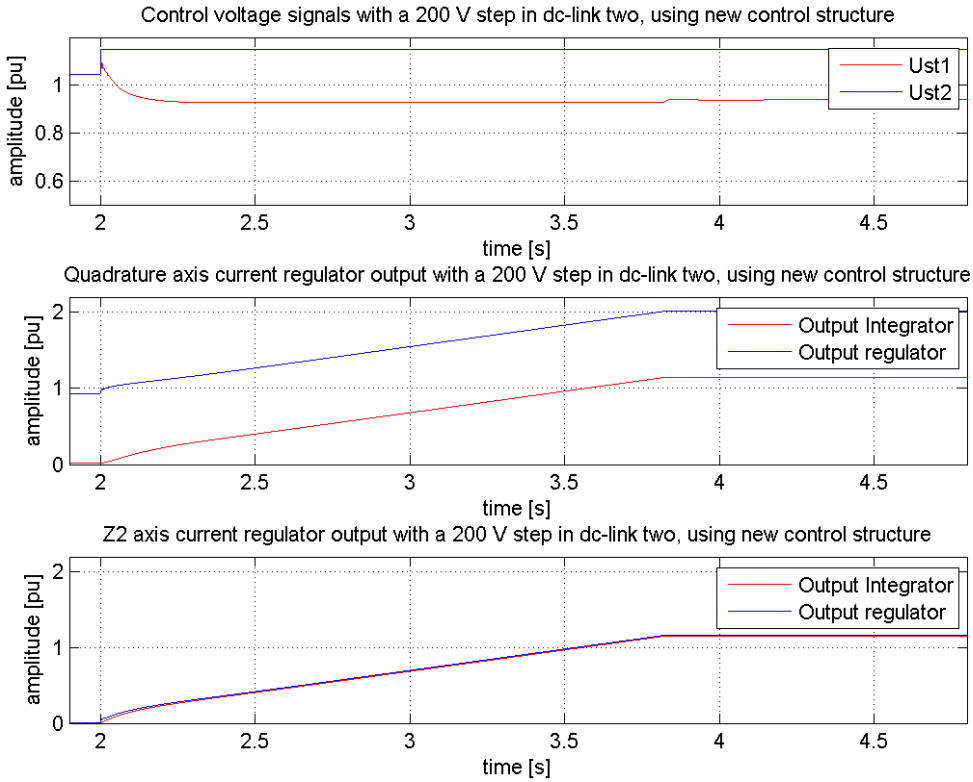

Figure 5.30: Transient control voltage and regulator responses to a negative 200 V step in dc-link voltage 2 with no output limitations to the regulators, using new control structure.

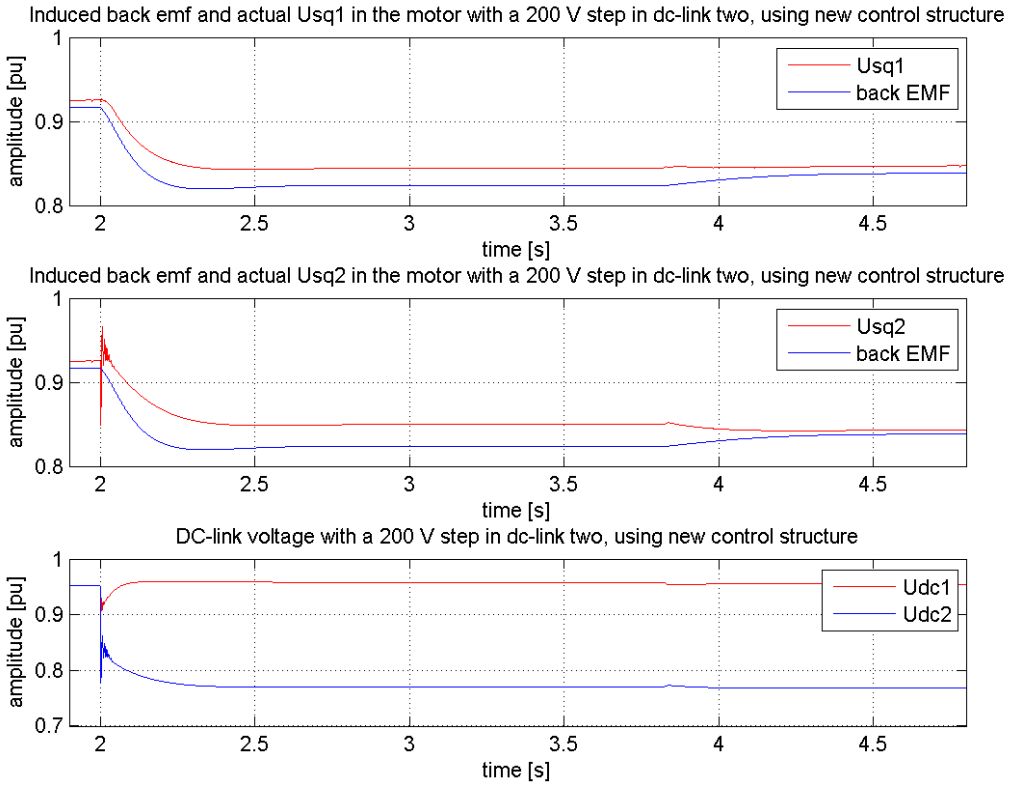

Figure 5.31 Transient voltage responses to a negative 200 V step in dc-link voltage 2 with no output limitations to the regulators, using new control structure.

Looking at Figure 5.29 there are a few key properties that need to be addressed. The first property is the initial leap of currents, and the high frequency oscillations that follows. The leap in the controlling currents is caused by the direct influence the drop in dc-link voltage two has on the rather large i_{q2}. As explained in chapter 4.3.2 and seen in Figure 5.29, the immediate drop in i_{q2} causes i_{q1} to leap upward. From equation (4.8) and Figure 5.29 this can be seen to cause a large deflection to the i_{z2} current, invoking the z_2 regulator to decrease the difference between i_{q1} and i_{q2}. Since i_{q2} decreases more than i_{q1} increases, the quadrature axis PI regulator also responds and tries to increase both values. However, since the deflection is far greater in the z_2 axis than in the total quadrature current, the z_2 regulator lowers i_{q1}. The high frequency oscillations that follow can be seen to originate from the quadrature axis regulator and z_2 regulator trying to raise i_{q2} thus making it oscillate against the lowered dc-link voltage.

The second property that needs to be addressed is the apparent steady state reached after the initial oscillations have died out. This is in fact not a steady state at all, but a state where the PI regulators controlling the different axes will increase/decrease their output, counteracting each other's influence. The key counteracting regulators is in this case the regulators controlling the quadrature and z_2 axis. As explained in chapter 4.3.2 the quadrature axis regulator is trying to increase the i_q to its reference value, thus increasing both i_{q1} and i_{q2}. The z_2 axis regulator is however trying to decrease the difference between i_{q1} and i_{q2} in order to reach its reference value. Since i_{q2} cannot be increased further, due to limitations added by the low dc-link voltage, the two regulators counteract each other's influence on i_{q1}. See equation (4.16). The response of the PI regulators can be seen in Figure 5.30.

It should be mentioned that the simulation regarding Figure 5.29 have been repeated in Appendix E.1 with faster regulators. This is in order to better illustrate the key properties of this simulation. For continuity, the responses included in chapter 5.4 have the same regulator parameters as in chapter 5.2 and 5.3.

The final and arguably the most crucial point is the leap into the permanent steady state. This happens when one of the regulators integrator reach its saturation limit, set at 1.15 for all regulators. When one regulator reaches saturation, the other regulator is able to freely control i_{q1} and i_{q2} before it also reaches saturation or reaches its reference value. Since two and two regulators are opposing each other, the integrators of the opposing regulators will increase at the same rate, given that their controlled currents remain constant, see Figure 5.30. This is true for the quasi steady state seen in Figure 5.29. However, the first transient response gives a greater difference between the reference value and actual value for the z_2 axis regulator than for the quadrature axis regulator. The result is that the z_2 regulator will always reach its saturation before the quadrature axis regulator reaches its saturation. This can be seen in Figure 5.29 at the end of the quasi steady state. Here the z_2 axis regulator reaches saturation, thereby allowing the quadrature axis regulator to increase i_{q1} and push i_{z2} further away from its reference value. This effect will be stronger for more tightly tuned regulators, as seen in Figure E.1 in appendix E.1. The explanation for this is that a faster quadrature axis regulator will have a greater affect on the quadrature axis currents in the time span from the integrator of the z_2 regulator reaches saturation until the integrator of the quadrature axis regulators also reaches saturation.

However, as the z_2 regulator reaches saturation, the effect on i_{q2} is to decrease rather than increase. This could be explained by considering the fact that the quadrature axis

regulator does not control each of the quadrature axis currents separately. When increasing u_q in order to increase i_q the controller tries to increase both i_{q1} and i_{q2}. Because of the low dc-link voltage on inverter two and the fact that u_{st2} has reached saturation, the effect of the raised control voltage u_q is diminished in the phase voltages outputted from inverter two. When i_{q1} is raised, because of the increased control voltage, this causes the rotor to accelerate. The accelerated rotor gives a larger back EMF and it is this effect that lowers i_{q2}. See Figure 5.31. The effects discussed in this paragraph are more prominent when the regulator parameters are tightened up to give faster regulators, see appendix E.1.

The consequences of the initial leap of quadrature currents and the z_2 regulator reaching saturation, will be severe for the operation of inverter one. The current protection scheme for this inverter will trip at the initial response or at the permanently increased i_{q1} in steady state.

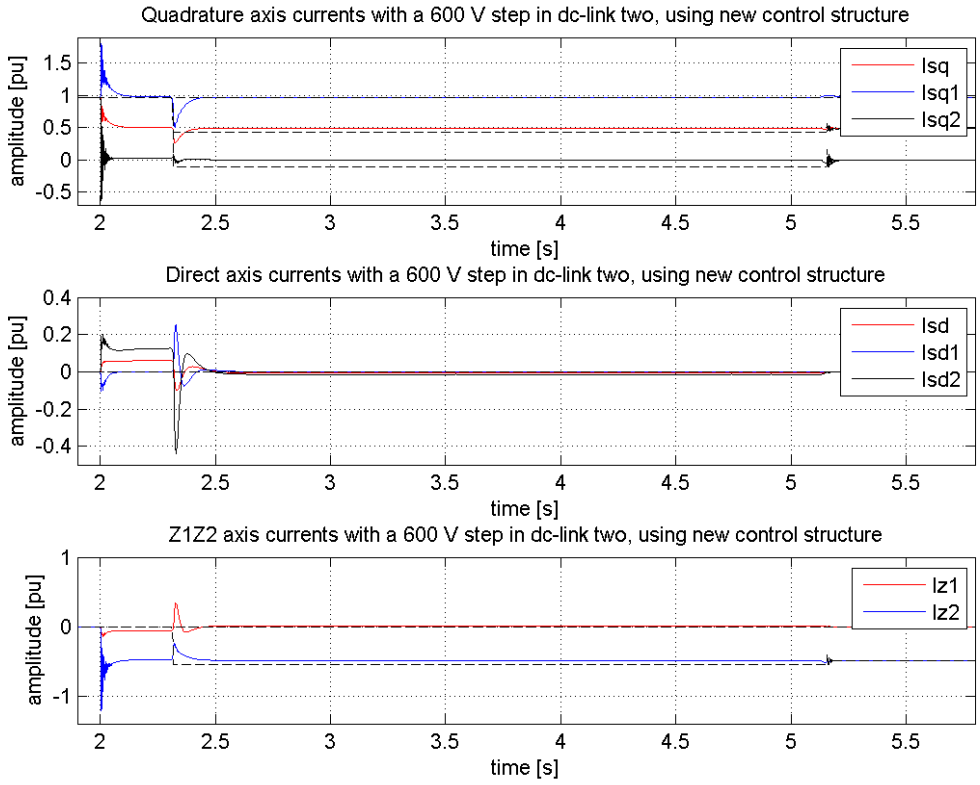

Figure 5.32: Transient current responses to a negative 600 V step in dc-link voltage 2 with no output limitations to the regulators, using new control structure.

In Figure 5.32 the same initial transient response as in Figure 5.29 can be seen. However, the voltage drop is so large that it triggers the undervoltage regulator to force the reference of i_{sq2} into a negative value. The response of the undervoltage regulator is dependent on the dc-link voltage reaching a certain threshold voltage. This threshold voltage is not reached at once because of the low current being demanded of inverter two. This delay causes the integrators in the PI regulators to integrate up. Because of this, the currents are seen to use a long time to reach their reference values after the undervoltage regulator have responded. This is seen in Figure 5.33.

The response of the undervoltage regulator is however vital, as it lowers the reference value of i_{q2} in response to the large drop in the dc-link voltage. The reference value of i_{q2} can be seen to go negative as the undervoltage regulator is trying to force the second inverter into generator mode in order to raise the dc-link voltage. With this change in reference value there will again be correspondence between the available output of the inverters and the output demanded by the reference values. This is seen in Figure 5.32 and Figure 5.33 as u_{st2} is no longer limited and the controllers are able to reach their reference values once the integrators have wound down. The time it takes to wind down is independent of the regulator speed.

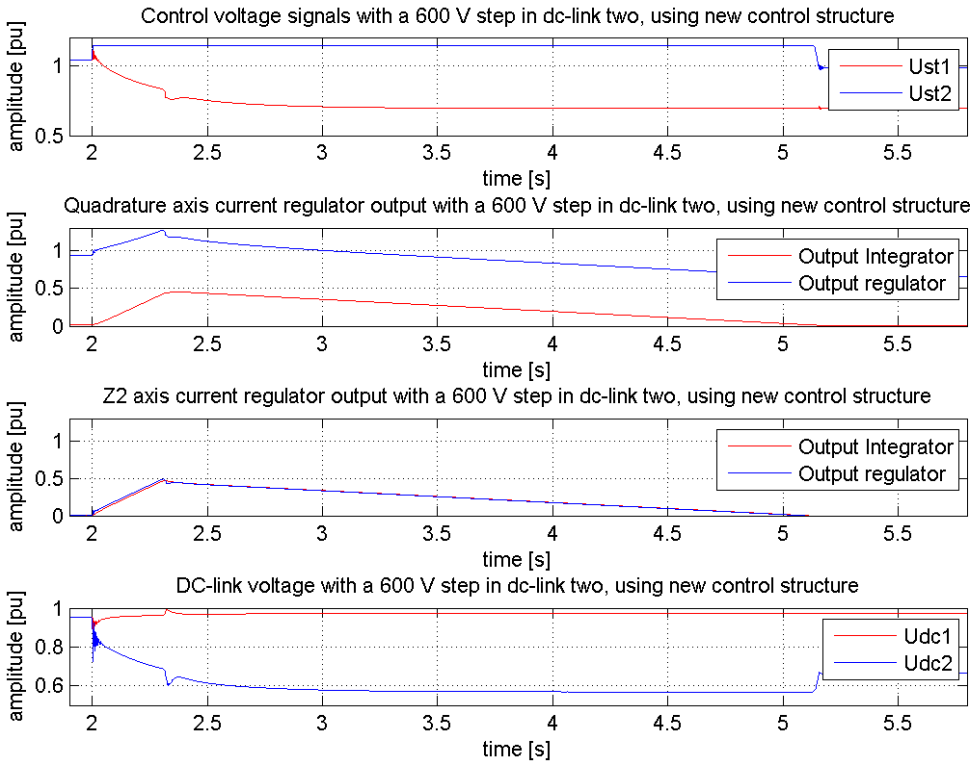

Figure 5.33: Transient voltage and regulator responses to a negative 600 V step in dc-link voltage 2 with no output limitations to the regulators, using new control structure.

The results given in Figure 5.32 and Figure 5.29 show a need to improve the control structures response to a drop in dc-link voltage. Both the 200 V and the 600 V drop of the dc-link voltage gave unsatisfying transient response. The 200 V drop also gave unsatisfactory steady state. In order to try to improve this response, certain elements were changed in the control structure. The changes are described in chapter 4.3.2. In short there was added limitation to the output of the four regulators and an anti windup scheme was connected to these limitations [16]. See Figure D.1 in appendix D. The new results are shown in Figure 5.34 and Figure 5.36.

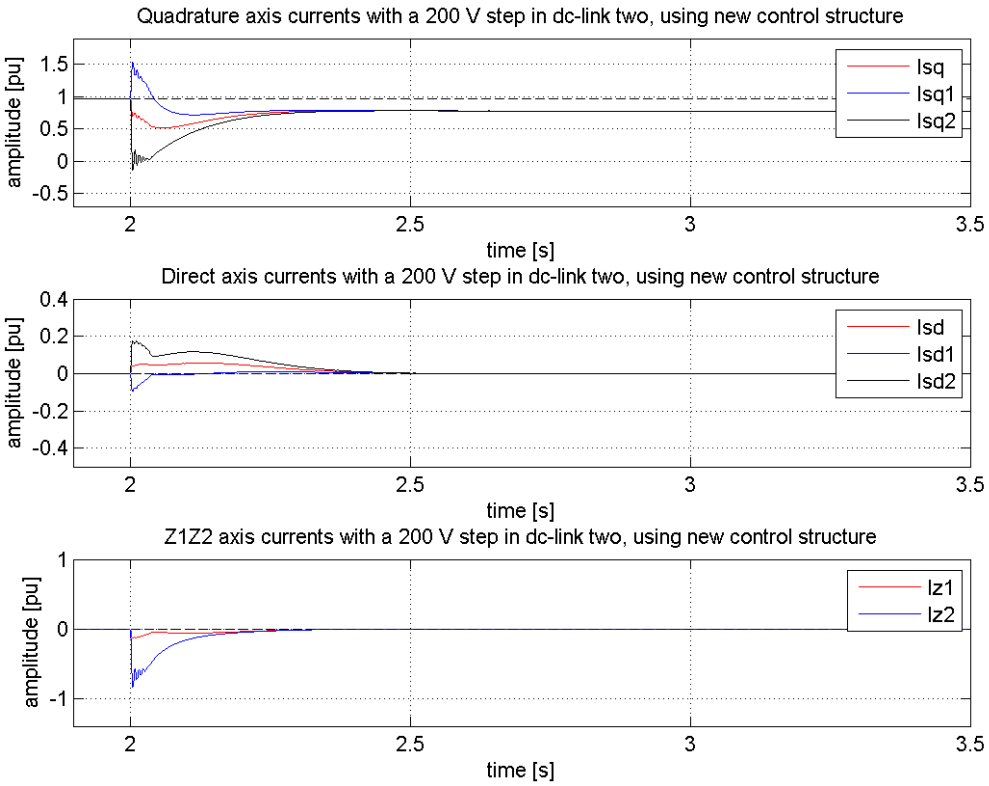

Figure 5.34: Transient current responses to a negative 200 V step in dc-link voltage 2 with output limitations on the regulators, using new control structure.

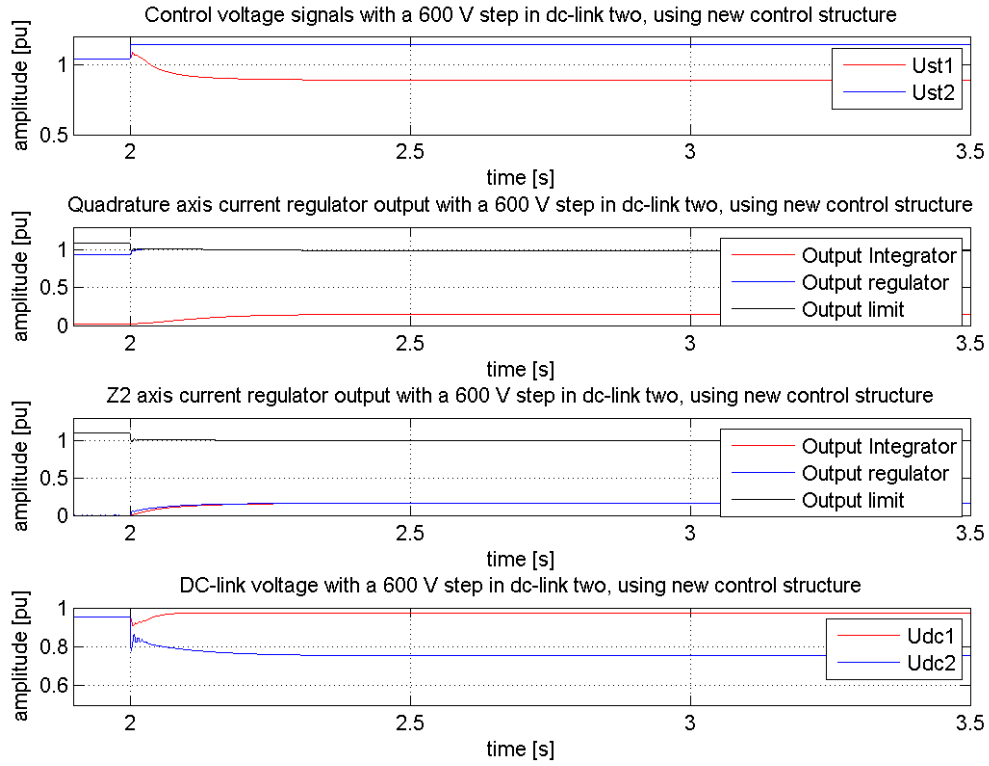

Figure 5.35: Transient voltage and regulator responses to a negative 200 V step in dc-link voltage 2 with output limitations on the regulators, using new control structure.

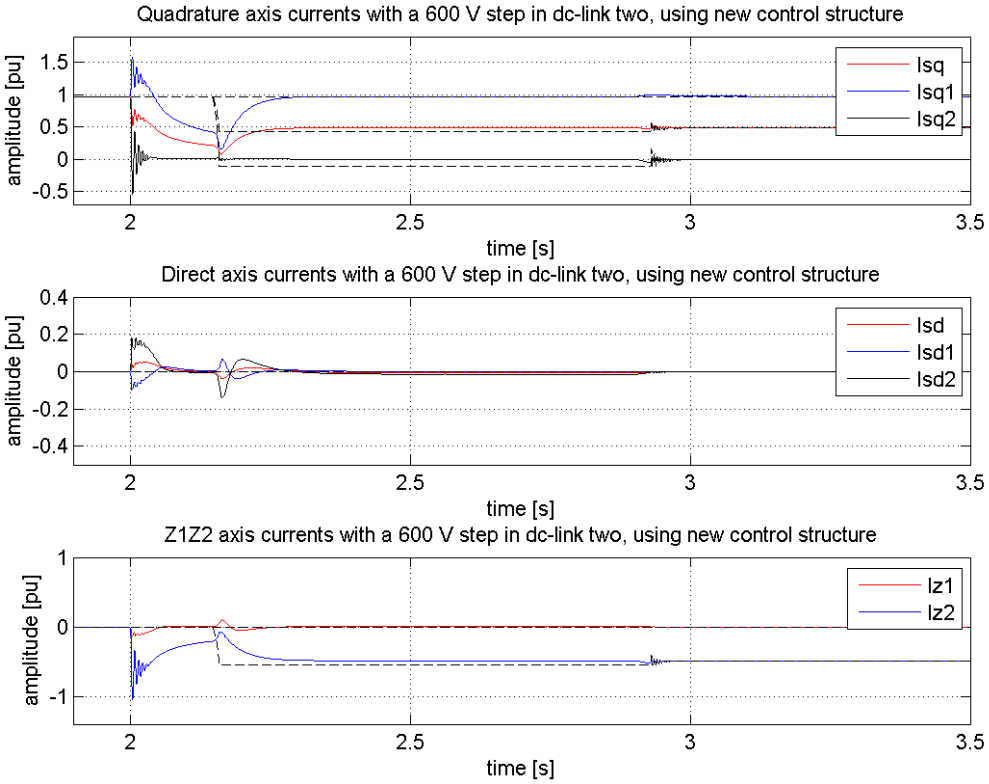

Figure 5.36: Transient current responses to a negative 600 V step in dc-link voltage 2 with output limitations on the regulators, using new control structure.

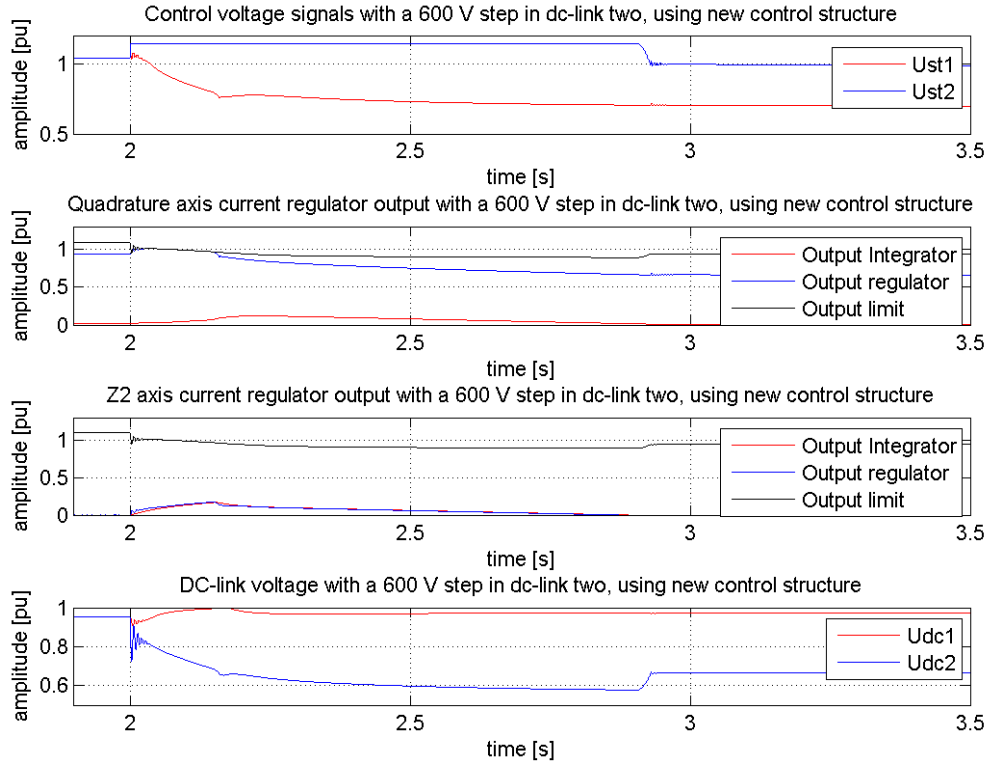

Figure 5.37: Transient voltage and regulator responses to a negative 600 V step in dc-link voltage 2 with output limitations on the regulators, using new control structure.

As seen in Figure 5.34 the response of the system to a 200 V drop in the dc-link voltage has improved. By limiting the output of each regulator as described in chapter 4.3.2, the quadrature axis regulator will now reach the output limit before it reaches the saturation limit on the inverter. This is because the quadrature axis regulator is already giving a certain output before the fault occurs, in order to keep the quadrature current equal to its reference value. See Figure 5.35. This gives the z_2 regulator the opportunity to regulate the difference between the two quadrature axis currents without the counter effect of the quadrature axis regulator.

Since the voltage drop was not large enough to invoke the undervoltage regulator, the reference values remain unchanged and the difference between the two quadrature axis currents will be regulated to zero. This gives a stable steady state solution that does not exceed the capabilities of either of the two inverters. However, this means that i_{q1} will be lowered to the same value as i_{q2}. This is not an optimal solution, as inverter one is capable of delivering full torque in the given scenario. Furthermore, the initial leap of the current values remains roughly the same, thus threatening the reliability of the motor drive.

As seen from Figure 5.36, the undervoltage regulator still works with the new limitations in place. The results can be seen to be similar to the results shown in Figure 5.32. However, the quadrature axis regulator reaches its output limits, and this reduces the value of i_{sq1} as the z_2 axis regulator is reducing the difference between the i_{q1} and i_{q2}. This causes reduced integral windup and reduces the wound down time of the integrators, thus making the system reach steady state quicker. See Figure 5.37.

With the undervoltage regulator changing the reference value of i_{q2} the reference value of i_{z2} is no longer zero. This gives the motor drive the capacity to run the two inverters at different states, even with the new output limitations. However, the initial current peak can still be seen in Figure 5.36.

The effect the direct and quadrature axis current has on the phase currents can be seen in Figure 5.38. The initial current peak seen in the quadrature axis current can be seen to be mirrored in the phase currents. The steady state increase of i_{q1} for a 200 V step without regulator output limitations, seen in Figure 5.29, also increases the steady state value of the phase currents from inverter one. This can also be observed in Figure E.4 in appendix E.1 with faster regulators

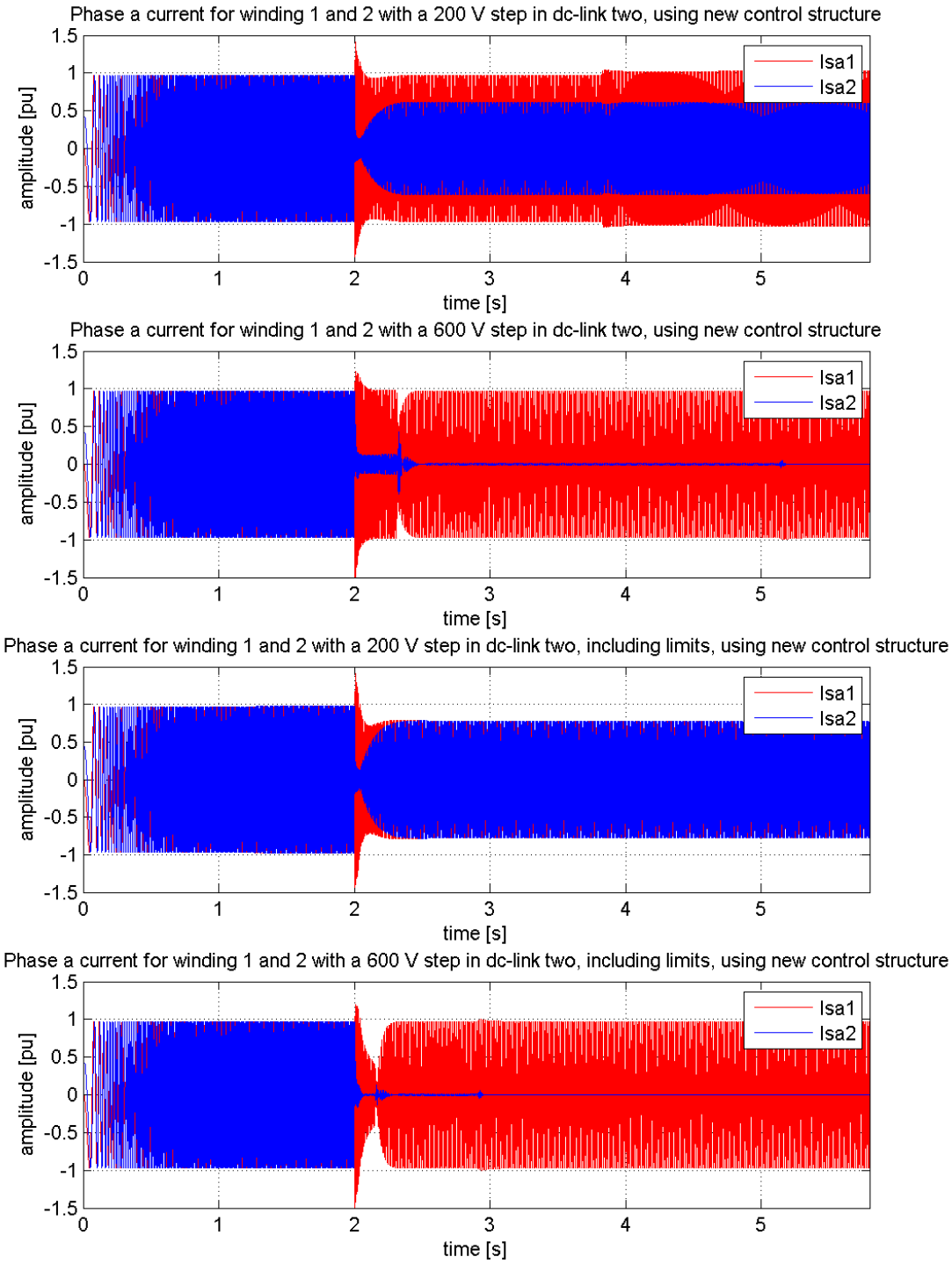

Figure 5.38: Transient phase a current responses to a negative step in dc-link voltage 2, using new control structure.

5.4.2 Start-up

The simulations performed in section 5.4.1 were repeated with a low dc-link voltage on start-up rather than a step in dc-link voltage. The simulated start-ups were conducted with dc-link voltage two set to 800 V and 400 V, corresponding to a voltage drop of 200 V and 600 V respectively. Dc-link voltage one and the torque reference was kept at 1 kV and 0.9 pu. This gave the following results.

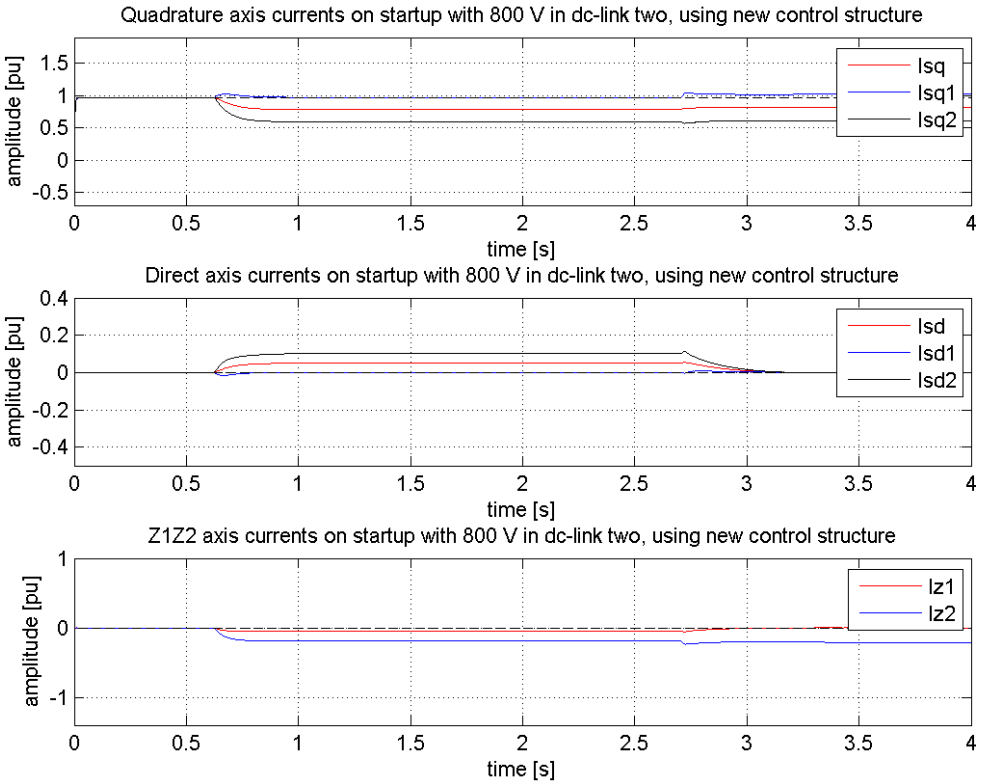

Figure 5.39: Transient current responses to a start-up with 800 V in dc-link two with no output limitations to the regulators, using new control structure.

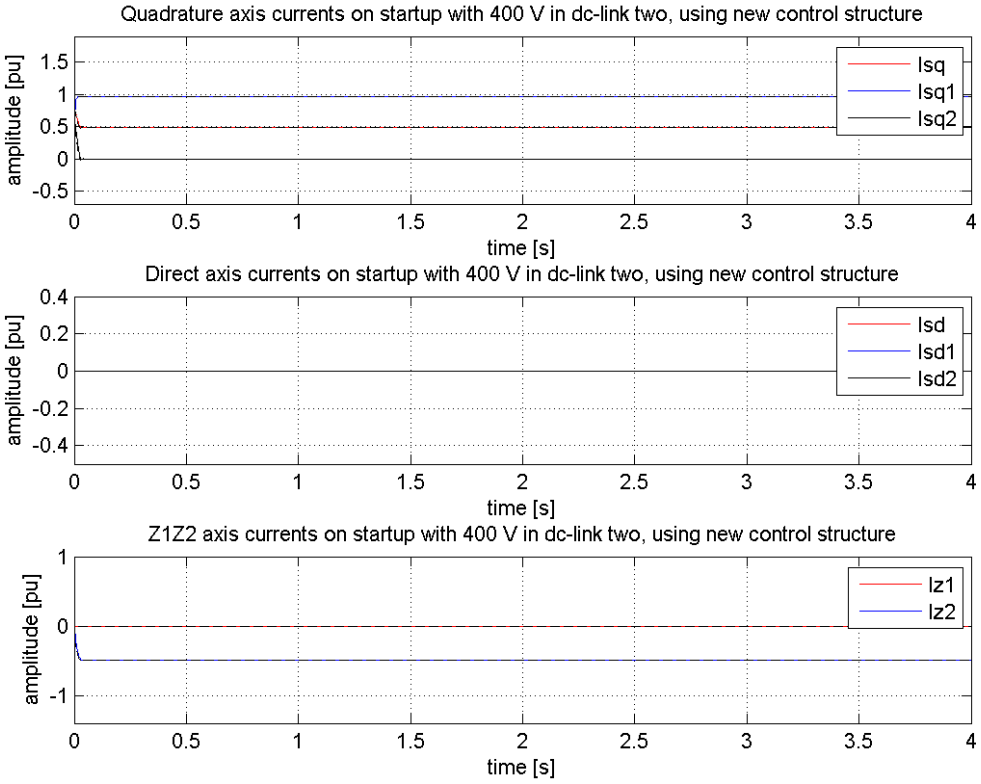

Figure 5.40: Transient current responses to a start-up with 400 V in dc-link two with no output limitations to the regulators, using new control structure.

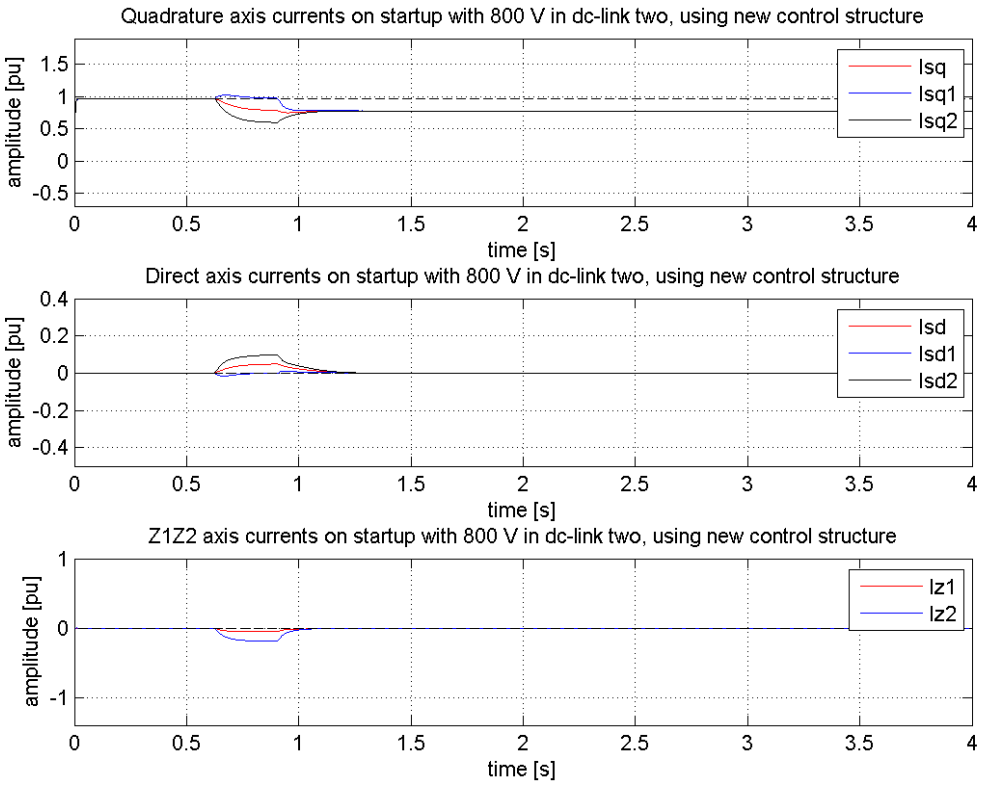

Figure 5.41: Transient current responses to a start-up with 800 V in dc-link two with output limitations on the regulators, using new control structure.

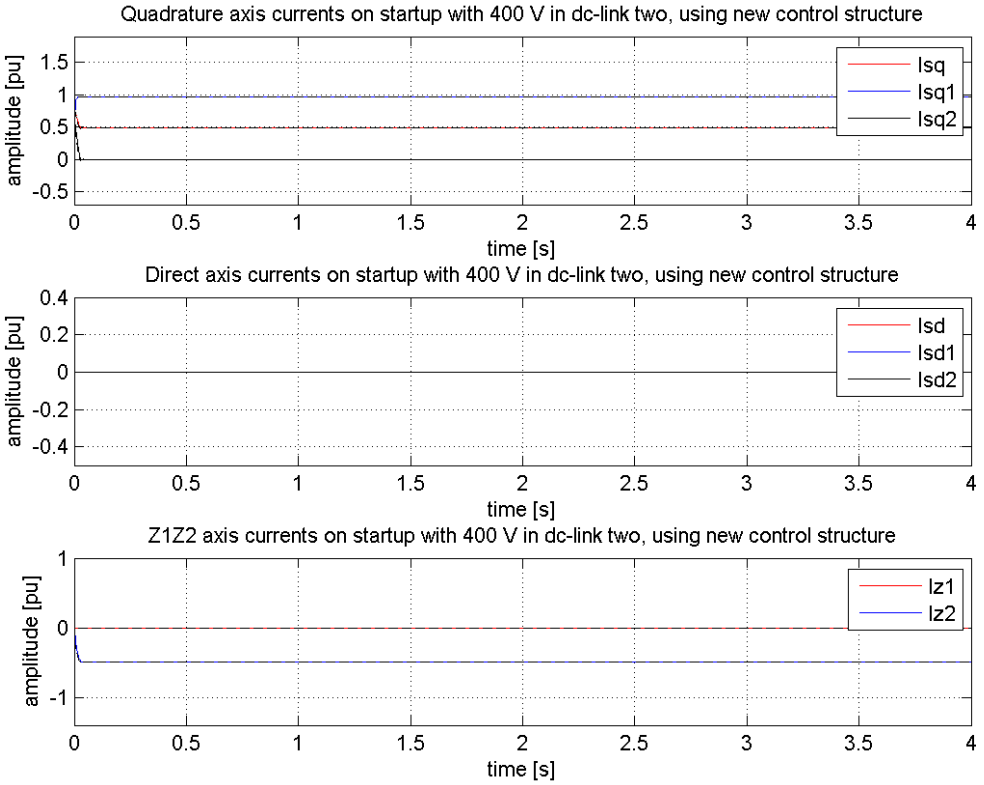

Figure 5.42: Transient current responses to a start-up with 400 V in dc-link two with output limitations on the regulators, using new control structure.

The results show that the performance of the control structure is in general better when dealing with low dc-link voltage start-ups than drop in dc-link voltage. This could be explained by realizing that the control structure does not need to deal with a sudden change in dc-link voltage which created the initial current peak in chapter 5.4.1. Rather it is the gradual increase of u_{st2} into saturation that triggers the response seen in the above figures.

In the simulations regarding the start-up with a 200 V drop in the dc-link voltage, we see the same phenomenon as in the corresponding simulations from chapter 5.4.1. From Figure 5.39, it can be observed that without the added output limits to the regulators the system enters the same quasi steady state as shown in Figure 5.29. The time period the system remains in this state is dependent on the speed of the regulators. However, with faster regulators the value of i_{q1} will be raised even more in the new steady state. Figure 5.41 shows the same simulations including the new output limits on the regulators. The system can be seen to enter the same quasi steady state as in Figure 5.39. The system is however quickly brought out of this state by the quadrature axis regulator reaching its limits. The z_2 axis regulator can thereby control the difference between the quadrature axis currents without interference from the quadrature axis regulator. The same steady state as in Figure 5.34 is then reached with the two components of the quadrature axis currents being equal.

Figure 5.40 and Figure 5.42 show the results of start-up with a 600 V drop in dc-link two. Here the undervoltage regulator can be seen to kick in immediately due to the low start-up value of dc-link two. This gives the correct reference values for the regulators before the control voltage u_{st2} reaches saturation, thereby allowing the control system to effectively control the response of the machine.

For corresponding plots of control voltage, output of regulators and dc-link voltage see appendix E.2.

The affect on the phase currents can be seen in Figure 5.43. The phase currents can again be seen to mirror the response of the direct and quadrature axis currents. The steady state increase of i_{q1} for start-up with 800 V in dc-link two without regulator output limitations, seen in Figure 5.40, also increases the steady state value of the phase current from inverter one. Including the regulator output limits, this affect can be seen to disappear in the phase currents.

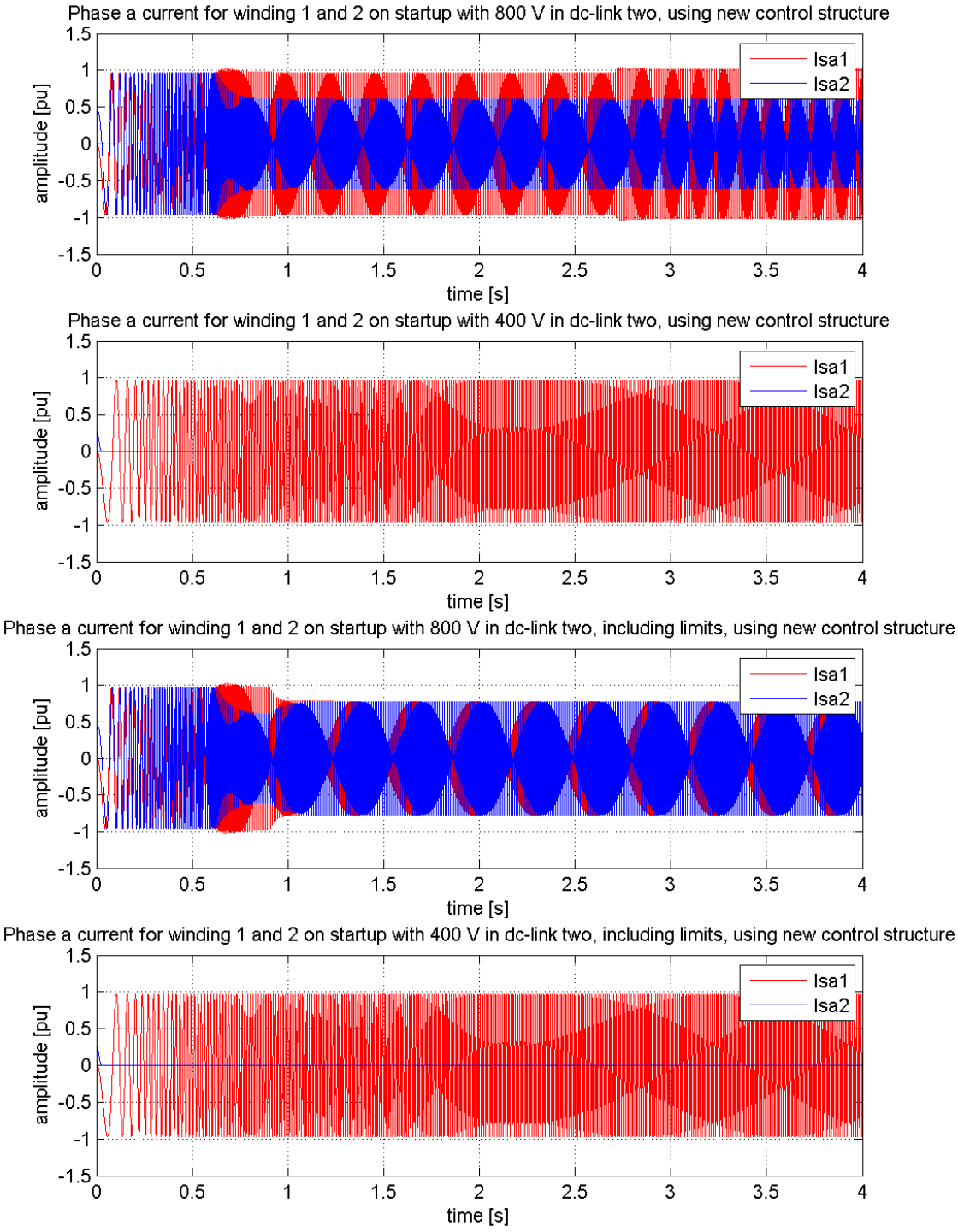

Figure 5.43: Transient phase a current responses to a start-up with low voltage on dc-link number two, using new control structure.

5.4.3 Summary

The response of the system without the additional output limitations is not satisfactory. Large initial current peaks can be seen when simulated with a step in dc-link voltage. Also, for small voltage drops, not invoking the undervoltage regulator, the steady state value of i_{q1} is raised. How much the steady state quadrature axis current of inverter one is raised is dependent on the speed of the regulators, with faster regulators giving a higher value of i_{q1}. In order to prevent the quadrature axis regulator from increasing the steady state value of i_{q1} the output of the four regulators were limited [16].

The results of the new simulation, including the new output limits on the regulator, show that the steady state solution has improved. Inverter one is no longer forced to deliver a quadrature axis current beyond its capacity. However, the transient state reached when the undervoltage regulator is not invoked, does not differentiate between the two quadrature axis currents. This is because the new output limits will always limit the quadrature axis regulator first, as it is already loaded, thereby giving the z_2 regulator the opportunity to control the difference between i_{q1} and i_{q2}. When the undervoltage regulator does not change the reference value of i_{q2}, the reference value of i_{z2} will be zero and the z_2 regulator will reduce i_{q1} so that it matches i_{q2}. This is not an optimal solution, as inverter one is capable of delivering full torque in the given scenario.

Including the new output limits does not significantly improve the amplitude of the initial current peaks, seen in Figure 5.29 and Figure 5.32. This could be explained by realizing that this peak is a consequence of the direct affect dc-link voltage two has on the current i_{q2} and the connection between i_{q1} and i_{q2} seen in equation (4.10). Limiting the output of the quadrature axis regulator does contribute to lowering i_{q1} as this regulator is trying to increase i_q and therefore also i_{q1} and i_{q2}. However the effect of the regulator is insignificant in this time span compared to the system response.

By increasing the threshold voltage of the undervoltage regulator some improvement may be obtained. This will cause smaller voltage drops to invoke the undervoltage regulator, thus changing the reference values. This value may need further fine tuning and work.

To conclude, the efforts made to improve the system response to low dc-link operations have improved some properties of the transient response, deteriorated other properties, but failed to give the system a satisfactory response to these kinds of faults. Further work is required in order to give the system an adequate response.

6 Conclusion and Scope of further work

6.1 Conclusion

In this work, a six-phase IPMSM with split dc-link has been investigated with the purpose of increasing the rated power and redundancy of motors onboard offshore vessels. A new control strategy has been developed in order to successfully control the machine during certain fault situations. The results show a large degree of correlation between the theory and simulations.

The control philosophy has been tested with analogue simulations. This includes tests of normal operation, faults leading to difference in current control torque reference, as well as faults leading to drop in the dc-link voltage. The simulations have been compared to the response of the double synchronous frame current control.

The new control structures ability to respond to changes in torque during normal operation were satisfactory. The control structure was able to quickly follow the torque reference and split the load evenly on the two inverters. This was done without excitation of the (z_1,z_2) subsystem.

The simulations of the system response to difference in torque reference also gave satisfactory results when including the decoupling elements for both subsystems. The direct and quadrature axis currents were rapidly regulated to their new steady state values for both inverters. This was done without considerable overshoot, and without endangering the integrity of the two inverters.

However, the system response to low dc-link voltage shows a need to implement additional control features in order to make the system successfully respond to a low dc-link voltage. This is in particular true for the step in dc-link voltage, where a large initial current peak may cause the trip of the motor drive.

6.2 Scope of further work

In this work, analogue inverters have been used, so new simulations should be considered in order to include the effect of digital control structure and inverter switches. In addition the following elements should be considered:

- Further study on the transient response of the system during low dc-link operations, especially considering new control features to improve the system response.
- Implementation of the current control scheme in a laboratory setup.

References

[1] **Hoem, Ø.** *Modelling and Control of Six-Phase Machines*, Norwegian University of Science and Technology, Department of Electrical Power Engineering, 2009

[2] **Nilsen, R.** *Strategy proposed during discussions on the present work,* Meeting to discuss problems related to the thesis, 2010

[3] **Nelson, R. H. og Krause, P. C.** *Induction machine analysis for arbitary displacement between multiple winding sets,* IEEE Trans. Power App. Syst., Vol. PAS-93, pp. 841-848, May/June 1974.

[4] **Clarke, E.** *Circuit analysis of a.c. power systems, Vol. I. Symmetrical and related components,* John Wiley & sons, Inc., 1943

[5] **Park, R.H.** *Two Reaction Theory of Synchronous Machines Part I,* AIEE Trans 48, pp. 716-730, 1929

[6] **Zhao, Y., Lipo, T.A.** *Space Vector PWM Control of Dual Three-Phase Induction Machine Using Vector Space Decomposition,* IEEE Trans. Ind. Applications, Vol. 31, No. 5, pp. 1100-1109, Sept./Oct. 1995.

[7] **Zhao, Y.** *Vector Space Decomposition Modeling and Control of Multiphase Induction Machines, Ph.D. Thesis University of Wisconsin, 1995*

[8] **Nilsen, R.** *Modelling of multi-phase Synchronous Machines,* Wärtsilä Norway, Ship Power Technology R&D, April 2009

[9] **Nilsen, R.** *Method proposed during discussions on the present work,* Meeting to discuss problems related to the thesis, 2010

[10] **Klingshirn, E. A.** *High Phase Order Induction Motors-Part I –Description and Theoretical Considerations,* IEEE Trans. Power App. Syst., Vol. PAS-102, no. 1, Jan. 1983.

[11] **Bojoi, R., Tenconi, A., Profumo, F., Griva, G., Martinello, D.** *Complete Analysis of Comparative Study of Digital Modulation Techniques for Dual Three-Phase AC Motor Drives*, IEEE PESC'02, pp. 851-857, 2002.

[12] **Bakhshai, A.R., Joos, G., Jin, H.** *Space Vector PWM Control of a Split-Phase Induction Machine Using The Vector Classification Technique,* in Conf. Rec. APEC, Vol. 2, pp. 802-808, 1998

[13] **Nilsen, R., Kvello, J. R.** *Simulation of a 6 phase PM Drive,* Wärtsilä Norway, Ship Power Technology R&D, 2009

[14] **Bojoi, R., Lazzari, M., Profumo, F., Teconi, A.** *Digital Field-Oriented Control of Dual Three-Phase Induction Motor Drives,* IEEE Trans. Ind. Applications, Vol. 39, No. 3, May/June 2003.

[15] **Hadioche, D., Razik, H., Rezzoug, A.** *On the Design of Dual-Stator Windings for Safe VSI Fed AC Machine Drives,* in Conf. Rec. IEEE-IAS Annu. Meeting, pp 1123-1130, 2001

[16] **Nilsen, R.** *Implementation in modell,* 2010

[17] **Robbins, W., Mohan, N., Undeland, T.** *Power electronics,* John Wiley & Sons, Inc., 2003.

A. Vectors and matrixes

A.1 Physical Model

The voltage, current and flux vectors of the physical model given in chapter 3.1.1.

$$\begin{aligned}\underline{U}^{SR} &= \left[U_{sa1} \quad U_{sa2} \quad U_{sb1} \quad U_{sb2} \quad U_{sc1} \quad U_{sc2} \quad U_f\right]^T \\ \underline{I}^{SR} &= \left[I_{sa1} \quad I_{sa2} \quad I_{sb1} \quad I_{sb2} \quad I_{sc1} \quad I_{sc2} \quad I_f\right]^T \\ \underline{\Psi}^{SR} &= \left[\Psi_{sa1} \quad \Psi_{sa2} \quad \Psi_{sb1} \quad \Psi_{sb2} \quad \Psi_{sc1} \quad \Psi_{sc2} \quad \Psi_f\right]^T\end{aligned} \tag{A.1}$$

The resistance and inductance matrix of the physical model:

$$\mathbf{R}^{SR} = \mathrm{diag}\left[R_s \quad R_s \quad R_s \quad R_s \quad R_s \quad R_s \quad R_f\right] \tag{A.2}$$

$$\frac{\partial \mathbf{L}}{\partial \theta}^{SR} = \begin{bmatrix} \frac{\partial \mathbf{L}_g^S}{\partial \theta} & \frac{\partial \mathbf{L}_{sf}^{SR}}{\partial \theta} \\ \frac{\partial \mathbf{L}_{fs}^{SR}}{\partial \theta} & 0 \end{bmatrix} \tag{A.3}$$

A.2 Transformed Model

The voltage, current and flux vectors after applying the transformation matrix given in equation (3.5):

$$\begin{aligned}\underline{U}^r &= \left[U_d \quad U_q \quad U_{z1} \quad U_{z2} \quad U_{01} \quad U_{02} \quad U_f\right]^T \\ \underline{I}^r &= \left[I_d \quad I_q \quad I_{z1} \quad I_{z2} \quad I_{01} \quad I_{02} \quad I_f\right]^T \\ \underline{\Psi}^r &= \left[\Psi_d \quad \Psi_q \quad \Psi_{z1} \quad \Psi_{z2} \quad \Psi_{01} \quad \Psi_{02} \quad \Psi_f\right]^T\end{aligned} \tag{A.4}$$

The resistance, inductance and **J** matrix after applying the transformation matrix given in equation (3.5):

$$\mathbf{R}^r = \mathbf{T}^r \cdot \mathbf{R}^{SR} \cdot \mathbf{T}^{-r} = \mathrm{diag}\left[R_s \quad R_s \quad R_s \quad R_s \quad R_s \quad R_s \quad R_f\right] \tag{A.5}$$

$$\mathbf{L}^{r} = \mathbf{T}^{r} \cdot \mathbf{L}^{SR} \cdot \mathbf{T}^{-r} = \begin{bmatrix} 3\cdot(L_{sh}+L_g)+L_{s\sigma} & 0 & 0 & 0 & 0 & 0 & L_{df} \\ 0 & 3\cdot(L_{sh}-L_g)+L_{s\sigma} & 0 & 0 & 0 & 0 & 0 \\ 0 & 0 & L_{s\sigma} & 0 & 0 & 0 & 0 \\ 0 & 0 & 0 & L_{s\sigma} & 0 & 0 & 0 \\ 0 & 0 & 0 & 0 & L_{s\sigma} & 0 & 0 \\ 0 & 0 & 0 & 0 & 0 & L_{s\sigma} & 0 \\ 3\cdot L_{df} & 0 & 0 & 0 & 0 & 0 & L_f \end{bmatrix} \tag{A.6}$$

$L_{s\sigma}$= Leakage inductance for each stator winding

L_g = Position dependent part of self inductance

L_{sh}= Stator Mutual inductance

$$\mathbf{J} = \begin{bmatrix} 0 & -1 & 0 & 0 & 0 & 0 & 0 \\ 1 & 0 & 0 & 0 & 0 & 0 & 0 \\ 0 & 0 & 0 & 1 & 0 & 0 & 0 \\ 0 & 0 & -1 & 0 & 0 & 0 & 0 \\ 0 & 0 & 0 & 0 & 0 & 0 & 0 \\ 0 & 0 & 0 & 0 & 0 & 0 & 0 \\ 0 & 0 & 0 & 0 & 0 & 0 & 0 \end{bmatrix} \tag{A.7}$$

The reactance matrix, a result of applying both the transformation matrix and the pu system to the physical model:

$$\mathbf{x}^{r} = \begin{bmatrix} x_{dh}+x_{s\sigma} & 0 & 0 & 0 & 0 & 0 & x_{dh} \\ 0 & x_{qh}+x_{s\sigma} & 0 & 0 & 0 & 0 & 0 \\ 0 & 0 & x_{s\sigma} & 0 & 0 & 0 & 0 \\ 0 & 0 & 0 & x_{s\sigma} & 0 & 0 & 0 \\ 0 & 0 & 0 & 0 & x_{s\sigma} & 0 & 0 \\ 0 & 0 & 0 & 0 & 0 & x_{s\sigma} & 0 \\ x_{dh} & 0 & 0 & 0 & 0 & 0 & x_{dh}+x_{f\sigma} \end{bmatrix} \tag{A.8}$$

$$x_{dh} = \frac{3\cdot(L_{sh}+L_g)\cdot\omega_n\cdot\hat{I}_n}{\hat{U}_n} \qquad x_{qh} = \frac{3\cdot(L_{sh}-L_g)\cdot\omega_n\cdot\hat{I}_n}{\hat{U}_n}$$

$$x_d = x_{dh}+x_{s\sigma} \qquad x_q = x_{qh}+x_{s\sigma}$$

B. Model parameters

In the following is listed the parameters used in Simulink to conduct the simulations documented in chapter 5.

Parameter	*Explanation*	*Value*
U_n	Nominal line-line voltage [V_{rms}]	601 V_{rms}
I_n	Nominal current [A_{rms}]	1310 A_{rms}
f_n	Nominal frequency [Hz]	125 Hz
p	number of pole pairs	15
r_s	Stator resistance [pu]	0.009 pu
x_d	Direct axis reactance [pu]	0.3558 pu
x_q	Quadrature axis reactance [pu]	0.3558 pu
x_σ	Leakage reactance [pu]	0.1 pu
ψ_m	Rotor Magnet flux [pu]	0.9255 pu

Table 7: Six-phase dual winding machine parameters

Parameter	*Explanation*	*Value*
K_{pd}	Gain factor in current controller direct axis	0.1510
K_{pq}	Gain factor in current controller quadrature axis	0.1510
K_{pz1}	Gain factor in current controller z_1 axis	0.0424
K_{pz2}	Gain factor in current controller z_2 axis	0.0424
T_{id}	Time constant of the direct axis controller	0.050
T_{iq}	Time constant of the quadrature axis controller	0.050
T_{iz1}	Time constant of the z_1 axis controller	0.0014
T_{iz2}	Time constant of the z_2 axis controller	0.0014
W_{max}	Max windup of the integrator	1.15

Table 8: dq and z_1z_2 current controller parameters

Parameter	*Explanation*	*Value*
T_v	Time delay in the inverter	0 or 1/6000
f_{sw}	Switching frequency [Hz]	3000

Table 9: Inverter parameters

Parameter	*Explanation*	*Value*
R	Resistance between stiff grid and capacitor	0.05 Ω
C	Capacitance of the dc-link capacitor	$12e^{-3}$ F

Table 10: DC-link parameters

C. Decoupling network

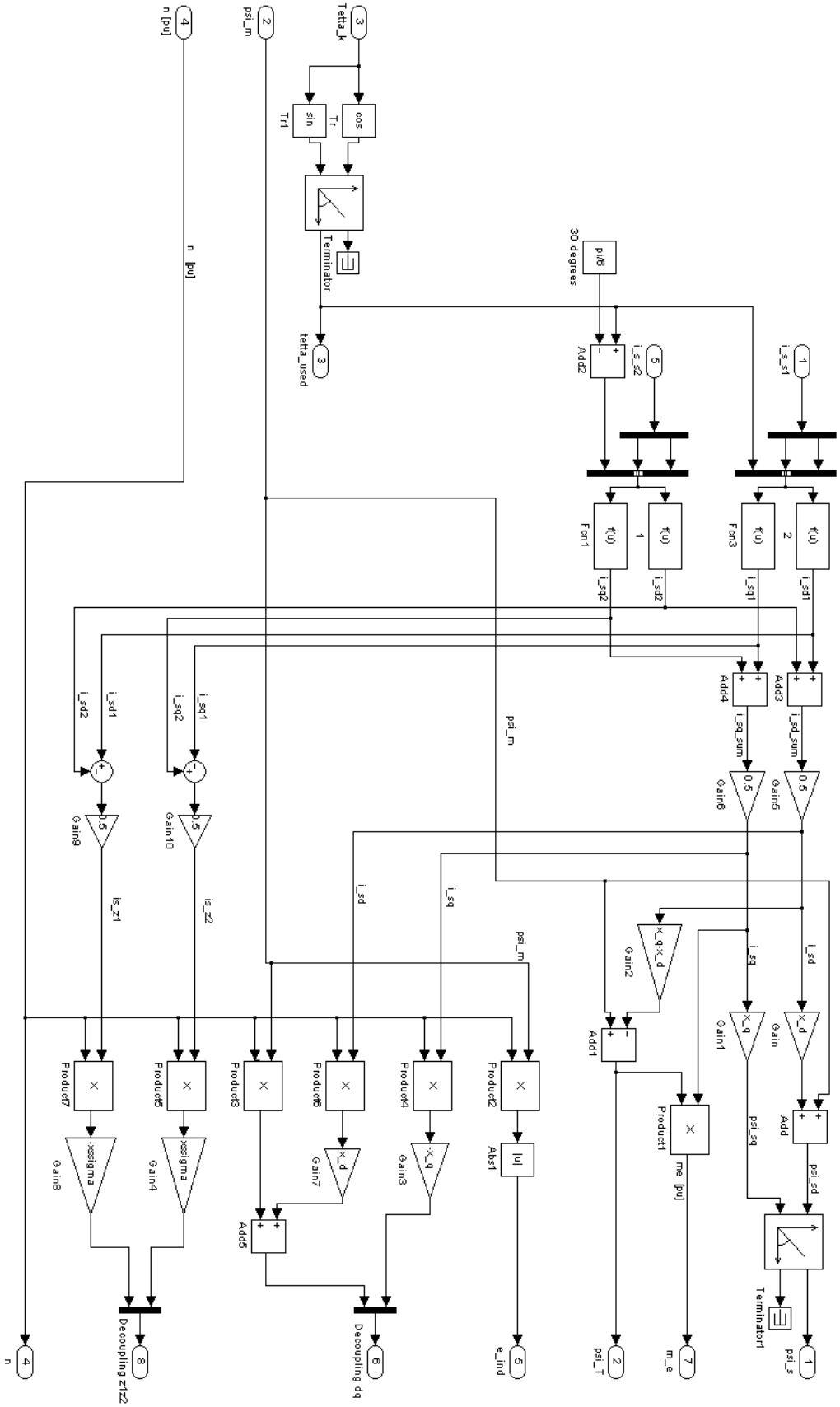

Figure C.1: Simulink model of the decoupling network

D. PI regulator with output limits

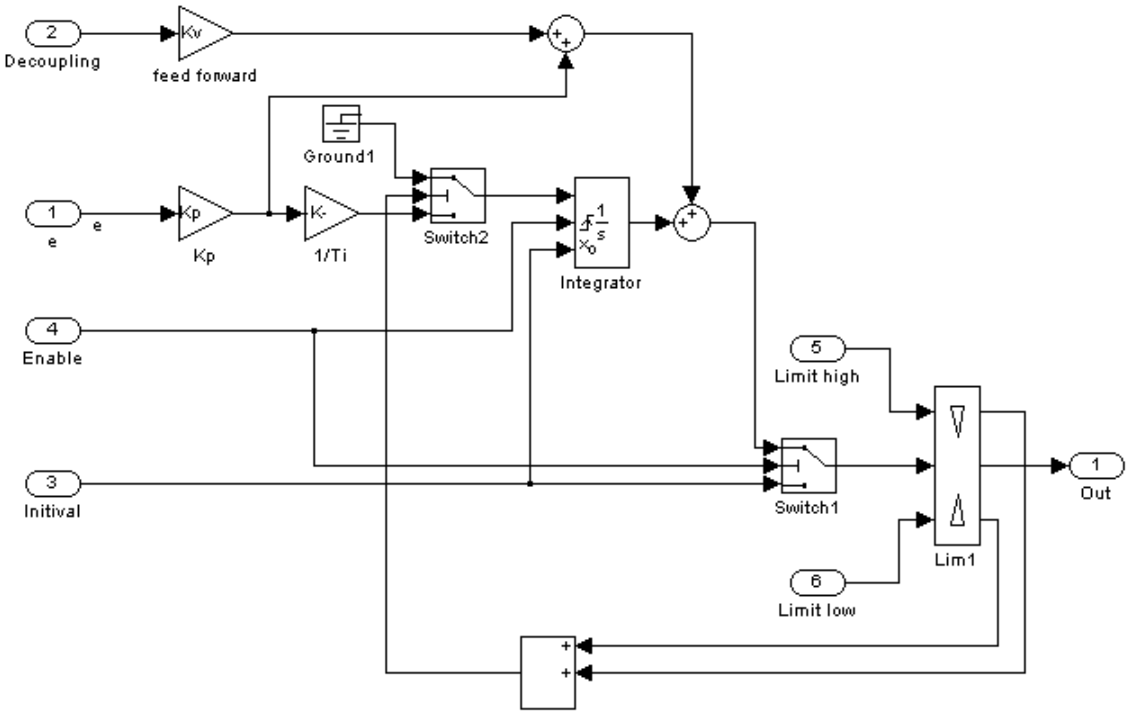

Figure D.1: Simulink model of the PI regulator with output limits

E. Additional Simulations results

E.1 200 V drop in dc-link voltage two with no output limits

In the simulations testing the original DSPC system response to a 200 V drop in dc-link number two, the current controller parameters was kept the same as for chapter 5.2 and 5.3 for the sake of continuity. However, the effects and results being discussed in relation to Figure 5.29 are much easier to convey when the regulators are set to operate at a higher speed. This is mainly because of the additional influence the quadrature axis regulator has on the system response before its integrator reaches saturation. This simulation has therefore been repeated, and the results are presented here. The controller parameters for this simulation are given in Table 11.

Parameter	*Explanation*	*Value*
K_{pd}	Gain factor in current controller direct axis	0.2831
K_{pq}	Gain factor in current controller quadrature axis	0.2831
K_{pz1}	Gain factor in current controller z_1 axis	0.0795
K_{pz2}	Gain factor in current controller z_2 axis	0.0795
T_{id}	Time constant of the direct axis controller	0.050
T_{iq}	Time constant of the quadrature axis controller	0.050
T_{iz1}	Time constant of the z_1 axis controller	0.0014
T_{iz2}	Time constant of the z_2 axis controller	0.0014
W_{max}	Max windup of the integrator	1.15

Table 11: Current controller parameters for simulations in appendix E.1

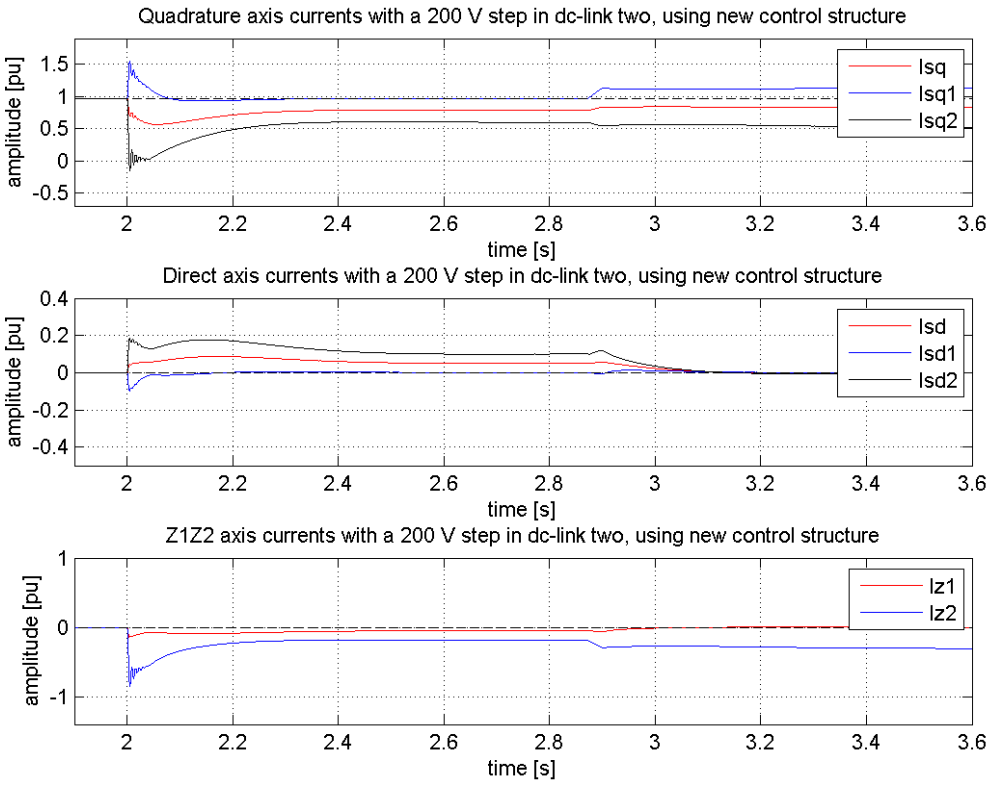

Figure E.1: Transient current responses to a negative 200 V step in dc-link voltage 2 with no output limitations to the regulators and faster regulators, using new control structure.

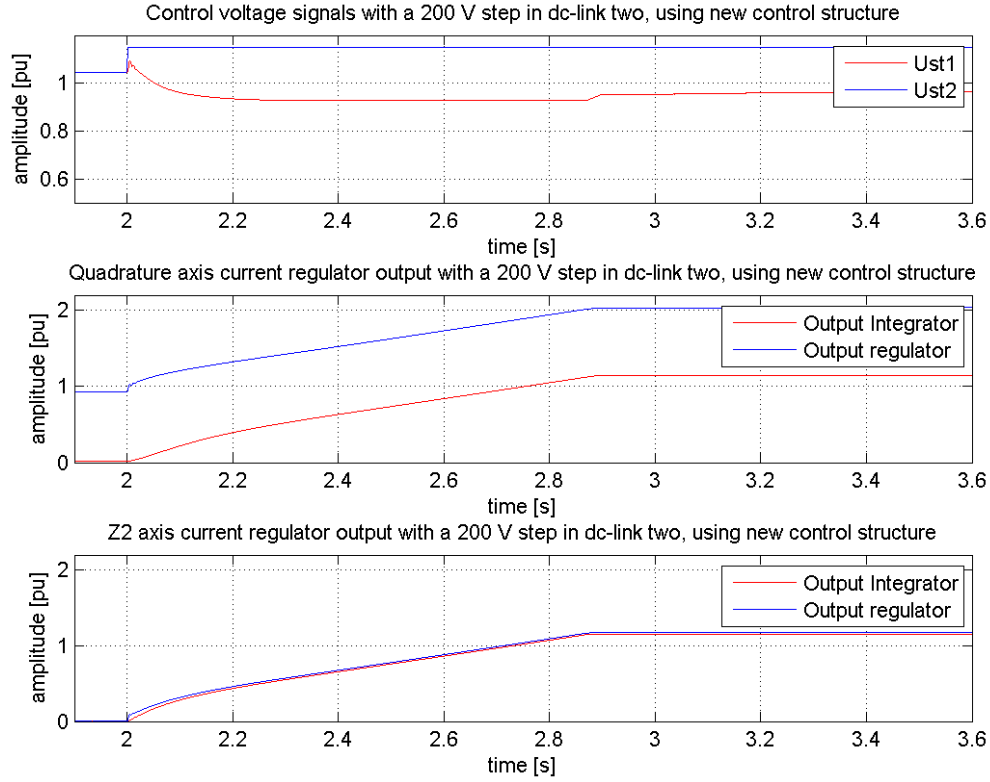

Figure E.2: Transient control voltage and regulator responses to a negative 200 V step in dc-link voltage 2 with no output limitations to the regulators and faster regulators, using new control structure.

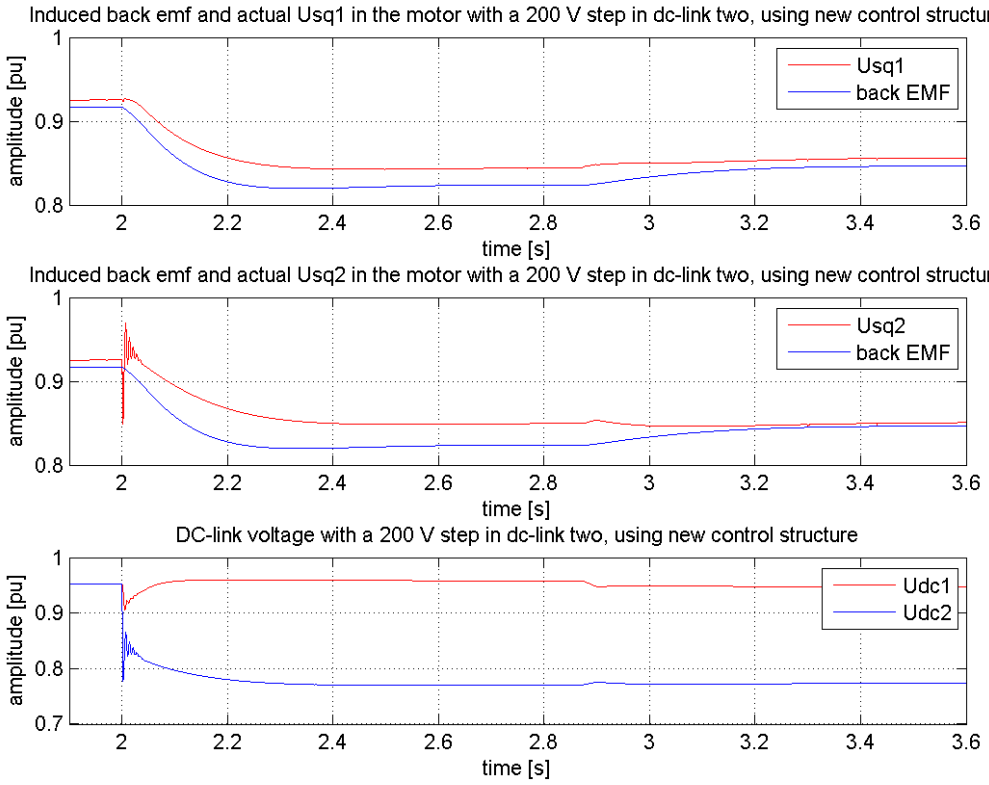

Figure E.3: Transient voltage responses to a negative 200 V step in dc-link voltage 2 with no output limitations to the regulators and faster regulators, using new control structure.

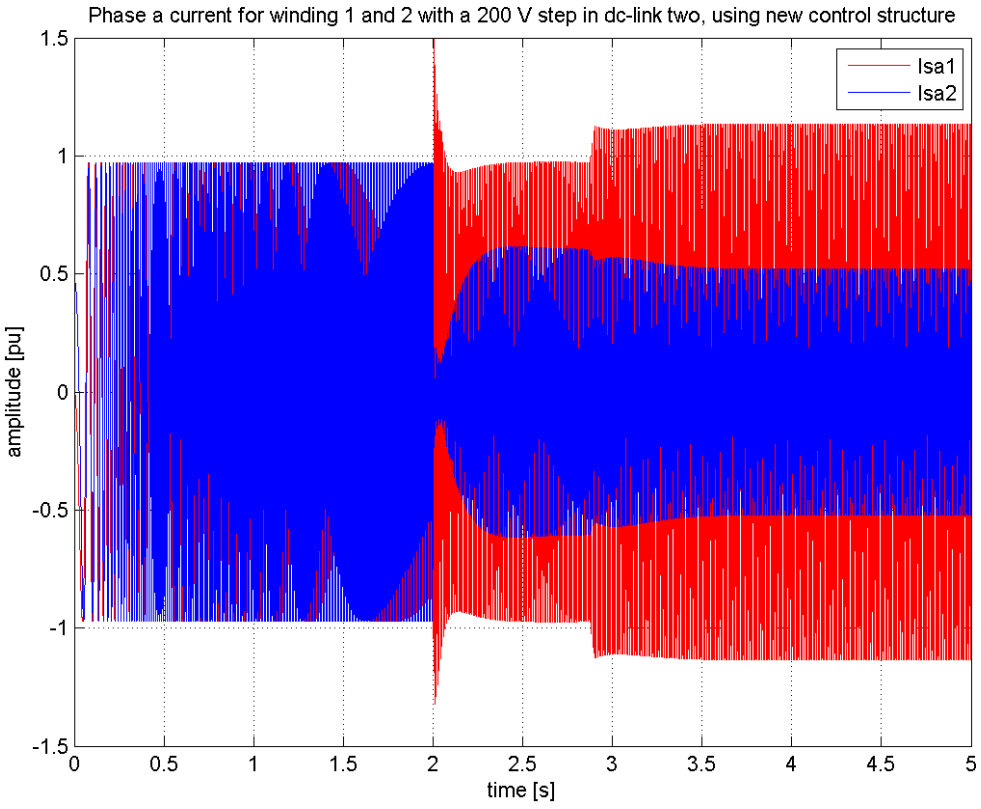

Figure E.4: Transient phase a current responses to a negative 200 V step in dc-link voltage 2 with no output limitations to the regulators and faster regulators, using new control structure.

E.2 Additional plots to start-up with low dc-link voltage.

In this section, additional plots from the low dc-link voltage simulations are included. These include plots of the control voltage, the dc-link voltage and the output of the quadrature axis and z_2 axis regulator.

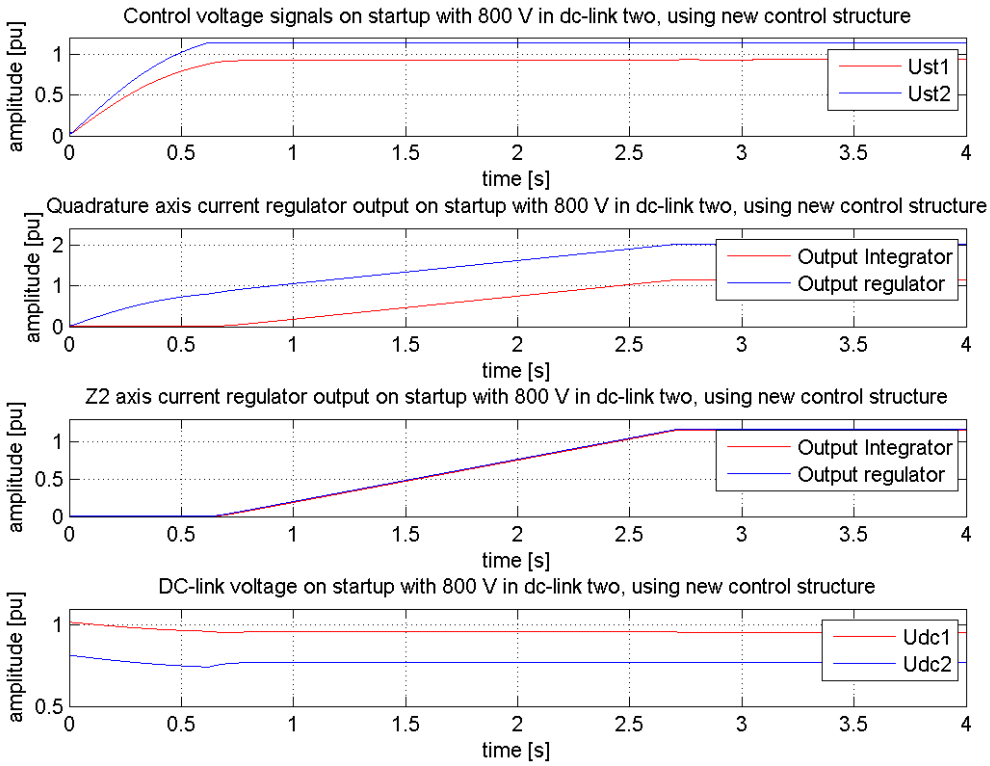

Figure E.5: Transient voltage and regulator responses to a start-up with 800 V in dc-link two with no output limitations to the regulators, using new control structure.

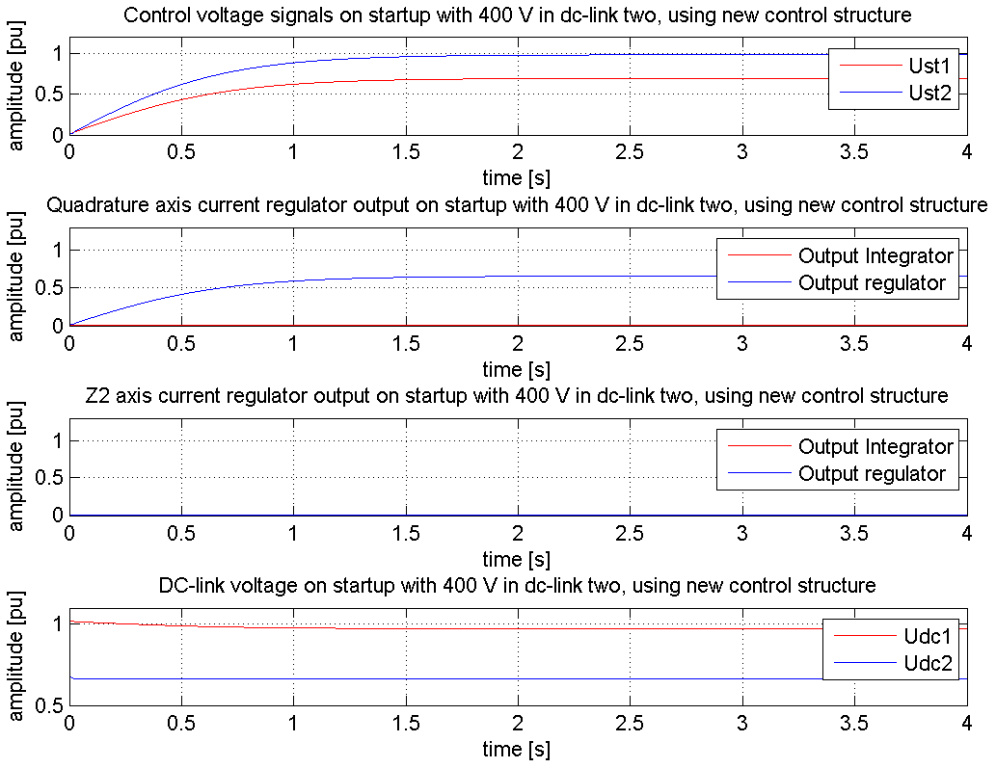

Figure E.6: Transient voltage and regulator responses to a start-up with 400 V in dc-link two with no output limitations to the regulators, using new control structure.

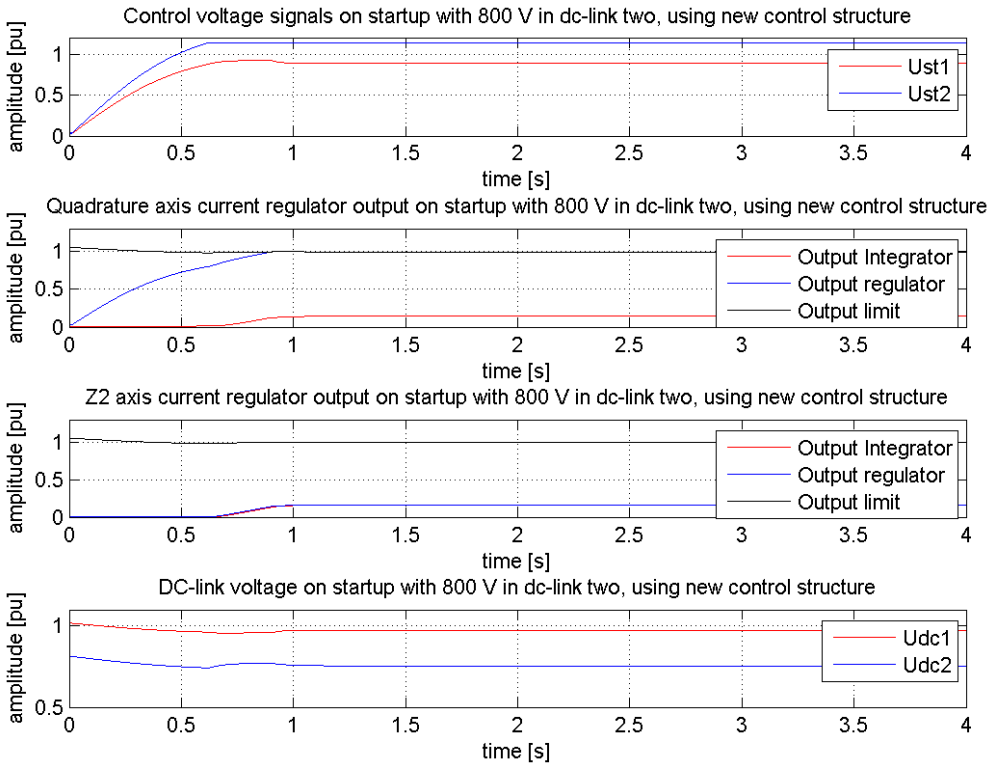

Figure E.7: Transient voltage and regulator responses to a start-up with 800 V in dc-link two with output limitations on the regulators, using new control structure.

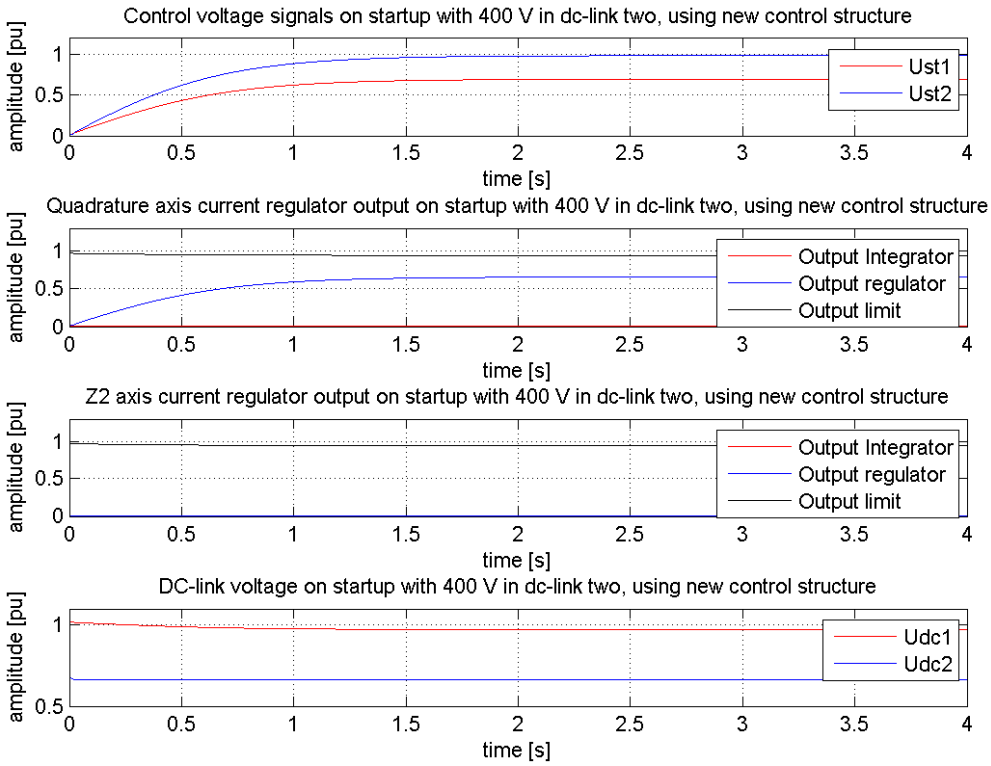

Figure E.8: Transient voltage and regulator responses to a start-up with 400 V in dc-link two with output limitations on the regulators, using new control structure.